JAEA-Technology
2006-017

JP0650381

JAEA-Technology

Applicability Assessment of Plug Weld to ITER Vacuum Vessel by Crack Propagation Analysis

Junji OHMORI, Masataka NAKAHIRA,
Nobukazu TAKEDA, Kiyoshi SHIBANUMA,
Hiromi SAGO* and Masanori ONOZUKA*

Plant System Group
Tokamak Device Group
Fusion Research and Development Directorate

March 2006

Japan Atomic Energy Agency

日本原子力研究開発機構

JAEA-Technology 2006-017

Applicability Assessment of Plug Weld to ITER Vacuum Vessel by Crack Propagation Analysis

Junji OHMORI, Masataka NAKAHIRA, Nobukazu TAKEDA,
Kiyoshi SHIBANUMA, Hiromi SAGO* and Masanori ONOZUKA*

ITER Project Unit
Fusion Research and Development Directorate
Japan Atomic Energy Agency
Naka-shi, Ibaraki-ken

(Received January 27, 2006)

In order to improve the fabricability of the vacuum vessel (VV) of International Thermonuclear Experimental Reactor (ITER), applicability of plug weld between VV outer shell and stiffening ribs/blanket support housings has been assessed using crack propagation analysis for the plug weld.

The ITER VV is a double-wall structure of inner and outer shells with ribs and housings between the shells. For the fabrication of VV, ribs and housings are welded to outer shell after welding to inner shell. A lot of weld grooves should be adjusted for welding outer shell. The plug weld is that outer shells with slit at the weld region are set on ribs/housings then outer shells are welded to them by filling the slits with weld metal. The plug weld can allow larger tolerance of weld groove gap than ordinary butt weld.

However, un-welded lengths parallel to outer shell surface remain in the plug weld region. It is necessary to evaluate the allowable un-welded length to apply the plug weld to ITER VV fabrication. For the assessment, the allowable un-welded lengths have been calculated by crack propagation analyses for load conditions, conservatively assuming the un-welded region is a crack. In the analyses, firstly allowable crack lengths are calculated from the stresses of the weld region. Then assuming initial crack length, crack propagation is calculated during operation period. Allowable initial crack lengths are determined on the condition that the propagated cracks should not exceed the allowable crack lengths.

The analyses have been carried out for typical inboard straight region and inboard upper curved region with the maximum housing stress. The allowable initial cracks of ribs are estimated to be 8.8mm and 38mm for the rib and the housing, respectively, considering inspection error of 4.4mm. Plug weld between outer shell and ribs/housings could be applicable.

Keywords: Fusion, ITER, Vacuum Vessel (VV), Plug Weld, Crack Propagation

---

* Mitsubishi Heavy Industries, LTD.

クラック進展解析によるプラグ溶接のITER真空容器への適用性評価

日本原子力研究開発機構
核融合研究開発部門　ITERプロジェクトユニット
大森　順次、中平　昌隆、武田　信和、柴沼　清
佐郷　ひろみ*、小野塚　正紀*

（2006年1月27日受理）

核融合実験装置（ITER）の真空容器の製作性を向上させるため、真空容器の外壁と、補強リブあるいはブランケット支持用ハウジングの溶接に、プラグ溶接を適用する可能性について、プラグ溶接部のクラック進展解析を行って評価した。

ITERの真空容器は、内壁と外壁からなる二重壁で構成され、二重壁間にはリブやハウジングが設けられる。真空容器の製作では、内壁にリブとハウジングを溶接した後、これらを外壁と溶接するため、外壁に溶接では、多数の溶接部の位置合わせが必要である。プラグ溶接は、溶接部分に溝を設けた外壁をリブやハウジングの上に乗せ、溶接金属でこの溝を埋めて接続する溶接方法で、通常の突き合わせ溶接に比べて、溶接部で大きな位置ずれを許容することができる。

しかしながら、プラグ溶接は溶接部に外壁表面に沿った非溶け込み部を生ずるので、ITER真空容器製作にプラグ溶接を適用するためには、許容非溶け込み長さを評価する必要がある。評価は、非溶け込み部を保守的に亀裂とみなし、荷重条件に対し亀裂進展解析を行って許容非溶け込み長さを求めた。解析では、まず溶接部にかかる応力から許容亀裂長さを求める。次に初期亀裂を仮定して、装置の運転期間中に進展する亀裂長さを計算し、進展した亀裂長さが許容亀裂長さを超えないように、許容初期亀裂長さを求めるものである。

インボード側の代表的直線部と、ハウジングの応力が最大となるインボード側上部曲線部について行った解析の結果、溶接部の非破壊検査による誤差を4.4mmと仮定して、真空容器のリブに許容される初期亀裂長さは8.8mm、ハウジングは38mmとなり、外壁の溶接部にプラグ溶接を適用することができる。

那珂核融合研究所(駐在)：〒311-0193　茨城県那珂市向山801-1
*三菱重工業株式会社

Contents

目　次

1. Introduction

The ITER main vessel is a large torus-shaped, double-wall structure of inner and outer shells with stiffening ribs and blanket housings between the shells to give the required mechanical strength and separate the shells. The basic vessel design is an all-welded structure.
Toroidal and poloidal ribs are used to reinforce the vessel structure. Each blanket module is attached directly to the VV by a set of four flexible supports located symmetrically with respect to the module center. The flexible supports are mounted in housings that are recessed inside the vessel and structurally integrated both with the inner and outer shells.
All weld joints within the VV are to be of the full-penetration type and most weld joints have conventional configurations in the reference design. Ribs and housings are welded to outer shell from outer shell side after welding to inner shell. Butt weld and ultrasonic testing of the joints have been proposed in the reference design. The groove gaps of the butt weld are about 2mm for manual weld and less than 1mm for automatic weld. By welding outer shells, weld deformations of the outer shells seem to be produced due to heat deposition of a lot of weld joints. Precise adjustment of groove gaps is to be required for welding outer shells.
In order to improve the fabricability of outer shell welding, plug weld joint has been proposed. The plug weld is that outer shells with slit at the weld position are set on ribs/housings then outer shells are welded to them by filling the slits with weld metal. The plug weld can allow larger tolerance of weld groove gaps than ordinary butt weld. However, un-welded lengths parallel to outer shell surface remain in the plug weld region. It is necessary to evaluate the allowable un-welded length to apply the plug weld to ITER vacuum vessel fabrication. In order to assess the applicability of plug welding, the allowable un-welded lengths have been calculated for operation conditions by crack propagation analyses, conservatively assuming the un-welded region is a crack. The analyzed regions are a typical inboard straight region with ribs/housings successively located and an inboard upper curved region with maximum housing stress. Additionally the allowable crack lengths perpendicular to outer shell surface, which are defects in weld metal, have been also assessed.

2. Structure of ITER vacuum vessel and plug weld

2.1 Structure of ITER vacuum vessel [1]

The ITER main vessel is a large torus-shaped, double-wall structure with shielding and cooling water between the shells. The vessel consists of inner and outer shells, ribs, shield structures, splice plates for field joints, and mechanical structures on the inner and outer shells to support in-vessel components and to support the vessel weight, shown in Fig.2.1.-1. The main parameters of the VV are summarized in Table 2.1-1.

The double-wall structure of the main vessel is made of SS 316L(N)-IG with stiffening ribs between the shells to give the required mechanical strength and separate the shells. The inner and outer shells are both 60 mm thick plates and the stiffening ribs mainly 40 mm thick plate. The basic vessel design is an all-welded structure. Although the VV is a double wall structure, the inner shell serves as the first confinement barrier. The minor and maximum radii of the main vessel are 3.2 m and 9.7 m respectively, and the overall height is 11.3 m. The total thickness of the double-wall structure is typically in the range of 0.34-0.75 m, shown in Fig.2.1-2. The inner and outer shells and stiffening ribs between them are joined by welding. These ribs also form the flow passages for the vessel cooling and baking water. Water flowing in the space between the shells is required to remove the nuclear heat deposition and also performs a shielding function.

Toroidal and poloidal ribs are used to reinforce the vessel structure. 40 mm thick plate is mainly used except a poloidal rib at the toroidal center of the 40° sector, which is 60 mm thick plate to provide sufficient strength of the vessel shells.

Each blanket module is attached directly to the VV by a set of four flexible supports located symmetrically with respect to the module center shown in Fig 2.1-3. The flexible supports are mounted in housings that are recessed inside the vessel and structurally integrated both with the inner and outer shells. The inner shell continues around the housing as the first confinement barrier.

2.2 Design of plug weld

Fig 2.2-1 shows the cross-section in inboard area. All weld joints within the VV are to be of the full-penetration type and most weld joints have conventional configurations in the reference design. For the welding of inner shell, the layout of the housings/keys allows the electron-beam welding of these components to the shell and radiographic testing as non-destructive testing (NDT) of the weld joints. It is because the inner shell is the confinement barrier.

For the welding joints between outer shell and rib/housing, butt weld and ultrasonic testing of the joints have been proposed in the reference design, shown in Figs.2.2-2 and 2.2-3. The groove gaps of the butt weld are about 2mm for manual weld and less than 1mm for automatic weld. By welding outer shells, weld deformations of the outer shells seem to be produced due to heat deposition of a lot of weld joints. Precise adjustment of groove gaps is to be required for welding outer shells.

In order to improve the fabricability of outer shell welding, plug weld joint has been proposed. Figs.2.2-4 and 2.2-5 show the plug weld joint between outer shell and rib, and between outer shell and housing. Outer shell with grooves are set on ribs and housings and welded to them using the grooves. The groove gaps of the plug welds can be larger than those of the butt weld. However, un-welded regions remain in the plug weld, shown in Figs.2.2-4 and 2.2-5. It is necessary to evaluate the allowable un-welded length to apply the plug weld to ITER vacuum vessel fabrication.

Reference

[2-1] ITER DDD 15, Vacuum Vessel, September 2004

Table 2.1-1 Main VV Parameters

	ITER-FEAT
Size	
- Torus OD	19.4 m
- Torus Height	11.3 m
- Double Wall Thickness	0.34-0.75 m
- Toroidal Extent of Sector	40°
- Number of Sectors	9
- Shell Thickness	60 mm
- Rib Thickness	40-60 mm
Structure	Double-wall structure
- Inboard Straight Region	Cylindrical
- Inboard Top/Bottom	Double curvature
- Outboard Region	4 Facets/Sector
Resistance	
- Toroidal	7.9 μΩ
- Poloidal	4.1 μΩ
Required Leak Rate	$\leq 1\times10^{-8}$ Pam^{-3}/s
Surface Area / Volume (Main Vessel)	
- Interior Surface Area	850 m^2
- Interior Free Volume (excluding IVC* volume)	1090 m^3
- Interior Total Volume (including IVC* volume)	1600 m^3
Materials[5]	
- Main Vessel and Double-wall Port Components	SS 316L(N)-IG
- Primary In-wall Shielding	SS 304B7 (inboard) and SS 304B4 (outboard)
- Ferromagnetic Insert Shielding	SS 430
- Single wall port components and Connecting Ducts	SS 304
- Fixing/supporting components (including fastening bolts)	Grade 660 or/and Alloy 718 (Inconel 718)
Mass (without water)	
- Main Vessel (without shielding)	1611 t
- Shielding	1733 t
- Port Structures	1487 t
- Connecting Ducts	294 t
- Total (not including water)	5124 t

* : In-vessel components (IVC)

G15GR7000-11-16W0.1

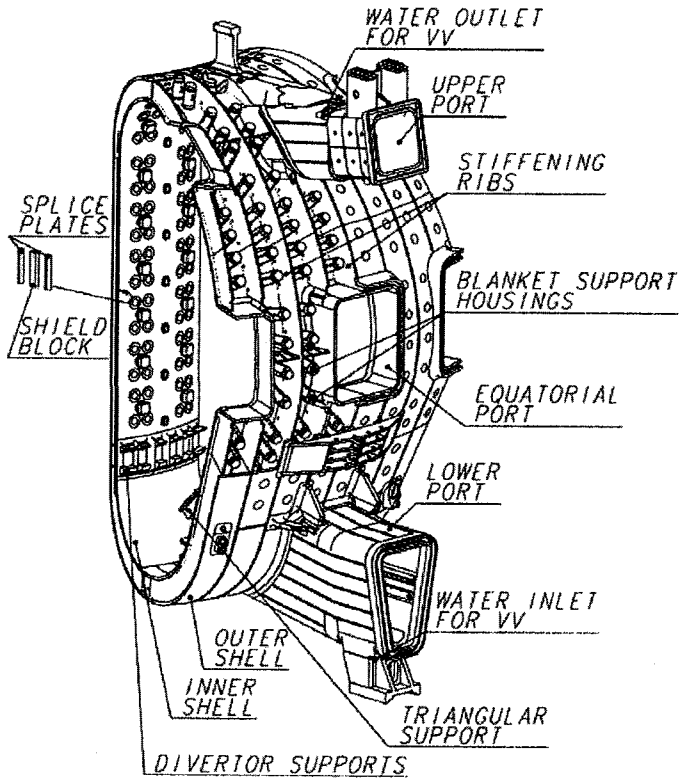

Fig.2.1-1 Vacuum Vessel Overall Structure

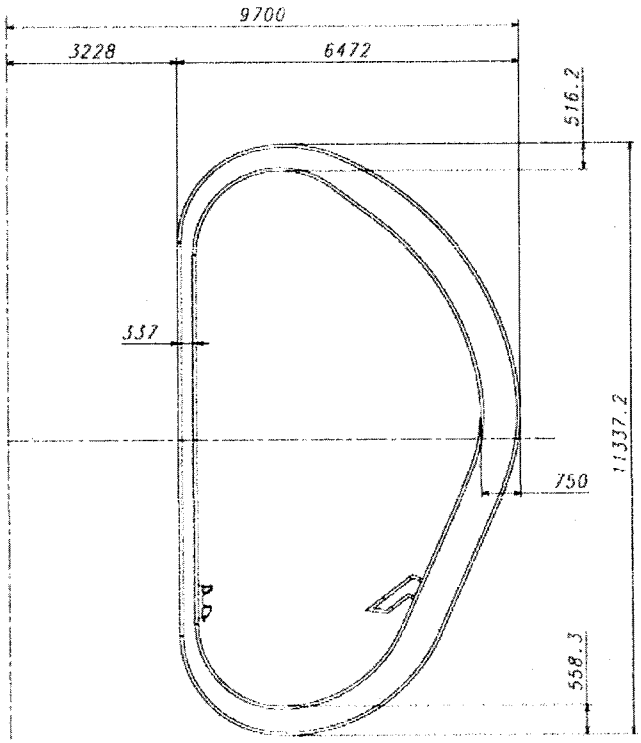

Fig.2.1-2 Vacuum Vessel Cross-Section

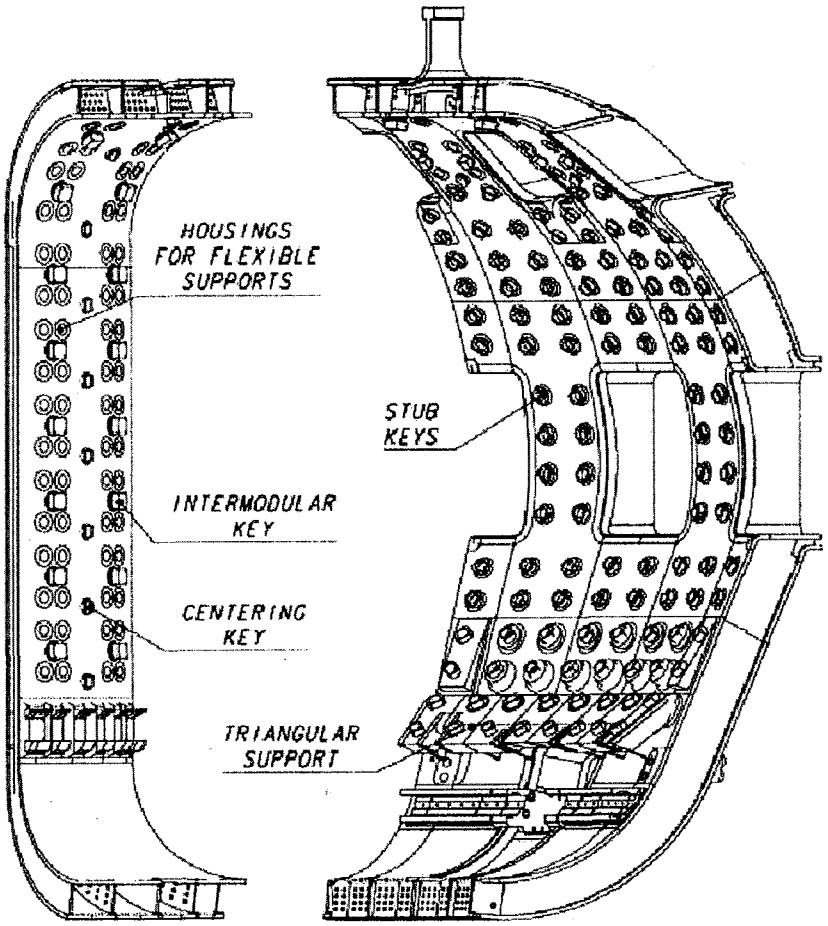

Fig.2.1-3 Arrangement of Housings and Keys for Attachment of the Blanket Modules

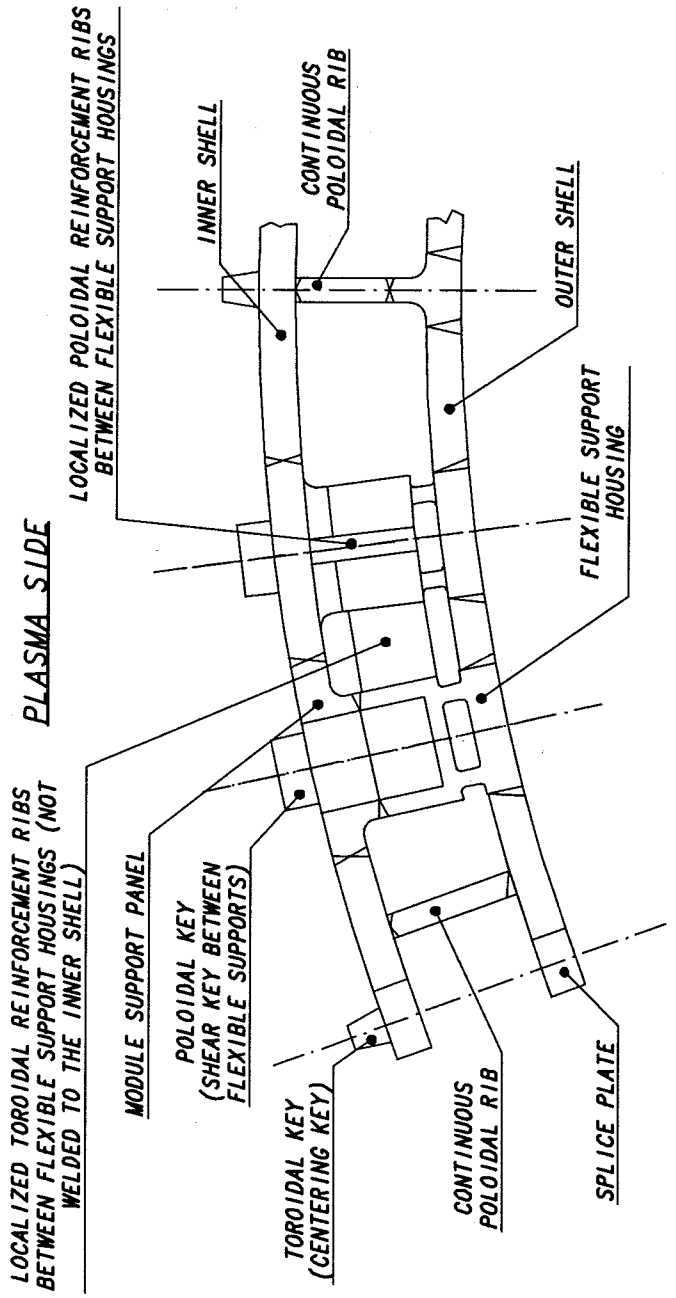

Fig. 2.2-1 Typical Toroidal Cross-Section in Inboard Region

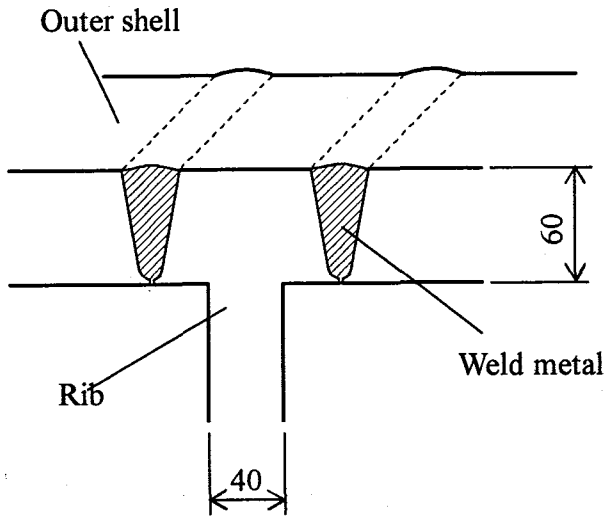

Fig.2.2-2 Butt Weld between Outer shell and Rib

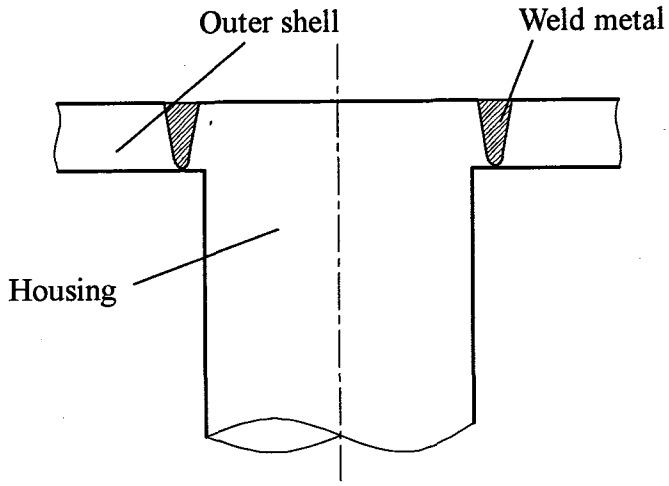

Fig.2.2-3 Butt Weld between Outer shell and Housing

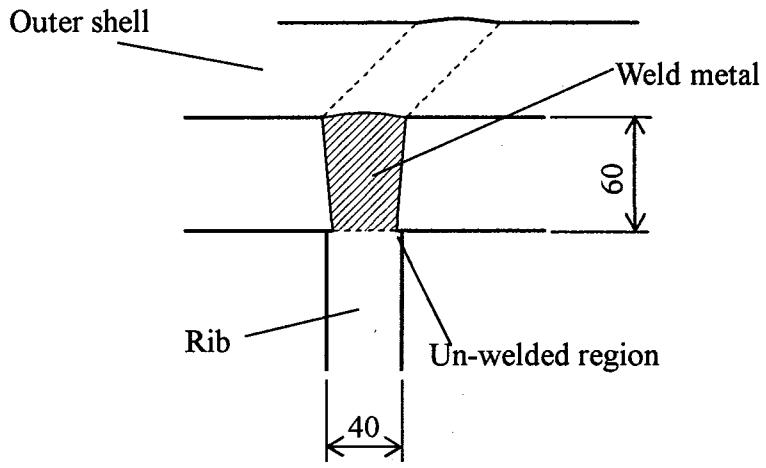

Fig.2.2-4 Plug Weld between Outer shell and Rib

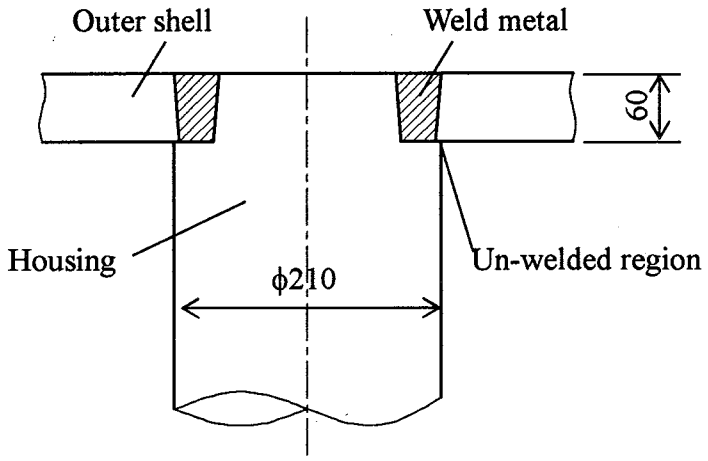

Fig.2.2-5 Plug Weld between Outer shell and Housing

3. Load conditions and combinations

Load conditions and combinations are shown in Table 3.-1[3-1]. The events producing electro-magnetic loads are major disruption(MD), vertical displacement event(VDE) and toroidal coil fast discharge(TFCFD). The event producing thermal load is nuclear heating. Stress analyses have been carried out for each load condition separately. The stresses for the load combinations are obtained by the summation of the stresses of the each analysis results. For the number of cycles of crack propagation analyses, operation events are grouped as follows; VDEII(MDII) of 3180 cycles, VDEII+ TFCFD of 101cycles, VDEIII of 1 cycle and thermal stress of 30000cycles, shown in Table3.-1.

Reference

[3-1] ITER DDD Load Specification, July 2004, P7.

Table 3-1 Load conditions and combinations

Cat.	Load Combination	No. of cycles	No. of cycles for crack propagation	Static allowable stress
I	MDI	3000(A)		Sm (Membrane) 1.5Sm (Bending) 3Sm (Thermal) 3 (Buckling)
	MDI+TFCFD	50(B)		
	VDEI	150(A)		
	VDEI+TFCFD	50(B)		
II	MDII	15(A)	3180(A) (=3000+150+15+15)	
	VDEII	15(A)		
III	VDEII+TFCFD	1(B)	101(B) (=50+50+1)	1.2Sm (Membrane) 1.8Sm (Bending) 2.5 (Buckling)
	VDEIII	1(C)	1(C)	
	Thermal stress	30000(D)	30000(D)	

Numbers of cycles used for crack propagation analyses are obtained by the summation of (A), (B), (C) and (D) events.

4. Evaluation method of plug weld applicability

4.1 Evaluation method

Plug weld has un-welded region in the welding between outer shell and housing/ribs. Although it is too conservative that the un-welded region is considered to be a crack, it is treated as a crack for the application assessment. In order to evaluate the allowable un-welded length, crack propagation has been analyzed for the un-welded lengths of housings and ribs of VV. Fig.4.1-1 shows the evaluation flow of the allowable initial crack length.

(i) Crack modeling
Plug welds of housing and ribs are modeled by a cylinder and a plate with a crack, respectively.
(ii) Load condition
The loads on the plug weld are calculated from operation conditions.
(iii) Calculation of critical crack length
ITER VV shells are made of ductile austenic steel. The fracture mode of the VV is considered to be plastic collapse. The critical crack length (a_n) is determined by plastic collapse load.
(iv) Assumption of initial crack length: a_0
(v) Calculation of crack propagation to obtain final crack length: a_f
The final crack length (a_f) is obtained by crack propagation calculation. The final crack length (a_f) is compared with the critical crack length a_n. When a_f is equal to a_n, failure of the plug weld is assumed to occur.
(vi)Allowable initial crack length
The allowable crack length is calculated by subtracting the crack propagation length caused by one operation cycle from the critical crack length (a_n).

4.2 Crack modeling

For plug weld with un-welded region, conservative assumptions have been performed for the welding of ribs and housings. Plate with double edged infinite crack is applied to the plug weld of ribs, shown in Fig.4.2-1(a). Circumferentially cracked cylinder is applied to the plug weld of housings, shown in Fig.4.2-1(b). Plate with a infinite surface crack is applied for the crack perpendicular to outer shell in the welding region, shown in Fig4.2-1(c) and (d). Tables 4.2-1 and 4.2-2 summarize the crack modeling and dimensions.

4.3 Critical crack length

4.3.1 Crack model of plug weld for rib

The critical crack length (a_n) is calculated by plastic collapse load. The plastic collapse load is defined as the load condition that the stress of the plate with the critical crack reaches the flow stress including safety factors.

For the rib, crack model of plate with double edged infinite crack is applied, shown in Fig.4.3-1. Under combined loading of axial force (F) and moment (M), shown in Fig.4.3-2, from equilibrium of the force and the moment, following formulas are obtained;

Equilibrium of axial force

$$F=2bz_1\sigma_f \quad (1)$$

Equilibrium of moment $$M = b\left(\frac{h^2}{4} - Z_1^2\right)\sigma_f \quad (2)$$

Where, b: rib thickness

h=t-2a t : rib width

a : crack length

$\frac{F}{SFm} = F_0$ F_0, M_0 : applied load

$\frac{M}{SF_b} = M_0$ SF_m, SF_b : safety factor

σ_f : flow stress

σ_f= (Sy+Su) / 2 = (184 + 462) /2 =323 MPa

Sy : yield strength (SS316L(N)-IG, 184 MPa, 100°C)

Su : ultimate strength (SS316L(N)-IG, 462 MPa, 100°C)

SFm : safety factor for membrane stress (=2.7) [4-1]

SFb : safety factor for bending stress (=2.3) [4-1]

4.3.2 Crack model of plug weld for housing

For housings, crack model of circumferentially cracked cylinder is applied, shown in Fig.4.3-3. Axial forces and moments are loaded on housings. Both the membrane and bending stresses are considered as the membrane stress because the consideration is conservative and the bending stresses of housings are not dominant from the results of stress analyses.

Circumferentially cracked cylinder for the housing

$$\sigma_m = \sigma_f \frac{(R_o - a)^2}{R_o^2} \tag{3}$$

where R_0 : diameter of the cylinder

a : circumferentially critical crack length

σ_m : membrane stress

$\frac{\sigma_m}{SF} = \sigma_0$ σ_0: applied load

SF : safety factor for membrane stress(= 3) [4-2]

4.3.3 Crack model for surface crack

For surface crack of welding region, elliptic crack is assumed, shown in Fig.4.3-4. The surface crack is perpendicular to outer shell surface. The crack would be assumed not only in plug weld region but also in butt weld region.

$$\sigma_m = \sigma_f \left(1 - \frac{\pi ac}{4bt}\right) \tag{4}$$

where a, c : crack depth and a half length

t : plate thickness (outer shell)

b : thickness

4.3.4 Calculation procedure of critical crack length

From the stress analyses of the typical inboard area, the critical crack lengths are calculated as follows;

(1) Define the evaluation cross section for calculating the critical crack length

For the ribs, the evaluation cross sections for calculating the critical crack lengths are shown in Fig.4.3-5(a). When plug welding is applied to the cross section, un-welded lengths exist on the both sides of the rib. For the housings, the evaluation cross sections are shown in Fig.4.3-5(b). The stresses in evaluation cross section distribute in toroidal and vertical directions. Therefore two directions of stress distributions are considered to calculate the critical crack length for the housing.

(2) Estimate membrane and bending stresses in the evaluation cross sections

From the results of stress analyses for the typical inboard region, membrane and bending stresses are obtained by linearization in the evaluation cross section. The mean stress corresponds to the membrane stress, and the linearized maximum stress corresponds to the membrane plus bending stress.

(3) Calculate critical crack length

Using formulas (1), (2), (3) and (4), critical crack length can be calculated for ribs and housings, respectively. For ribs, axial force F and moment M in the evaluation cross section are obtained by the membrane and bending stresses from the stress analyses. For housings, using formula (3) circumferentially critical crack length can be calculated assuming membrane plus bending stresses are membrane stresses. For surface crack, critical crack lengths are calculated for three cases of stress to apply; safety factor multiplied membrane stress, safety factor multiplied combined stress (membrane plus bending stress) and membrane stress plus safety-factor multiplied bending stress.

If the critical crack length exceeds 75 percents of rib/housing thickness, the 75 percents of rib/housing thickness is assumed to be the critical crack length [4-2].

4.3.5 Crack propagation analysis

Crack propagation is calculated by stress intensity and crack growth rate.

For ribs, stress intensity is calculated by the following formulas where membrane stress (σm) is considered as membrane plus bending stresses.

(i) Stress intensity factor for a plate with cracks on both side [4-3]

$$K_I = \sigma_m \sqrt{\pi a} \cdot F_m, \qquad \left(0 < \frac{a}{t} < 0.5\right) \tag{4}$$

where $\sigma_m = \dfrac{P}{2bt}$

$$F_m = \left[1 + 0.122\cos^4\left(\frac{\pi a}{t}\right)\right]\sqrt{\frac{t}{\pi a}\tan\left(\frac{\pi a}{t}\right)}$$

For housings, the following formulas are applied.

(ii) Stress intensity factor for a cylinder with circumferential crack [4-3]

$$K_I = \left(F_m\sigma_m + F_b\sigma_b\right)\sqrt{\pi a}, \qquad \left(0 < \frac{a}{R_o} < 1\right) \tag{5}$$

where $\sigma_m = \dfrac{P}{\pi R_o^2}$, $\sigma_b = \dfrac{4M}{\pi R_o^3}$

$$\varsigma = 1 - \frac{a}{R_o}$$

$$F_m = 0.5\sqrt{\varsigma}\left(1 + 0.5\varsigma + 0.375\varsigma^2 - 0.363\varsigma^3 + 0.731\varsigma^4\right)$$

$$F_b = 0.375\sqrt{\varsigma}\left(1 + 0.5\varsigma + 0.375\varsigma^2 + 0.313\varsigma^3 + 0.274\varsigma^4 + 0.537\varsigma^5\right)$$

(iii) Stress intensity factor for a plate with elliptic crack [4-4]

$$K_I = (\sigma_m + H_S\sigma_b)\sqrt{\pi\frac{a}{Q}}\cdot F_S, \qquad \left(0 < \frac{a}{t} < 0.8,\ 0 < \frac{a}{c} < 2,\ 0 < \frac{c}{b} < 0.5\right) \tag{6}$$

where $\sigma_m = \dfrac{P}{2bt}$, $\sigma_b = \dfrac{3M}{bt^2}$

$$F_S = \left[M_1 + M_2\left(\frac{a}{t}\right)^2 + M_3\left(\frac{a}{t}\right)^4\right]\cdot g \cdot f_\phi \cdot f_W$$

$$f_W = \left[\sec\left(\frac{\pi c}{2b}\cdot\sqrt{\frac{a}{t}}\right)\right]^{1/2}$$

$$H_S = H_1 + (H_2 - H_1)\cdot\sin^p\phi$$

where ϕ is the parameter of elliptic crack angle. $\phi = 0°$ means surface of crack and $\phi = 90°$ means the deepest point of crack depth.

For $a/c \le 1$

$$Q = 1 + 1.464\cdot\left(\frac{a}{c}\right)^{1.65}$$

$$M_1 = 1.13 - 0.09\cdot\frac{a}{c}$$

$$M_2 = -0.54 + \frac{0.89}{0.2 + \dfrac{a}{c}}$$

$$M_3 = 0.5 - \frac{1}{0.65 + \dfrac{a}{c}} + 14\cdot\left(1 - \frac{a}{c}\right)^{24}$$

$$g = 1 + \left[0.1 + 0.35\cdot\left(\frac{a}{c}\right)^2\right]\cdot(1 - \sin\phi)^2$$

$$f_\phi = \left[\left(\frac{a}{c}\right)^2\cdot\cos^2\phi + \sin^2\phi\right]^{1/4}$$

$$p = 0.2 + \frac{a}{c} + 0.6\cdot\frac{a}{t}$$

$$H_1 = 1 - 0.34 \cdot \frac{a}{t} - 0.11 \cdot \frac{a}{c} \cdot \frac{a}{t}$$

$$H_2 = 1 + G_{21} \cdot \frac{a}{t} + G_{22} \cdot \left(\frac{a}{t}\right)^2$$

$$G_{21} = -1.22 - 0.12 \cdot \frac{a}{c}$$

$$G_{22} = 0.55 - 1.05 \cdot \left(\frac{a}{c}\right)^{0.75} + 0.47 \cdot \left(\frac{a}{c}\right)^{1.5}$$

For $a/c > 1$

$$Q = 1 + 1.464 \cdot \left(\frac{a}{c}\right)^{1.65}$$

$$M_1 = \sqrt{\frac{c}{a}} \cdot \left(1 + 0.04 \cdot \frac{c}{a}\right)$$

$$M_2 = 0.2 \cdot \left(\frac{c}{a}\right)^4$$

$$M_3 = -0.11 \cdot \left(\frac{c}{a}\right)^4$$

$$g = 1 + \left[0.1 + 0.35 \cdot \frac{c}{a} \cdot \left(\frac{a}{t}\right)^2\right] \cdot (1 - \sin\phi)^2$$

$$f_\phi = \left[\left(\frac{c}{a}\right)^2 \cdot \sin^2\phi + \cos^2\phi\right]^{1/4}$$

$$p = 0.2 + \frac{c}{a} + 0.6 \cdot \frac{a}{t}$$

$$H_1 = 1 + G_{11} \cdot \frac{a}{t} + G_{12} \cdot \left(\frac{a}{t}\right)^2$$

$$H_2 = 1 + G_{21} \cdot \frac{a}{t} + G_{22} \cdot \left(\frac{a}{t}\right)^2$$

$$G_{11} = -0.04 - 0.41 \cdot \frac{c}{a}$$

$$G_{12} = 0.55 - 1.93 \cdot \left(\frac{c}{a}\right)^{0.75} + 1.38 \cdot \left(\frac{c}{a}\right)^{1.5}$$

$$G_{21} = -2.11 - 0.77 \cdot \frac{c}{a}$$

$$G_{22} = 0.55 - 0.72 \cdot \left(\frac{c}{a}\right)^{0.75} + 0.14 \cdot \left(\frac{c}{a}\right)^{1.5}$$

(iv) Crack growth rate [4-2]

$$\frac{da}{dN}[\text{m/cycle}] = \frac{C \cdot t_r^{0.5} (\Delta K)^m}{(1-R)^{2.12}} \tag{7}$$

where $C = 8.17 \times 10^{-12}$

$m = 3.0$

$t_r = 1000$

$$R = \frac{K_{\min}}{K_{\max}}$$

$\Delta K = K_{\max} - K_{\min}$ (R≥0)

$\Delta K = K_{\max}$ (R<0)

The initial crack is assumed to be 0.1mm for the crack propagation analysis.

4.3.6 Determine the allowable crack length

According to crack propagation analyses, the multiple number of total design loading operation cycles are calculated. The allowable crack length is the crack length corresponding to total design loading operation cycles minus one operation cycle. The inspection error is assumed to be 4.4mm for UT application [4-5].

References

[4-1] ASME Sec. XI Division 1 Appendix C C-2621.

[4-2] Rules on Fitness-for-Service for Nuclear Power Plants (JSMES NA1-2002)

[4-3] Tada, H. Paris, P.C. and Irwin, G.R., "The stress Analysis of Cracks Handbook", Del Research Corporation (1973)

[4-4] Newman, J. C. Jr and Raju, I. S., "Stress Intensity Factor Equations for Cracks in Three-Dimensional Finite Bodies Subjected to Tension and Bending Loads", NASA Technical Memorandum 85793, NASA (1984).

[4-5] Application of UT for inspection of pipes etc. in primary loop recirculation system, Nuclear and Industrial Safety Agency in JA, July, 2004.

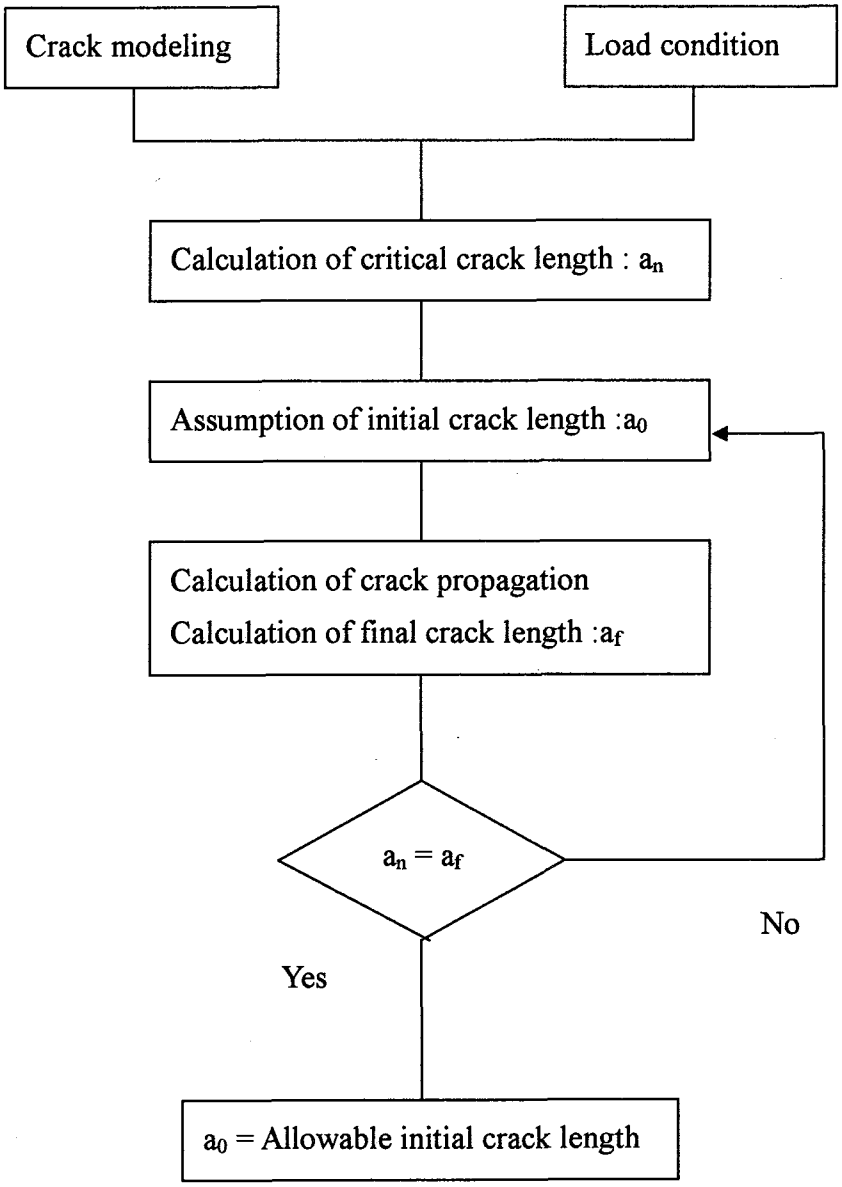

Fig. 4.1-1 Evaluation flow of allowable initial crack length

Table4.2-1 Crack modeling

	Rib	Housing
Crack in un-welded region	Plate with double edged infinite crack	Circumferentially cracked cylinder
Crack perpendicular to outer shell surface	Plate with a finite surface crack	Plate with a finite surface crack

Table 4.2-2 Dimensions

	Rib	Housing
Crack in un-welded region [mm]	$t = 60$	$R_o = 105$
Crack perpendicular to outer shell surface [mm]	$t = 60$ $2b = 1000$	$t = 60$ $2b = 660\ (= 2\pi R)$

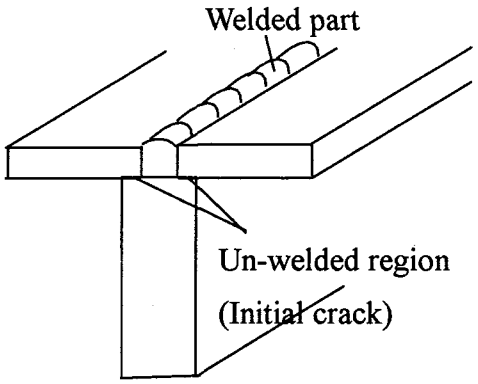

(a) Rib (Un-welded region)

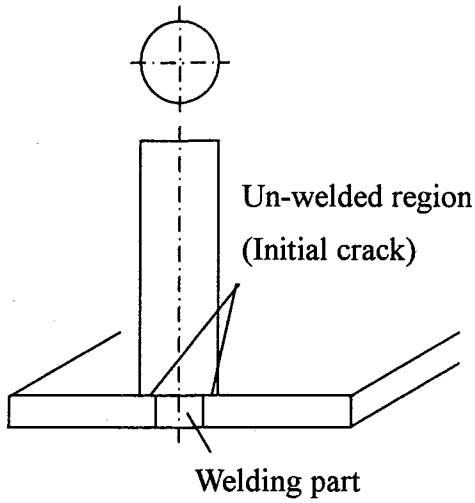

(b) Housing (Un-welded region)

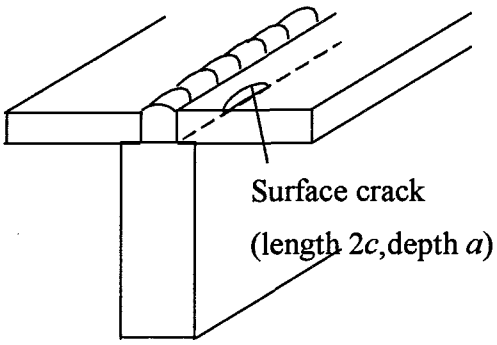

(c) Rib (Welding region)

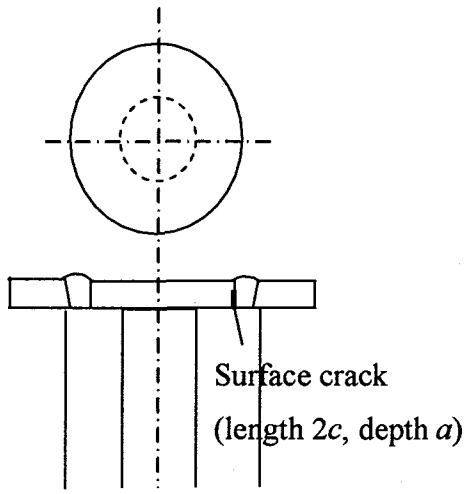

(d) Housing (Welding Region)

Fig.4.2-1 Crack Models of Ribs and Housings

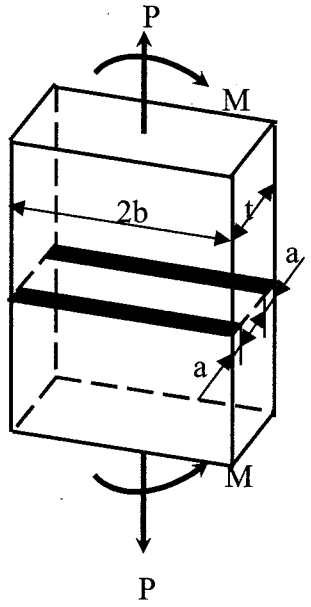

Fig.4.3-1 Crack model of plate with double edged infinite crack for rib

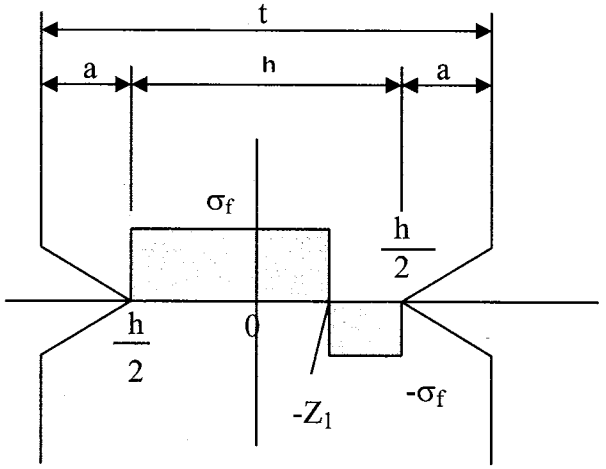

Fig 4.3-2 Model of collapse load for rib with cracks on both sides

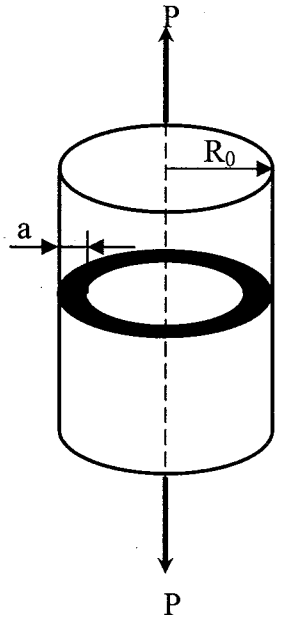

Fig.4.3-3 Crack model of circumferentially cracked cylinder for housing

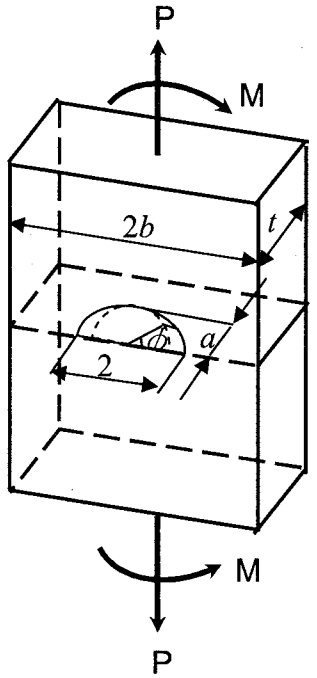

Fig.4.3-4 Crack model of plate with a finite surface crack for welding region

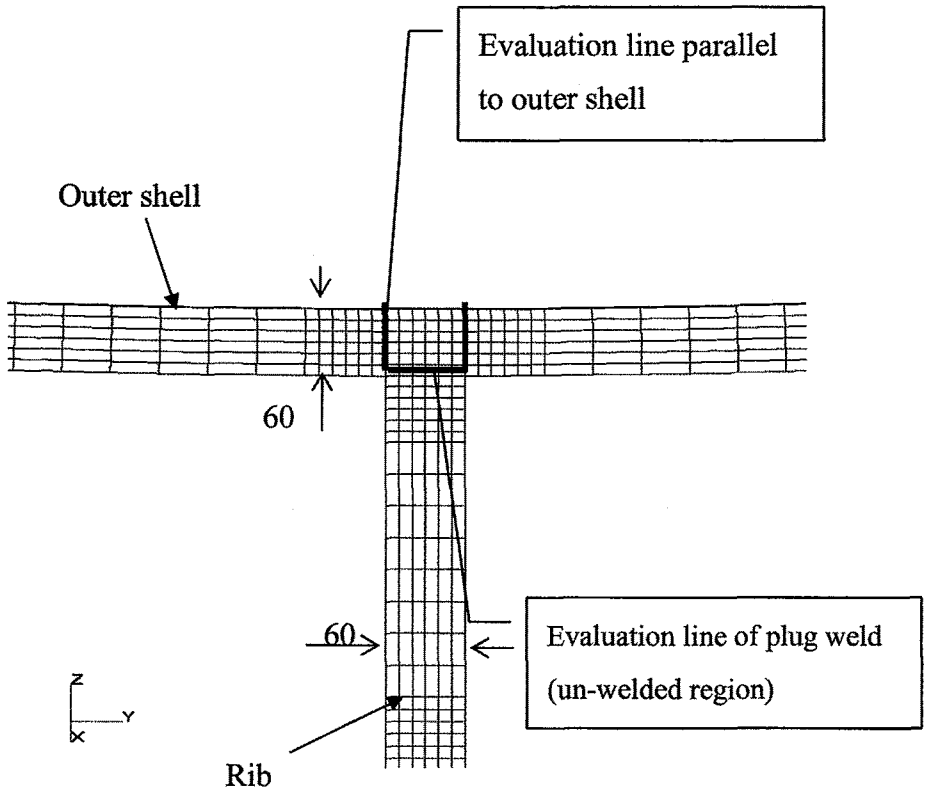

(a)Rib

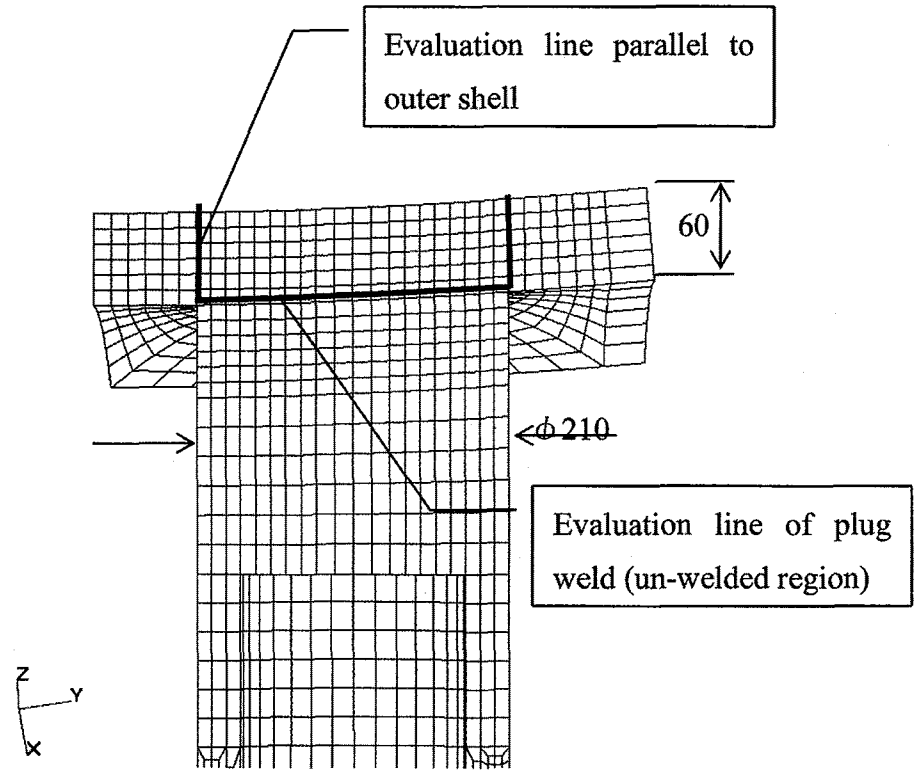

(b) Housing

Fig.4.3-5 Evaluation line for crack analysis

5. Electro-magnetic and stress analyses of the whole VV structure

In order to evaluate the stresses of the weld regions between ribs/housings and the VV outer shell, the electro-magnetic (EM) and stress analyses of the whole VV structure have been performed for load conditions shown in Sec.3.

5.1 Electro-magnetic analyses of the whole VV structure

5.1.1 Analysis model

A toroidal 20-degree three dimensional model with three port openings has been established in the EM analysis, shown in Fig. 5.1-1. Shell-element has been used for all components of VV shells and ribs.
No.1 blanket and No.18 blanket on the triangular support are modeled as the contact points between plasma and blankets for the calculation of halo current.

5.1.2 Analysis conditions

(1) Material properties

Electrical resistivity of 0.797 μΩm for the VV shells at 100 °C was applied taking the component temperatures at the start of burn into account.

(2) Load conditions

Five load conditions due to plasma disruptions have been considered for the analyses of the VV structure. The EM loads due to eddy current are as follows;
i) Major disruption II with 40ms linear current decay
ii) Vertical displacement event III (VDE) with fast downward plasma movement with 40ms linear current decay
iii) Vertical displacement event III (VDE) with fast upward plasma movement with 40ms linear current decay
The plasma disruption scenarios are shown in Figs. 5.1-2~4. The eddy currents of the VV structures are calculated at the end of the disruptions.
The EM loads due to halo current are as follows;
iv)Vertical displacement event III (VDE) with slow downward plasma movement
v) Vertical displacement event III (VDE) with slow upward plasma movement
vi) TF coil fast discharge with time constant of 11sec [5-1]
The halo currents are assumed to be 0.58*Ip for the slow downward plasma movement and 0.35* Ip for slow upward plasma movement [5-2].

$$I_{halo} * Pf/I_{plasma} = 0.58$$

where Pf is toroidal peaking factor of the halo current.

(3) Boundary conditions

The condition of toroidal edges of the VV model is rotational symmetry in toroidal direction. For halo current of downward VDEIII, the contact points between plasma and blanket modules are No.1 and No.18 modules. For those of upward VDEIII are No.7 and No.11 modules.

5.1.3 Analysis Results

Calculated eddy and halo current distributions are shown in Fig.5.1-2 ~ 5.1-7. Table 5.1-1 shows the EM analysis conditions and VV currents. Halo currents are obtained from the ratio of VV upper and lower current-pass resistances. The VV currents for VDEIII (Slow, Downward) are 3.2MA and 5.5MA in upper and lower parts of VV, respectively. Those for VDEIII (Slow, Upward) are 5.5MA and 1.5MA in upper and lower parts of VV, respectively. The eddy current distribution of TFCFD has been calculated at 1.2sec after TFCFD start. The maximum EM forces of TFCFD are produced at the time [5-3]. Figs.5.1-8 ~ 5.1-13 show EM forces for the load conditions. The EM loads of downward VDE III and TFCFD are understandable compared with ITER DDD [5-4].

References

[5-1] ITER DRG2 G A0 GDRD 3 01-07-19 R1.0, Chapter2 Page3.

[5-2] ITER DDD Load Specification, July 2004, P21.

[5-3] I.Senda, The analysis of TF fast discharge with detail modeling of TF coils, June 2001,JAHT.

[5-4] ITER DDD 15 Vacuum Vessel, September 2004, P113, P119.

Table 5.1-1 EM analysis condition and VV currents

Analysis case	Condition	VV current
(1) MD II	Linear 40ms decay	
(2)VDE III (Fast Downward)	Linear 40ms decay	
(3)VDE III (Fast Upward)	Linear 40ms decay	
(4) Halo current VDEIII (Slow, Downward)	I halo ×Pf/I plasma =0.58	I upper=3.2MA I lower=5.5MA
(5) Halo current VDEIII (Slow, Upward)	I halo ×Pf/I plasma =0.46 I upward/I downward=0.8	I upper=5.5MA I lower=1.5MA
(6) TFCFD	TFC current = 58kA EM load is calculated at the time of 1.2 sec after TFCFD	I vv= 2.88MA

Pf is toroidal peaking factor of the halo current

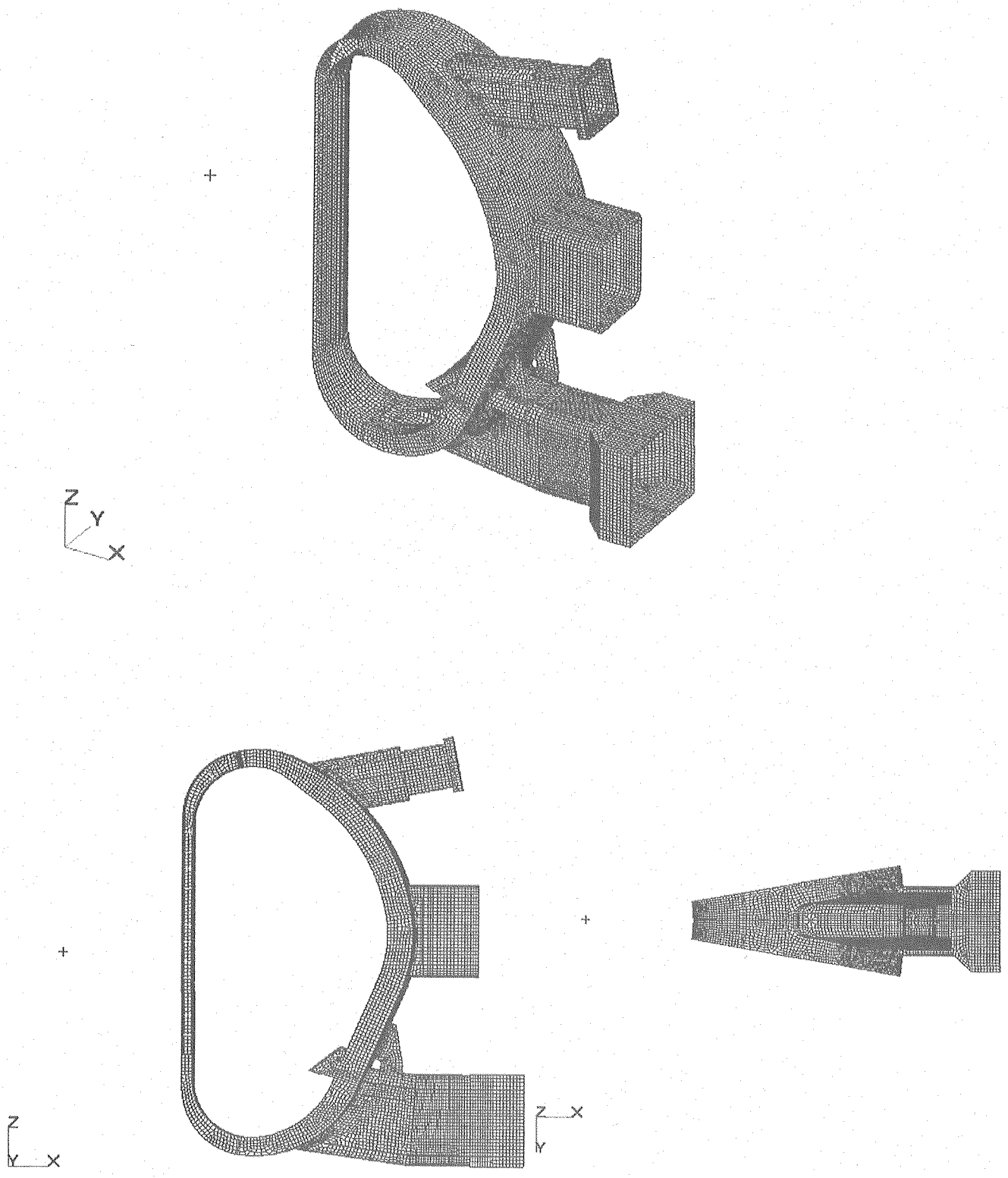

Fig.5.1-1 EM Analysis Model

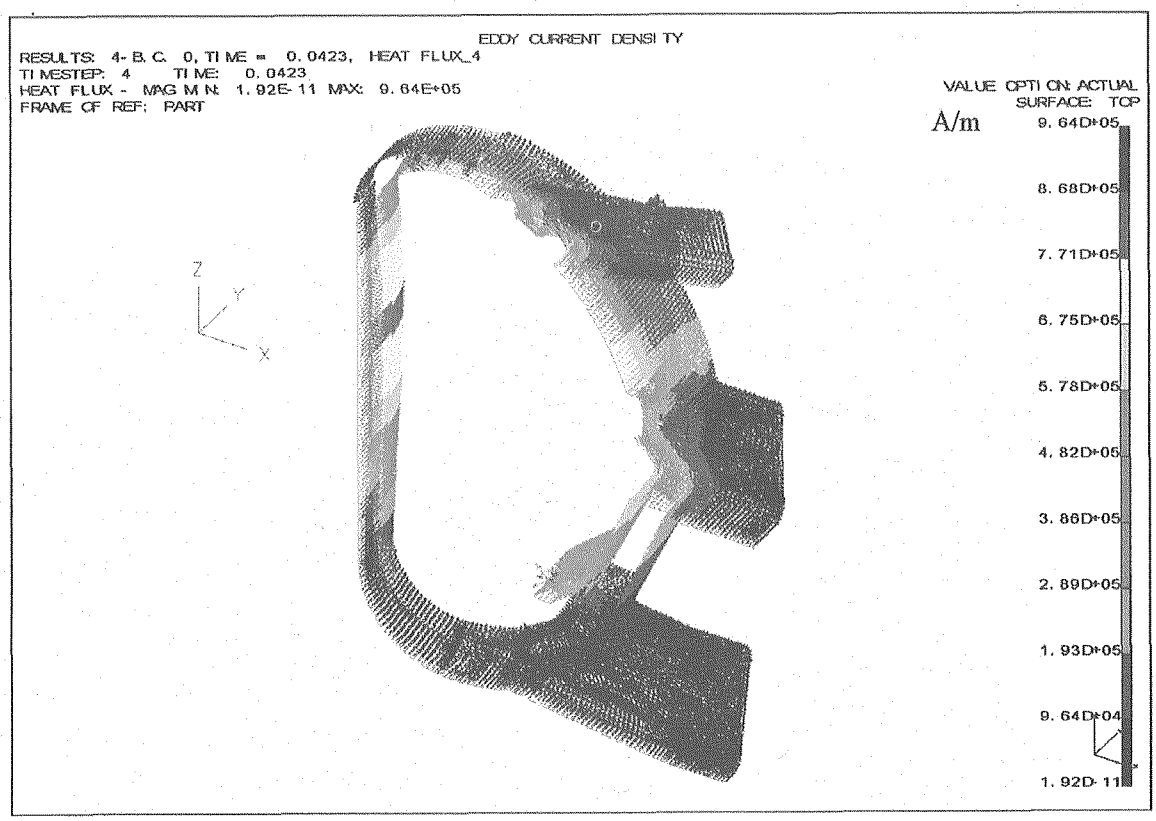

Fig. 5.1-2 Eddy current in VV at major disruption, t=42.3msec

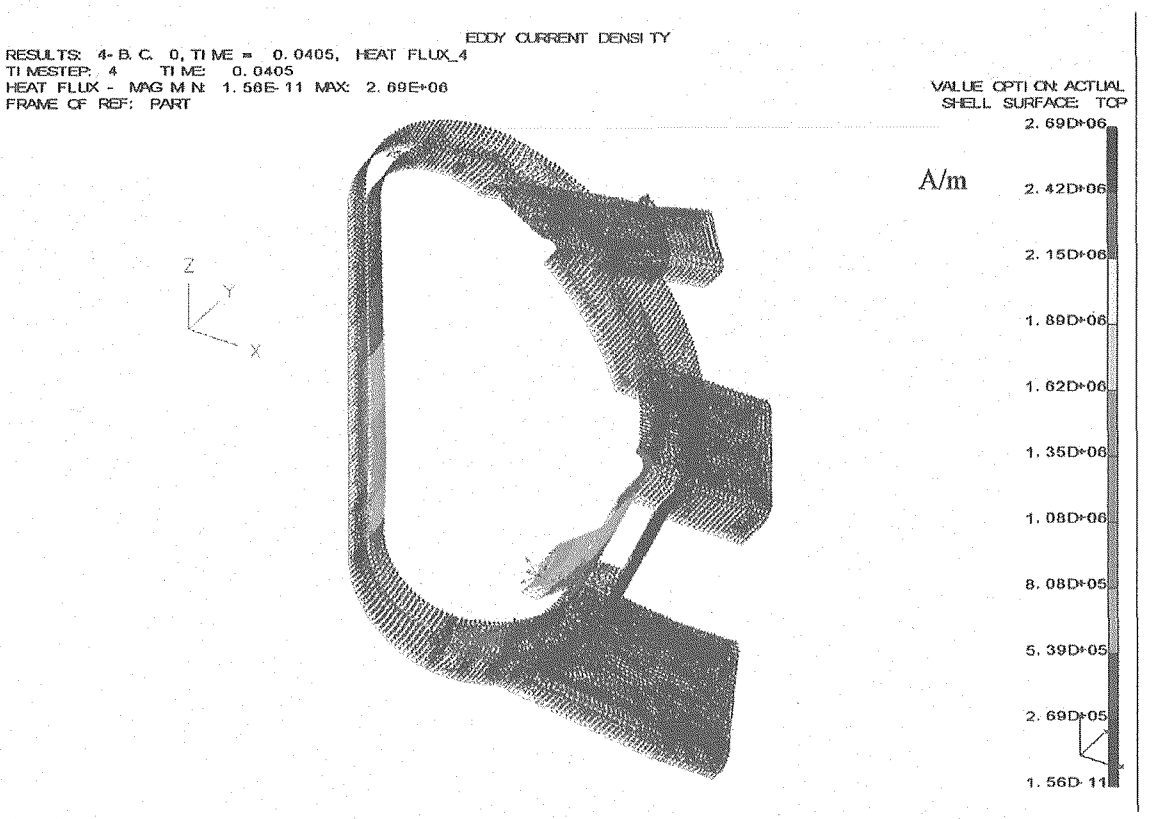

Fig. 5.1-3 Eddy current in VV at VDEIII (F,D) t=40.5msec

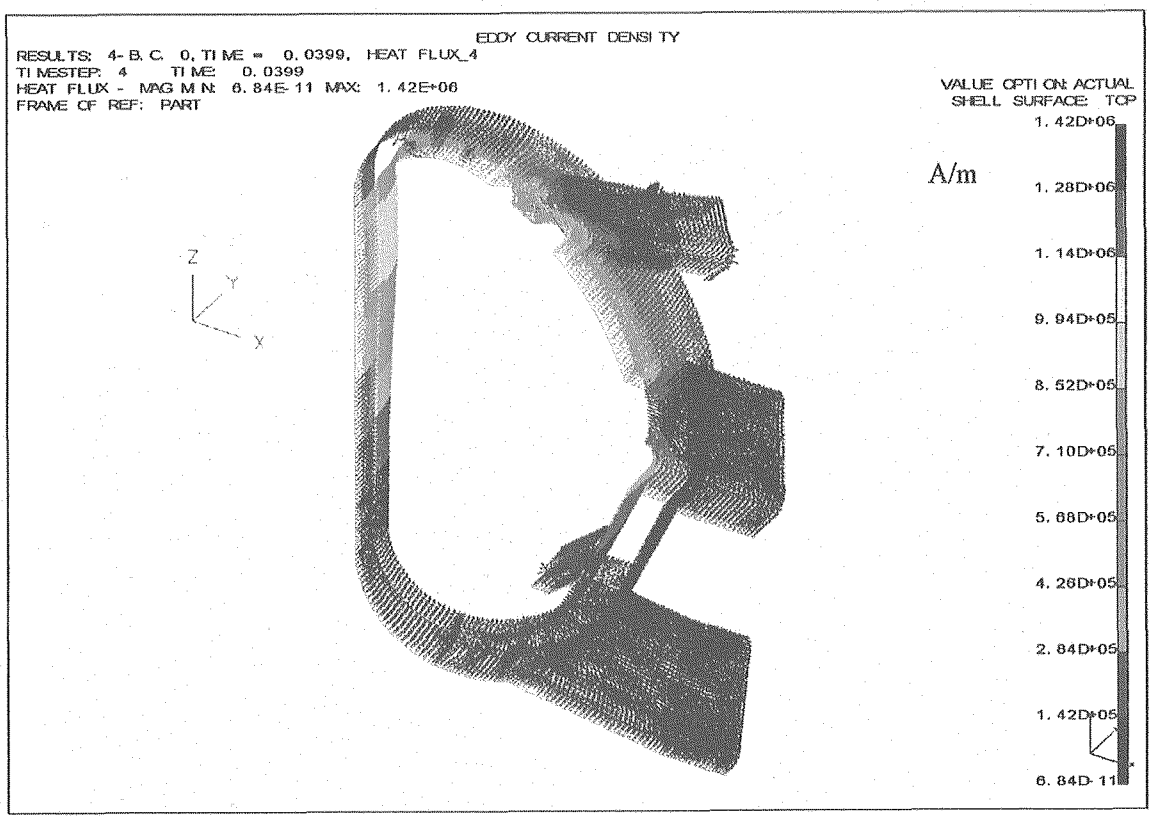

Fig. 5.1-4 Eddy current in VV at VDEIII (F,U) t=39.9msec

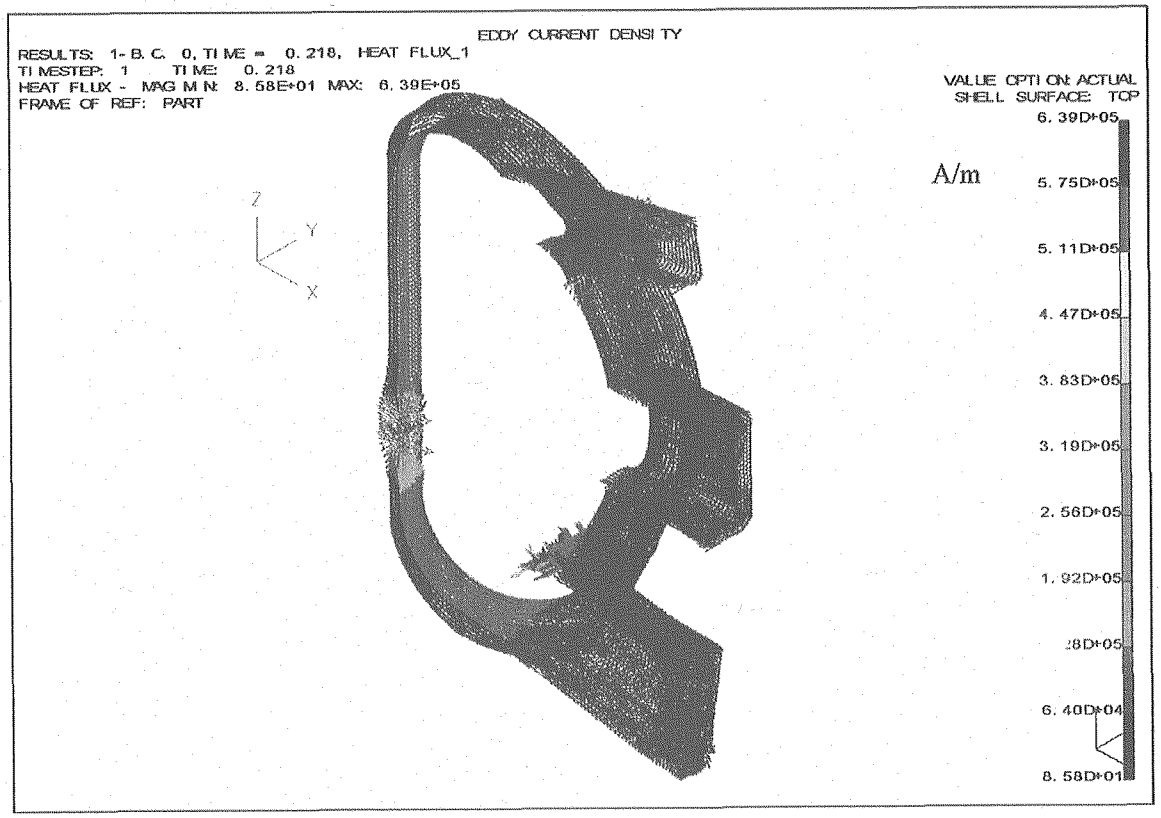

Fig. 5.1-5 Halo current in VV at VDE III (S,D)

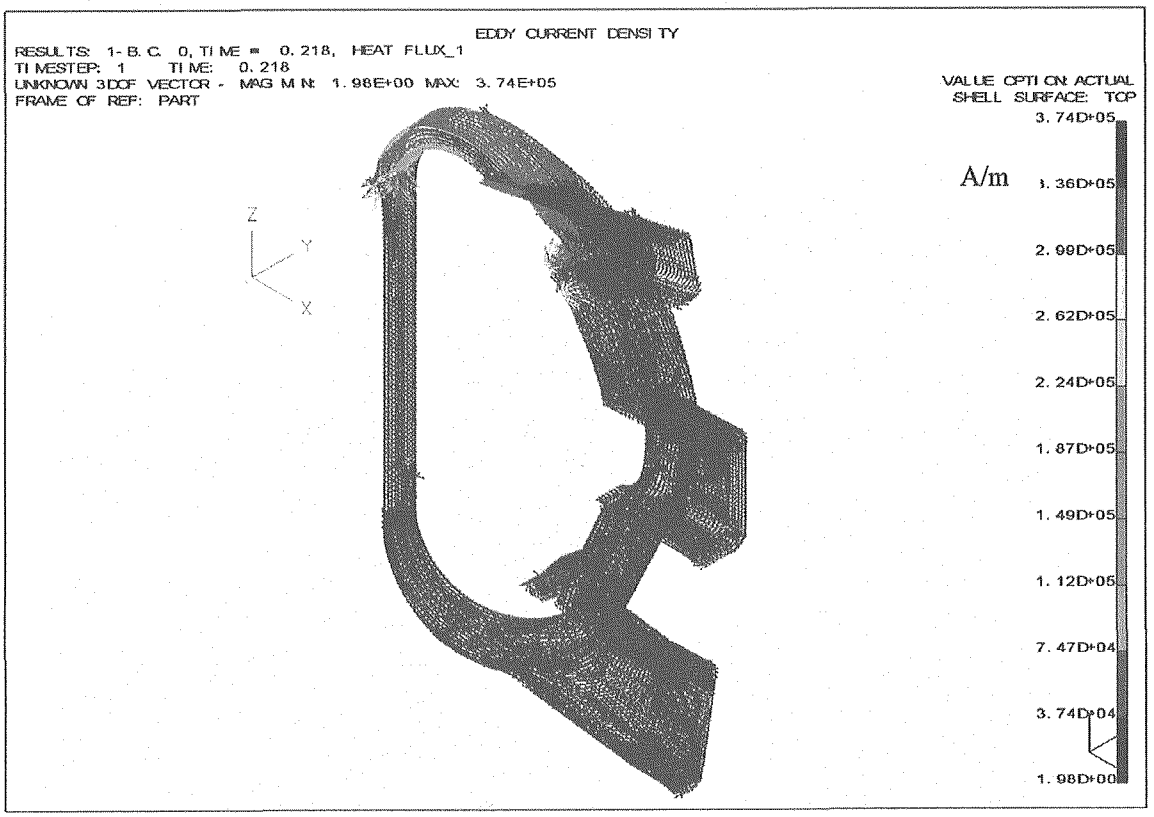

Fig. 5.1-6 Halo current in VV at VDEIII(S,U)

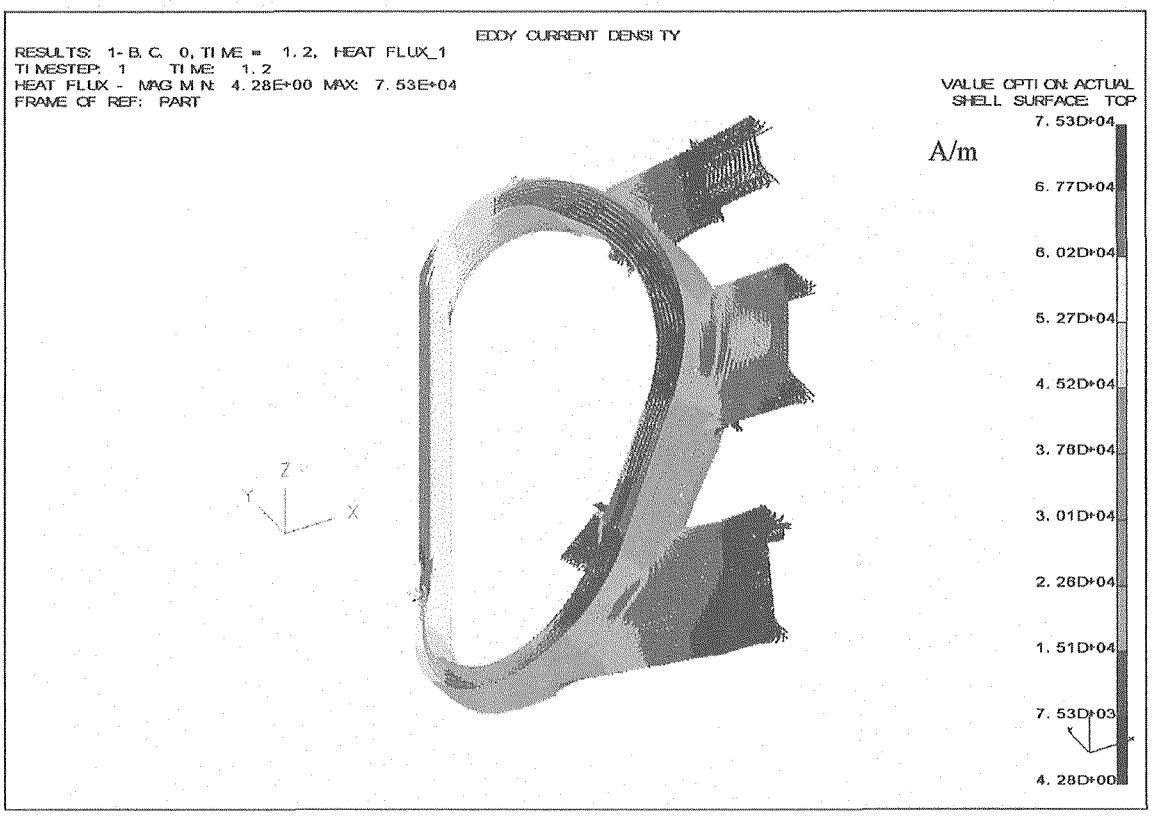

Fig. 5.1-7 Eddy current in VV at TFCFD, t=1.2sec

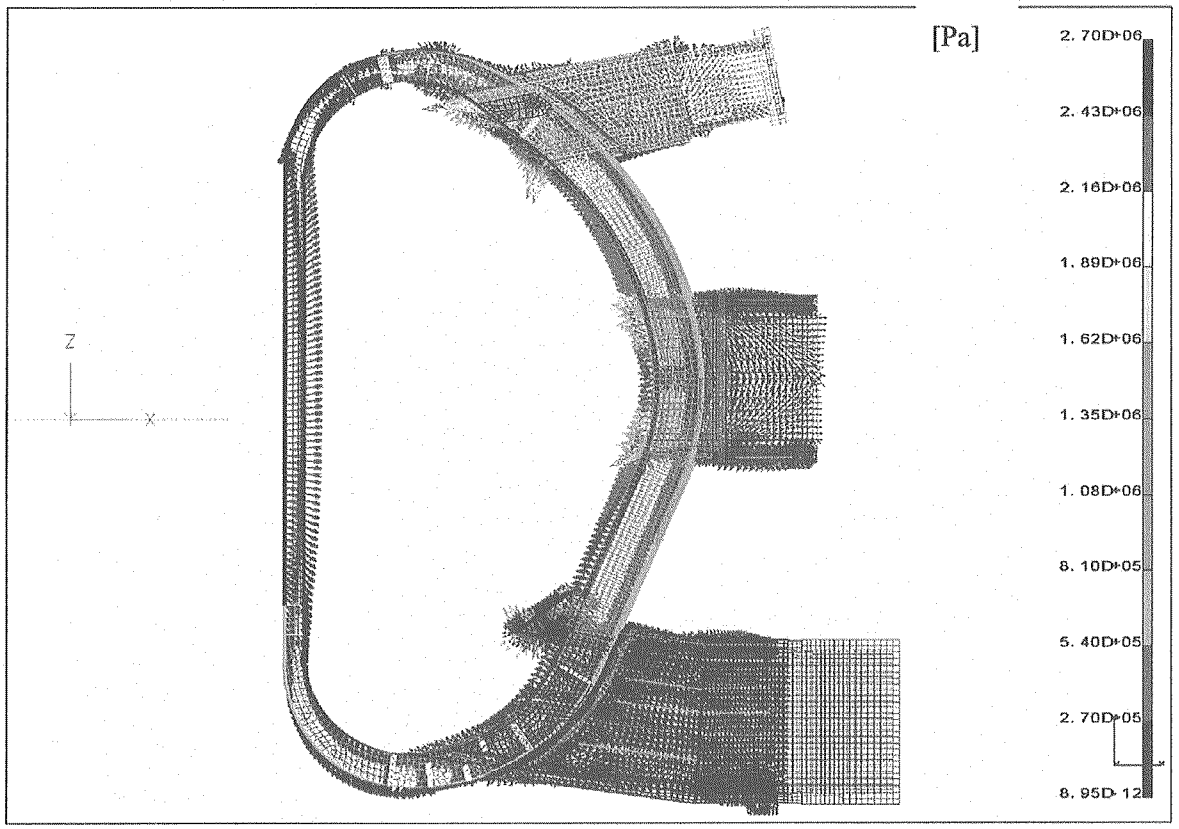

Fig.5.1-8 EM force distribution at MD

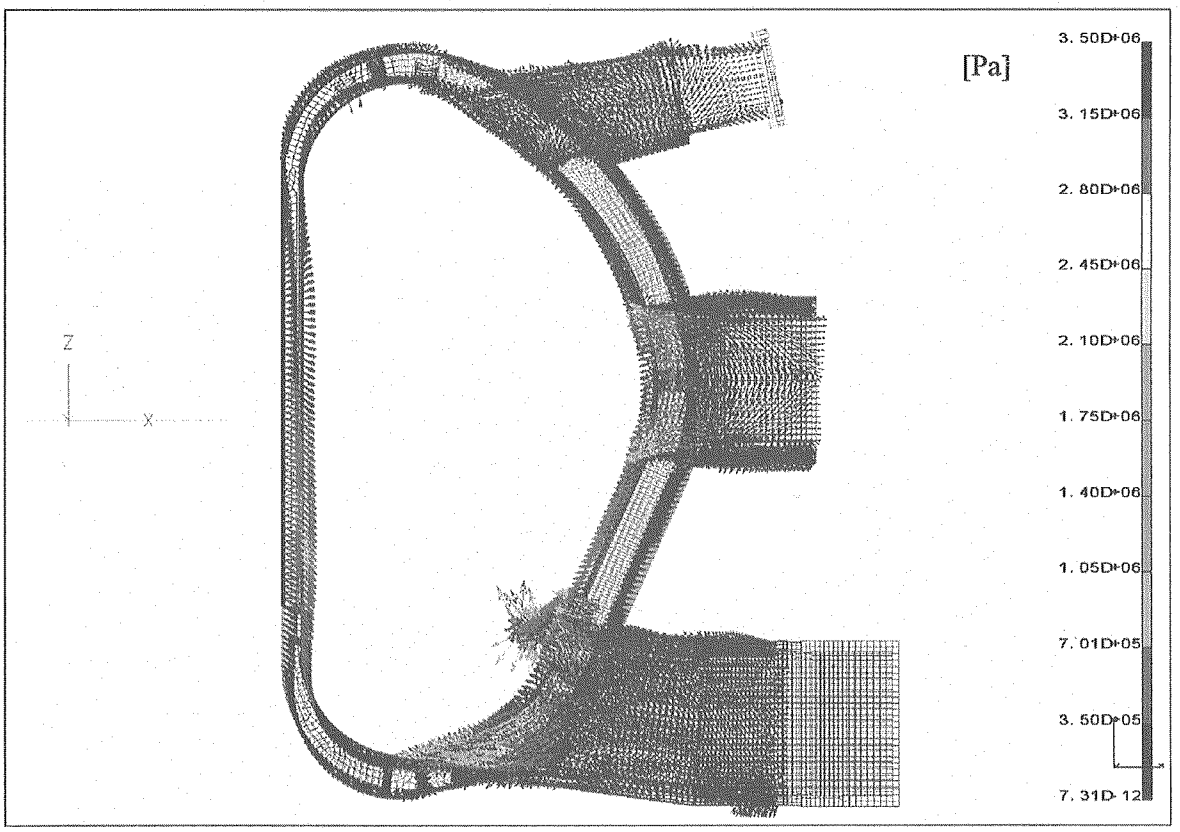

Fig.5.1-9 EM force distribution at VDE III(F,D)

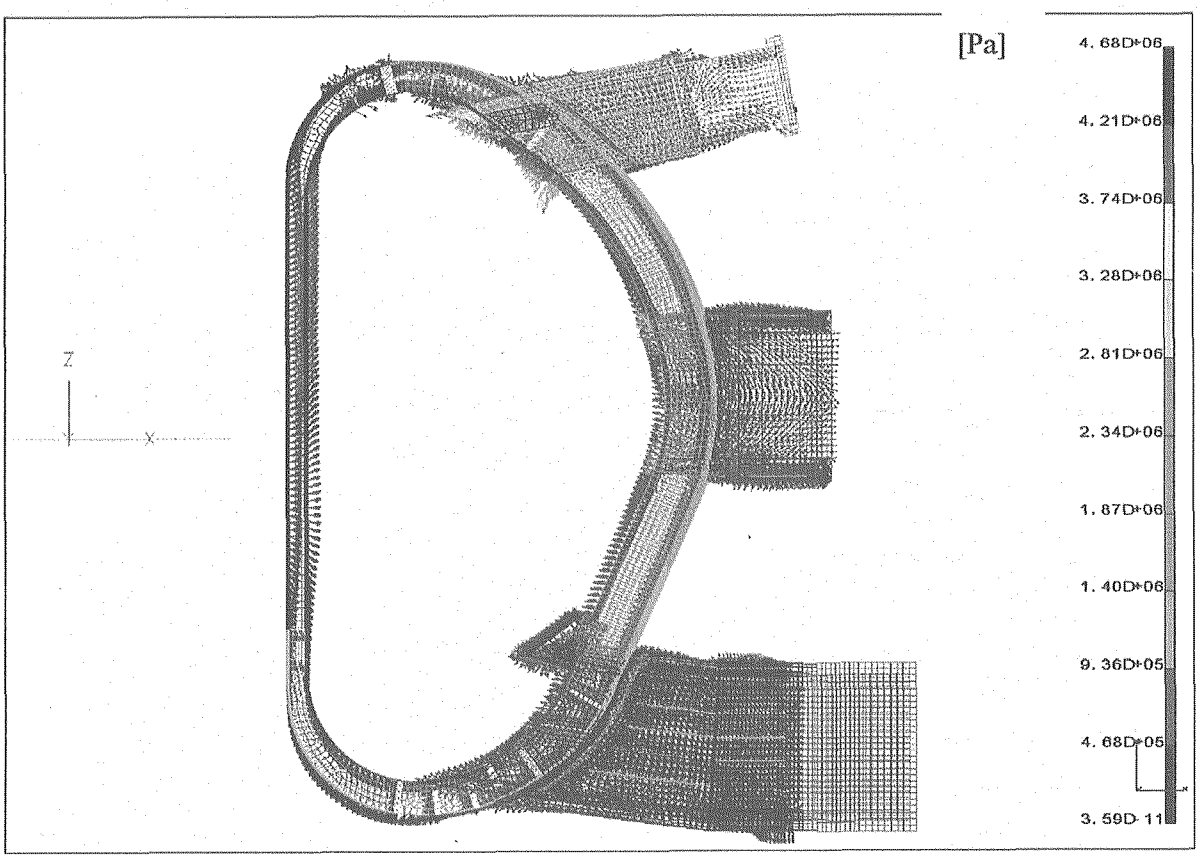

Fig.5.1-10 EM force distribution at VDE III(F,U)

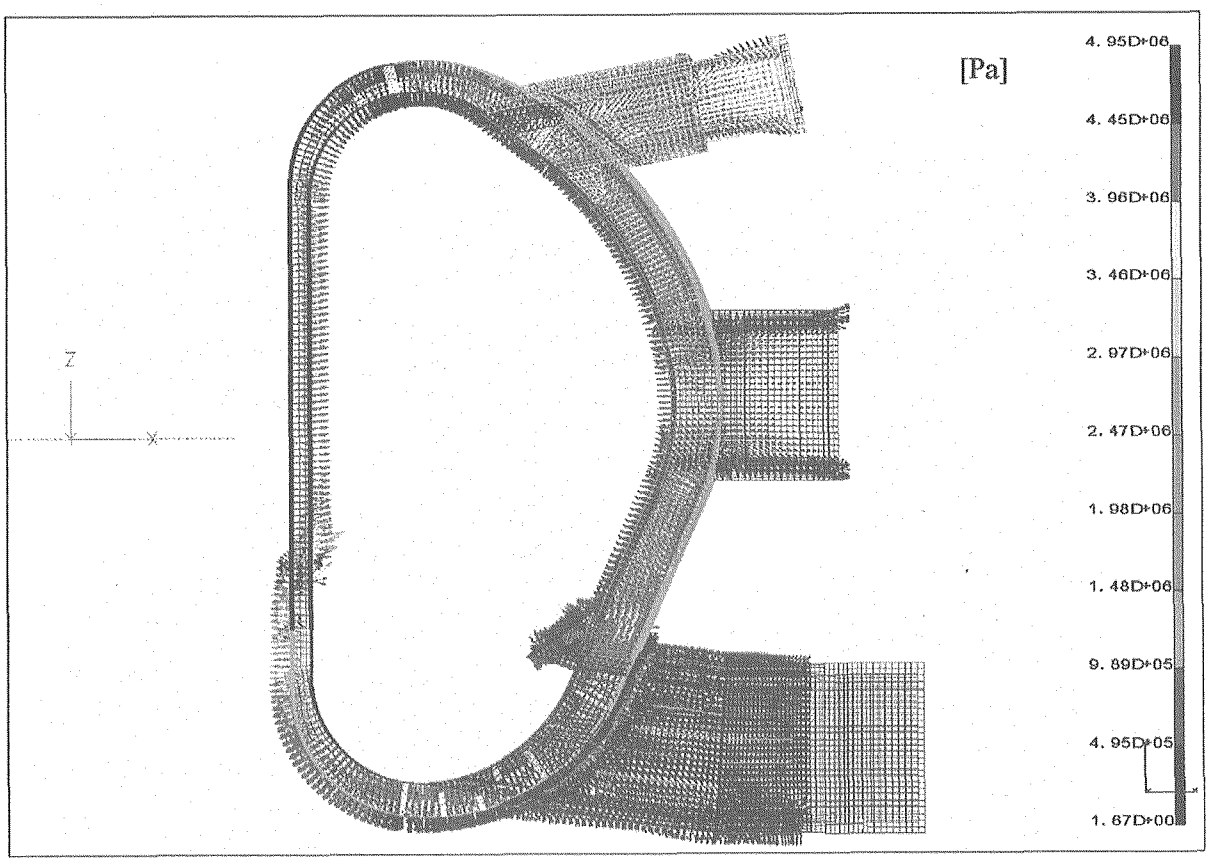

Fig.5.1-11 EM force distribution at VDE III(S,D)

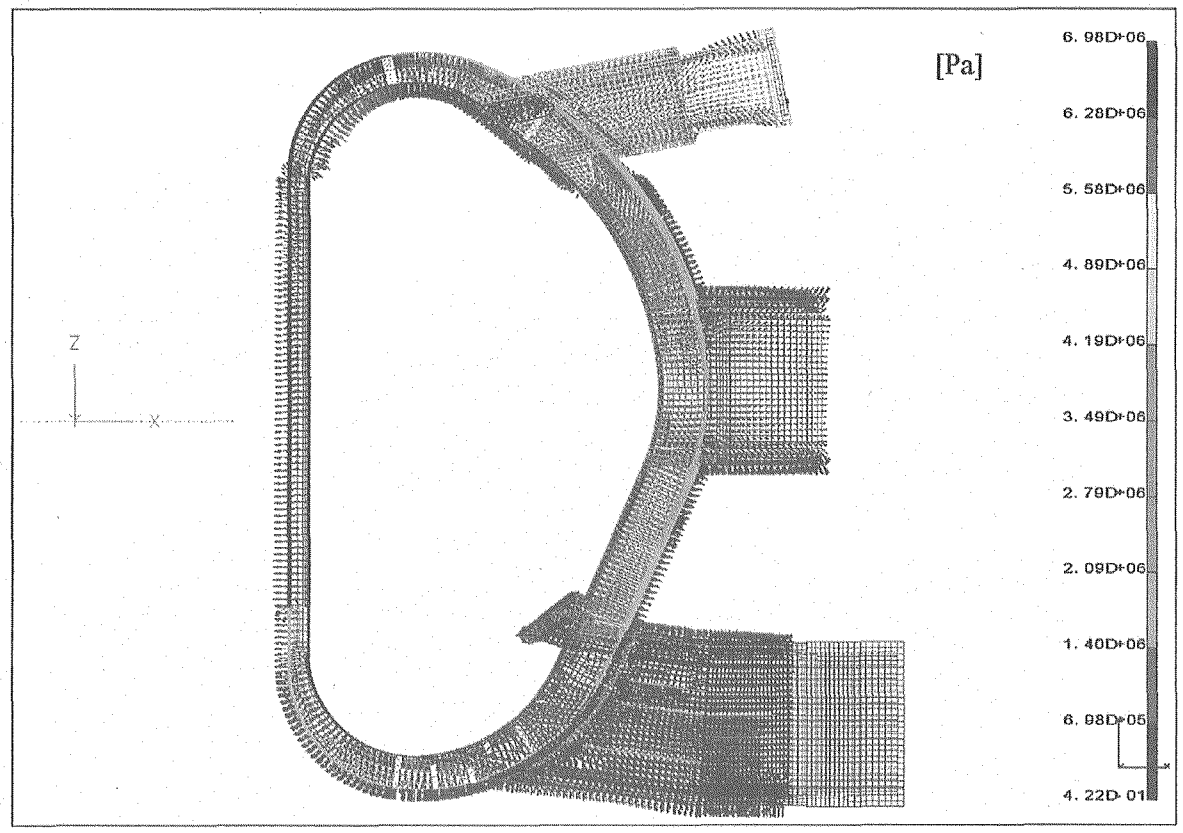

Fig.5.1-12 EM force distribution at VDE III(S,U)

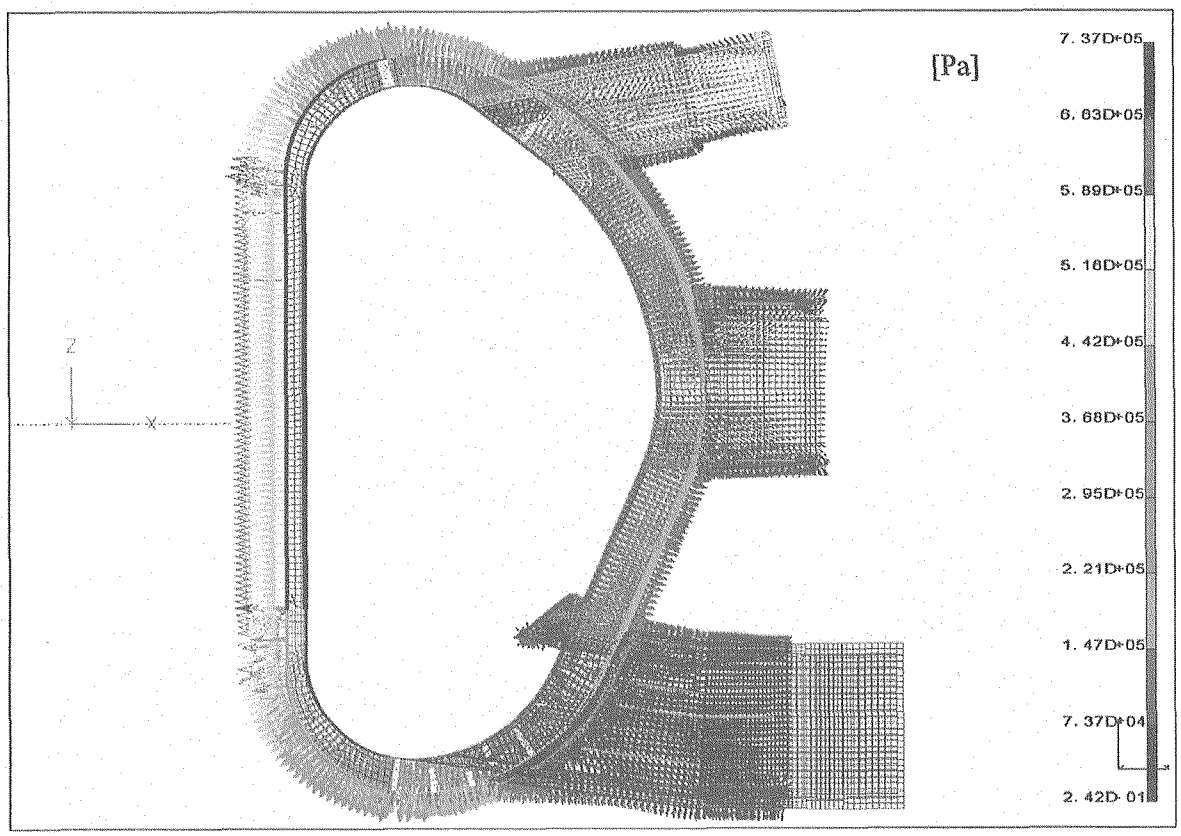

Fig.5.1-13 EM force distribution at TFCFD

5.2 Global stress analysis of the whole VV structure

Stress Analyses of the whole VV structure have been performed in order to find high stress regions of welding between ribs and housings. Load conditions for the stress analyses are coolant pressure and EM loads resulted from EM analyses.

5.2.1 Analysis model

The analysis model of the stress analyses is the same as that of EM analysis, shown in Fig.5.1-1. The VV shells and ribs are modeled using shell elements. The beam elements of housing model are added to the analysis model.

5.2.2 Analysis conditions

(1) Material Properties

Young's modulus and Poisson ratio of the VV shell material are 198GPa and 0.29, respectively. The dimensions of beam elements for housing are inner and outer diameters of 152mm and 210mm, respectively.

(2) Load conditions

Load conditions for the stress analyses are coolant pressure load, EM load due to TF coil fast discharge (TFCFD) and EM loads due to plasma disruptions. The stress analysis for each load condition has been performed separately. The stresses for load combination are obtained by summation of the analysis results for each load condition. The factors of stresses for load combinations are shown in Table5.2-1. EM forces of blanket module on housing of ± 500kN are not included in the stress analyses.

Load conditions;

i) Coolant pressure of 1.3 MPa between VV inner and outer shells
ii) Major disruption II with 40ms linear current decay
iii) Vertical displacement event III (VDE) with fast downward plasma movement with linear current decay of 40ms
iv) Vertical displacement event III (VDE) with fast upward plasma movement with linear current decay of 40ms
v) Vertical displacement event III (VDE) with slow downward plasma movement
vi) Vertical displacement event III (VDE) with slow upward plasma movement
vii) TF coil fast discharge (TFCFD) with time constant of 11sec

(3) Boundary conditions

The condition of toroidal edges of the VV model is cyclic symmetry in toroidal direction. For the support of the VV structure, attached area of the support on the lower port bottom is fixed in all directions, shown in Fig.5.2-1

5.2.3 Analysis results

For each load condition, maximum membrane and bending stresses are shown in Tables 5.2-2 and 5.2-3 where σy means the stress along VV outer shell surface. The positive membrane stress is tensile stress of the weld lines of ribs and housings. Stresses of the bold letters mean that the stresses are high for each disruption. The stresses due to downward disruption are higher than those due to upward disruption for toroidal rib. Table 5.2-4 summarized the maximum membrane and membrane plus bending stresses for each disruption. The locations are shown in Figs 5.2-2 and 5.2-3 for ribs and housings, respectively.

For toroidal ribs, the maximum membrane stress is produced at the side rib of the lower port, shown in Fig5.2-2(1/3). The rib is not welded to inner shell. The maximum membrane plus bending stress is produced at the side rib of the lower port and the rib of VV upper part. The stress distributions are shown in Fig.5.2-4 for load combinations. High stress elements such as element No.38296 and No.34574 are located at the edge of the toroidal rib and the stress concentrates at the edge.

For poloidal ribs, maximum stresses are produced in the VV upper part and the side of the lower port, shown in Fig.5.2-2(3/3) and Fig.5.2-4. The stress concentrates at the edge of the ribs.

For housings, maximum stresses are produced in those of blanket No. 7in the VV upper part, shown in Fig.5.2-3.

In order to assess crack propagation, detail stress distributions of the weld region are required. The detail stress analyses have been carried out for the VV inboard region and the upper region, described in Sec.6 and Sec.7, respectively. The inboard region is selected for a typical VV region with ribs/housings successively located, and the upper region is for that of the maximum housing stress.

Table 5.2-1 Factors of stresses for load combinations

	Coolant pressure (CP)	MD (Eddy current)	TFCFD	VDE III(Fast upward) (Eddy current)	VDE III (Fast downward) (Eddy current)	VDE III(Slow upward) (Halo current)	VDE III(Slow downward) (Halo current)
VDE II(Fast, upward)+CP	1.0			0.75		0.45	
VDE II(Fast downward d)+CP	1.0				0.75		0.45
VDE II(Slow upward)+CP	1.0					0.75	
VDE II(Slow downward)+CP	1.0						0.75
MD II +CP	1.0	1.0				0.41	
VDE II(Fast upward)＋TFCFD+CP	1.0		1.0	0.75		0.45	
VDE II(Fast downward)＋ TFCFD+CP	1.0		1.0		0.75		0.45
VDE II(Slow upward)＋TFCFD+CP	1.0		1.0			0.75	
VDE II(Slow downward)＋ TFCFD+CP	1.0		1.0				0.75
VDE III(Fast upward)+CP	1.0			1.0		0.6	
VDE III(Fast downward)+CP	1.0				1.0		0.6
VDE III(Slow upward)+CP	1.0					1.0	
VDE III(Slow downward)+CP	1.0						1.0

Table 5.2-2 Maximum element stress (σy) of ribs for each load condition

	Rib									
	σy Membrane [Pa]		σy Bending [Pa]				σy Membrane + Bending [Pa]			
	Max	Min	Z1 Max	Z1 Min	Z2 Max	Z2 Min	Z1 Max	Z1 Min	Z2 Max	Z2 Min
MD+Coolant pressure	3.599E+07	-7.693E+07	8.743E+06	-8.025E+07	8.025E+07	-8.743E+06	2.486E+07	-1.038E+08	9.001E+07	-6.237E+07
VDE II(Fast upward)+CP	8.304E+07	-3.504E+07	3.521E+07	-9.125E+07	9.125E+07	-3.521E+07	8.100E+07	-8.858E+07	9.400E+07	-3.473E+07
VDE II(Fast downward)+CP	**1.110E+08**	-7.127E+07	1.550E+08	-3.436E+07	3.436E+07	-1.550E+08	**1.659E+08**	-6.976E+07	9.079E+07	-1.441E+08
VDE II(Slow upward)+CP	7.724E+07	-2.645E+07	3.628E+07	-7.262E+07	7.262E+07	-3.628E+07	7.182E+07	-6.752E+07	8.929E+07	-2.593E+07
VDE II(Slow downward)+CP	**1.151E+08**	-5.780E+07	1.230E+08	-3.157E+07	3.157E+07	-1.230E+08	**1.683E+08**	-5.639E+07	7.553E+07	-1.125E+08
VDE II(Fast upward)+TFCFD+CP	8.796E+07	-3.276E+07	4.208E+07	-8.603E+07	8.603E+07	-4.208E+07	8.574E+07	-8.244E+07	9.998E+07	-3.920E+07
VDE II(Fast downward)+TFCFD+CP	**1.119E+08**	-6.636E+07	1.602E+08	-3.541E+07	3.541E+07	-1.602E+08	**1.720E+08**	-6.508E+07	1.031E+08	-1.484E+08
VDE II (Slow upward)+TFCFD+CP	7.751E+07	-2.417E+07	4.315E+07	-6.737E+07	6.737E+07	-4.315E+07	7.407E+07	-6.136E+07	9.527E+07	-2.571E+07
VDE II (Slow downward)+TFCFD+CP	**1.160E+08**	-5.689E+07	1.282E+08	-2.893E+07	2.893E+07	-1.282E+08	**1.698E+08**	-6.251E+07	8.503E+07	-1.168E+08
VDE III (Fast upward)+CP	1.055E+08	-5.260E+07	4.159E+07	-1.214E+06	1.214E+08	-4.159E+07	1.031E+08	-1.205E+08	1.224E+08	-6.026E+07
VDE III (Fast downward)+CP	**1.301E+08**	-1.003E+08	2.069E+08	-4.514E+07	4.514E+07	-2.069E+08	**2.188E+08**	-9.824E+07	1.113E+08	-1.950E+08
VDE III (Slow upward)+CP	9.290E+07	-4.114E+07	3.944E+07	-9.652E+07	9.652E+07	-3.944E+07	9.081E+07	-9.237E+07	1.056E+08	-3.988E+07
VDE III (Slow downward)+CP	**1.355E+08**	-8.229E+07	1.643E+08	-3.650E+07	3.650E+07	-1.643E+08	**1.937E+08**	-8.014E+07	8.715E+07	-1.529E+08

Stresses of bold letters mean that the locations of the stresses are checked because the stresses are high for each load category.

Table 5.2-3 Maximum element stress (σy) of housings for each load condition

	Housing											
	Membrane [Pa]		Bending[Pa]				Membrane + Bending [Pa]					
	Max	Min	P1 Max	P1 Min	P2 Max	P2 Min	P1 Max	P1 Min	P2 Max	P2 Min	Max SQRT ($P1^2+P2^2$)	MinSQRT ($P1^2+P2^2$)
MD+CP	1.638E+07	5.447E+06	1.464E+07	-1.283E+07	6.346E+06	-7.718E+06	2.734E+07	-1.899E+06	1.563E+07	1.048E+06	2.738E+07	7.510E+06
VDE II (Fast upward)+CP	1.910E+07	7.221E+05	1.807E+07	-1.514E+07	1.430E+07	-1.205E+07	3.497E+07	-4.488E+06	1.631E+07	-6.945E+06	3.528E+07	3.783E+06
VDE II (Fast downward)+CP	**2.680E+07**	4.345E+06	8.107E+06	-9.156E+06	1.634E+07	-1.020E+07	3.297E+07	-3.028E+06	3.859E+07	1.299E+06	**3.905E+07**	5.452E+06
VDE II (Slow upward)+CP	1.891E+07	4.010E+06	1.372E+07	-1.498E+07	1.585E+07	-9.147E+06	3.263E+07	-9.163E+05	2.084E+07	-6.799E+05	3.326E+07	7.492E+06
VDE II (Slow downward)+CP	**2.390E+07**	4.868E+06	9.265E+06	-9.199E+06	1.294E+07	-5.929E+06	2.911E+07	-1.658E+06	3.446E+07	2.115E+06	**3.491E+07**	5.701E+06
VDE II (Fast upward)+TFCFD+CP	1.973E+07	2.720E+06	1.795E+07	-1.496E+07	1.504E+07	-1.147E+07	3.530E+07	-5.510E+06	1.792E+07	-5.106E+06	3.549E+07	6.421E+06
VDE II (Fast downward)+TFCFD+CP	**2.881E+07**	4.298E+06	8.302E+06	-8.828E+06	1.703E+07	-9.455E+06	3.511E+07	-2.226E+06	4.076E+07	-2.226E+06	**4.120E+07**	5.282E+06
VDE II (Slow upward)+TFCFD+CP	1.935E+07	6.009E+06	1.361E+07	-1.481E+07	1.659E+07	-8.455E+06	3.296E+07	-2.151E+06	2.326E+07	1.211E+06	3.369E+07	7.737E+06
VDE II (Slow downward)+TFCFD+CP	**2.591E+07**	4.761E+06	9.150E+06	-9.022E+06	1.363E+07	-6.439E+06	3.125E+07	-8.557E+05	3.664E+07	1.820E+06	**3.706E+07**	5.589E+06
VDE III(Fast upward)+CP	2.017E+07	-3.577E+06	1.978E+07	-1.587E+07	1.597E+07	-1.580E+07	3.702E+07	-9.170E+06	1.658E+07	-1.279E+07	3.781E+07	-7.147E+04
VDE III(Fast downward)+CP	**3.163E+07**	8.834E+05	1.032E+07	-1.242E+07	2.204E+07	-1.669E+07	3.938E+07	-5.024E+06	4.642E+07	5.796E+05	**4.706E+07**	4.784E+06
VDE III (Slow upward)+CP	1.991E+07	1.236E+06	1.398E+07	-1.567E+07	1.804E+07	-1.193E+07	3.390E+07	-3.608E+06	2.102E+07	-4.992E+06	3.487E+07	6.966E+06
VDE III (Slow downward)+CP	**2.775E+07**	4.445E+06	9.835E+06	-1.028E+07	1.751E+07	-1.100E+07	3.422E+07	-3.198E+06	4.093E+07	1.668E+06	**4.155E+07**	5.647E+06

Stresses of bold letters mean that the locations of the stresses are checked because the stresses are high for each load category.

Table 5.2-4 Maximum stress and location

(a) Toroidal rib

	σy Membrane		σy Membrane+Bending	
	Max	Location	Max	Location
VDE II (Fast downward)+Coolant pressure	1.110E+08	O4-T-L1-0-1 (38296)	1.659E+08	I1-T-L1-0-1 (34574)
VDE II (Slow downward)+Coolant pressure	1.151E+08	O4-T-L1-0-1 (38296)	1.683E+08	O4-T-L1-0-1 (38296)
VDE II (Fast downward)＋TFCFD+Coolant pressure	1.119E+08	O4-T-L1-0-1 (38296)	1.720E+08	I1-T-L1-0-1 (34574), I1-T-R1-0-1 (12663)
VDE II (Slow downward)＋TFCFD+Coolant pressure	1.160E+08	O4-T-L1-0-1 (38296)	1.689E+08	O4-T-L1-0-1 (38296)
VDE III (Fast downward)+Coolant pressure	1.301E+08	O4-T-L1-0-1 (38296)	2.188E+08	I1-T-R1-0-1 (12663)
VDE III (Slow downward)+Coolant pressure	1.355E+08	O4-T-L1-0-1 (38296)	1.937E+08	O4-T-L1-0-1 (38296)

(b)Poloidal rib

	σy Membrane		σy Membrane+Bending	
	Max	Location	Max	Location
VDE II (Fast downward)+Coolant pressure	8.848E+07	O1-P-C-0-1 (16038)	9.079E+07	O1-P-C-0-1 (16038)
VDE II (Slow upward)+Coolant pressure	7.259E+07	O3-P-L1-0-1 (22461)	7.657E+07	O3-P-L1-0-1 (22461)
VDE II (Fast downward)＋TFCFD+Coolant pressure	9.990E+07	O1-P-C-0-1 (16038)	1.031E+08	O1-P-C-0-1 (16038)
VDE II (Slow downward)＋TFCFD+Coolant pressure	8.370E+07	O1-P-C-0-1 (16038)	8.503E+07	O1-P-C-0-1 (16038)
VDE III (Fast downward)+Coolant pressure	1.082E+08	O1-P-C-0-1 (16038)	1.113E+08	O1-P-C-0-1 (16038)
VDE III (Slow upward)+Coolant pressure	9.156E+07	O3-P-L1-0-1 (22461)	9.710E+07	O3-P-L1-0-1 (22461)

(c) Housing

	Membrane		Membrane+Bending	
	Max	Location	Max	Location
VDE II(Fast downward)+Coolant pressure	2.680E+07	H7-2-4	3.905E+07	H7-2-4
VDE II(Slow downward)+Coolant pressure	2.390E+07	H7-2-4	3.491E+07	H7-2-4
VDE II (Fast downward)+TFCFD+Coolant pressure	2.881E+07	H7-2-4	4.120E+07	H7-2-4
VDE II (Slow downward)+TFCFD+Coolant pressure	2.591E+07	H7-2-1, H7-2-4	3.706E+07	H7-2-1, H7-2-4
VDE III (Fast downward)+Coolant pressure	3.163E+07	H7-2-4	4.706E+07	H7-2-4
VDE III (Slow downward)+Coolant pressure	2.775E+07	H7-2-1, H7-2-4	4.155E+07	H7-2-1, H7-2-4

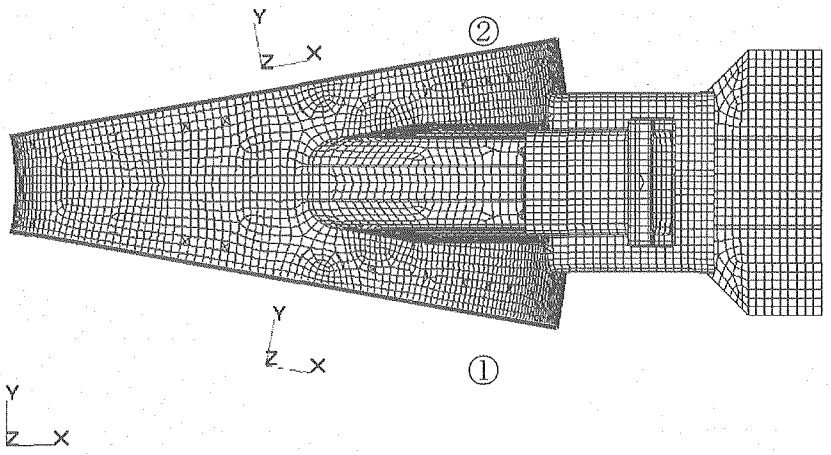

Cyclic symmetry condition

[Nodes of Side ① and Side ② connected by MPC]

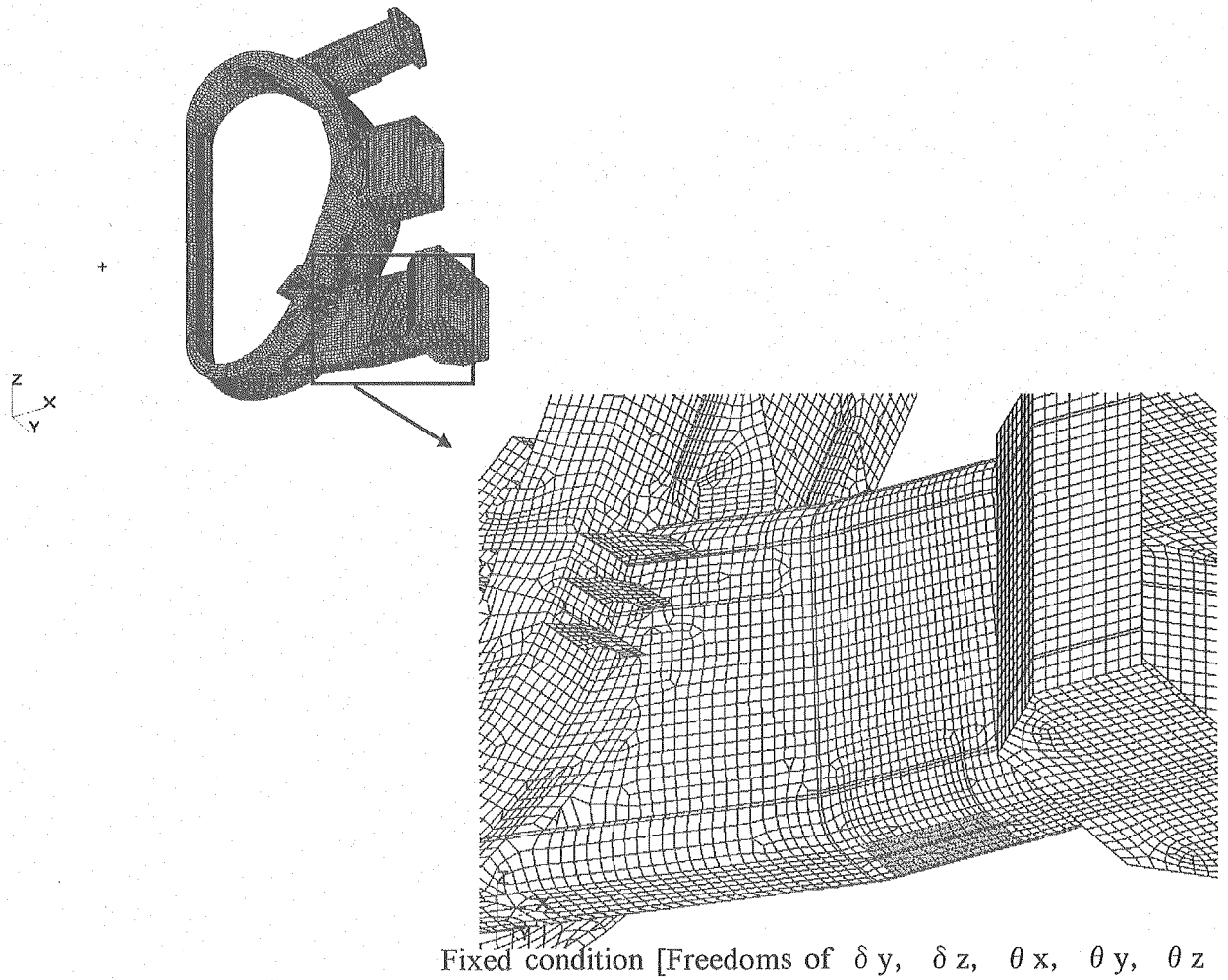

Fixed condition [Freedoms of δ y, δ z, θ x, θ y, θ z constrained area for attaching VV support structure]

Fig.5.2-1 Boundary condition for stress analysis

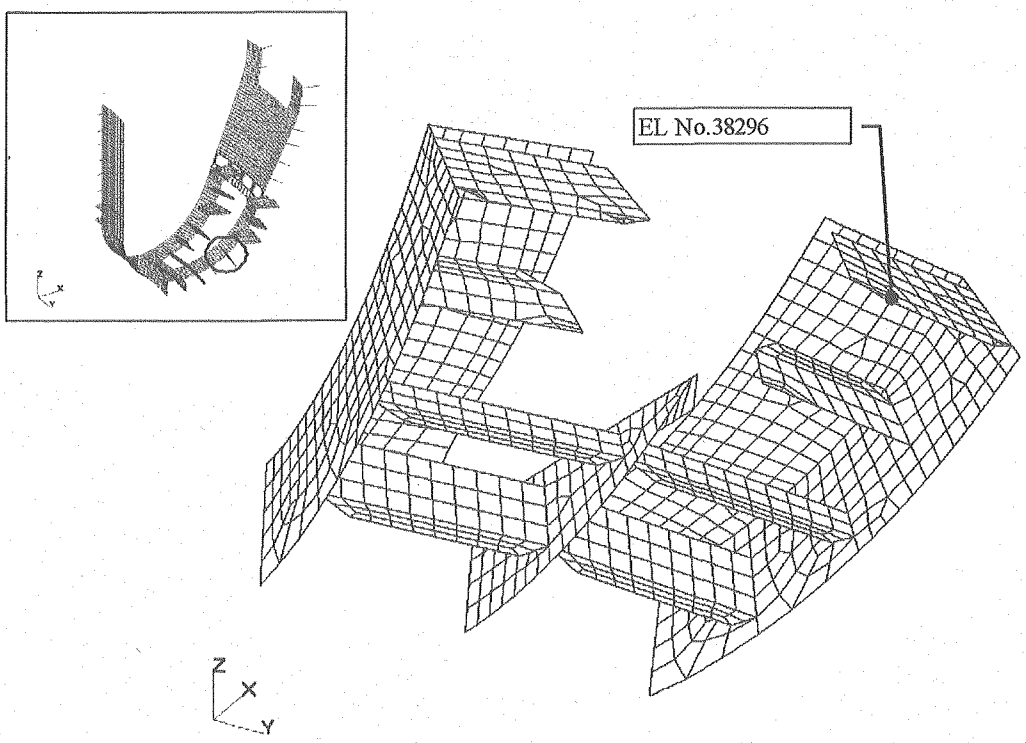

O4-T-L1-0-1

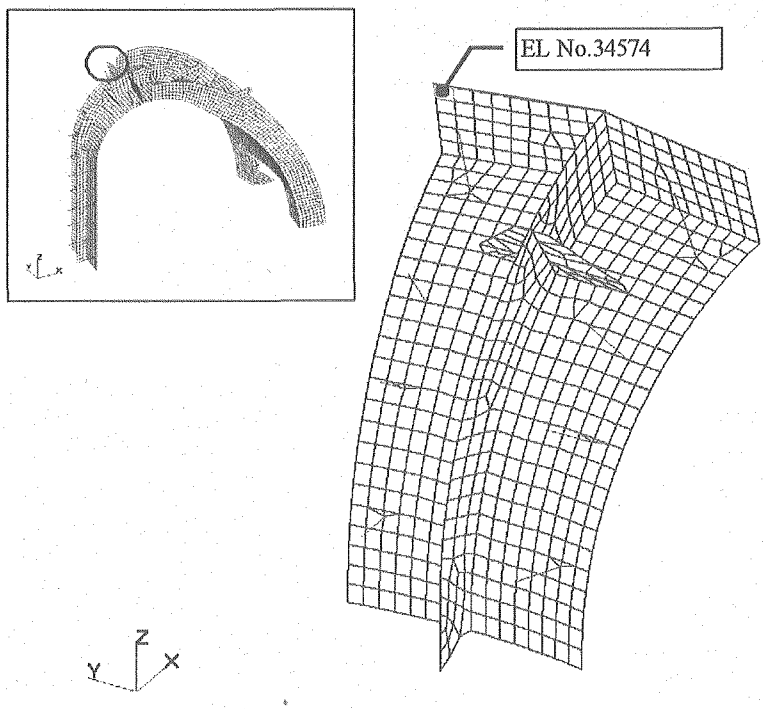

I1-T-L1-0-1

Fig. 5.2-2(1/3) Location of maximum stress of ribs

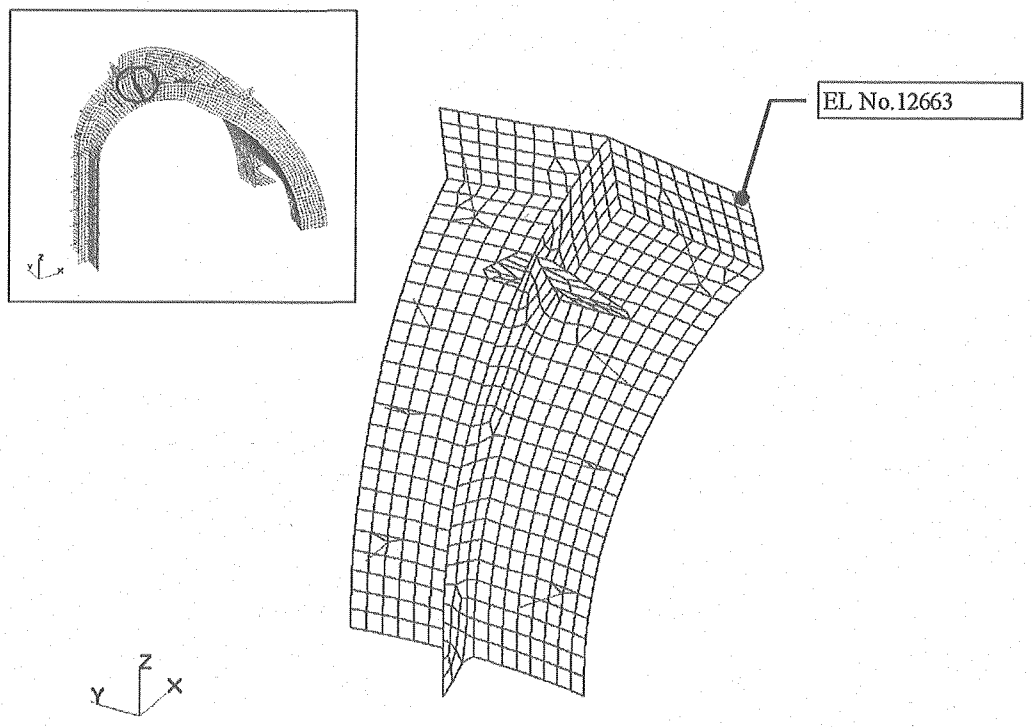

I1-T-R1-0-1

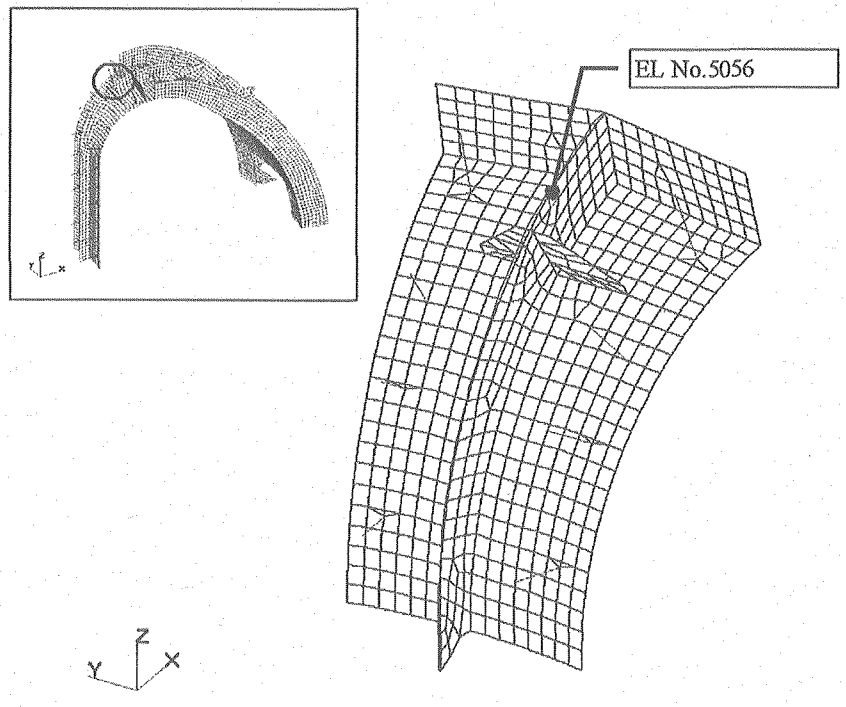

I1-P-C-0-1

Fig. 5.2-2(2/3) Location of maximum stress of ribs

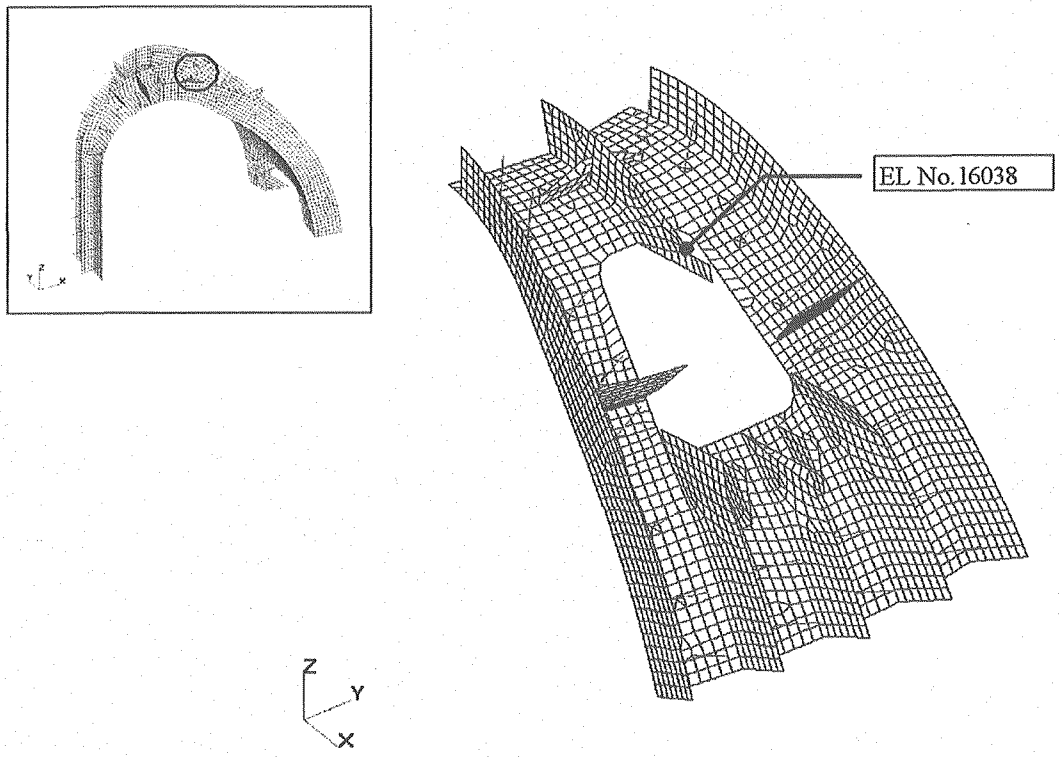

O1-P-L1-0-1

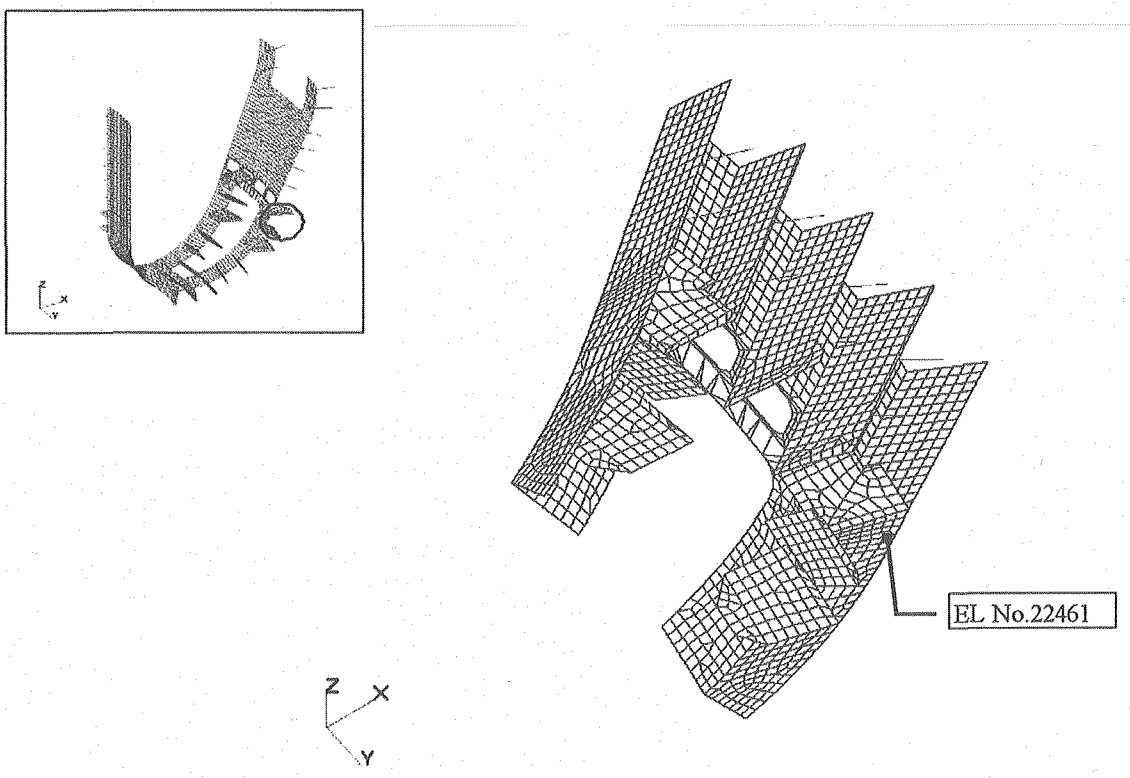

O3-P-L1-0-1

Fig. 5.2-2(3/3) Location of maximum stress of ribs

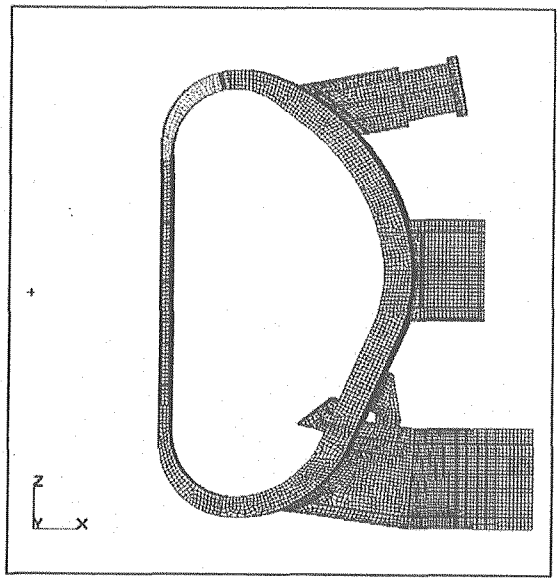

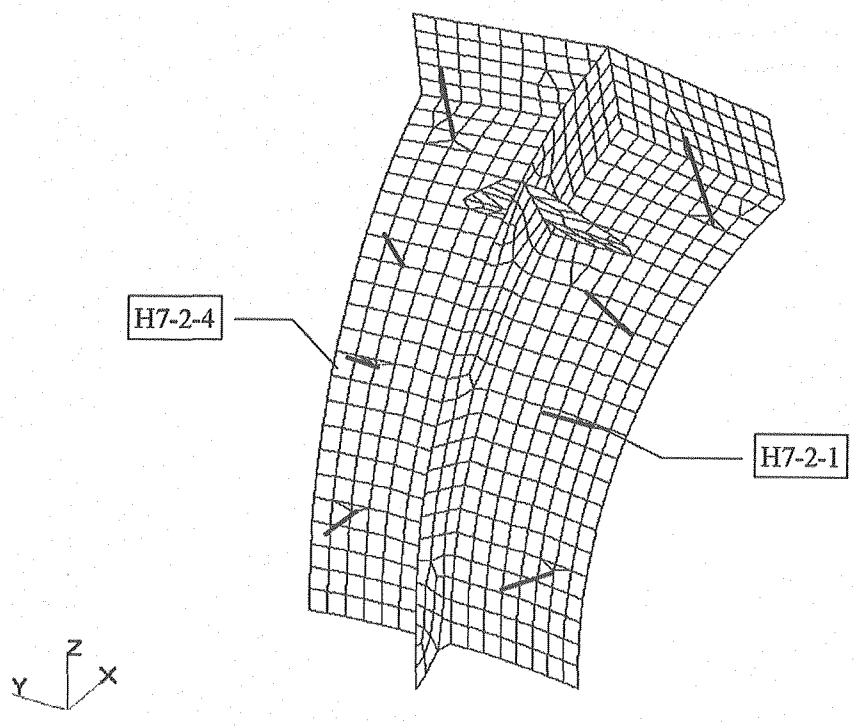

Fig. 5.2-3 Location of maximum stress of housingss

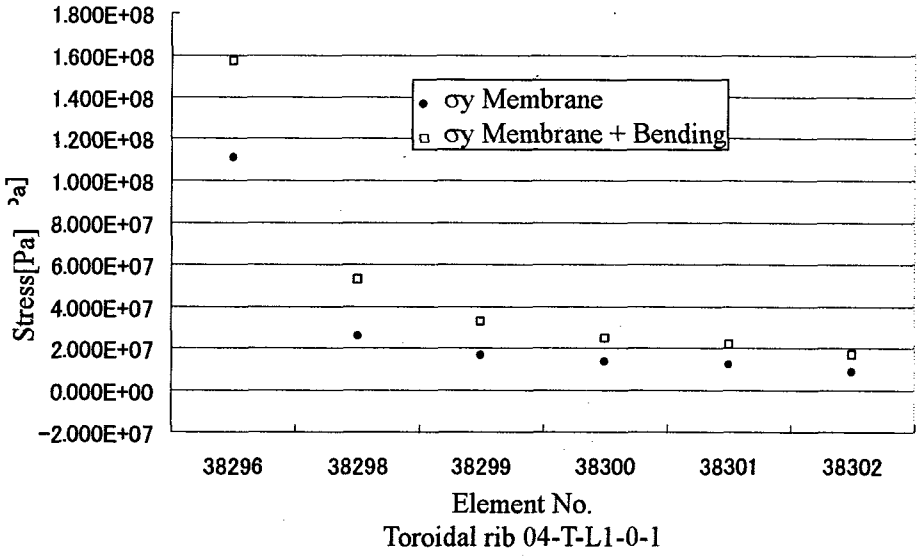

Toroidal rib 04-T-L1-0-1

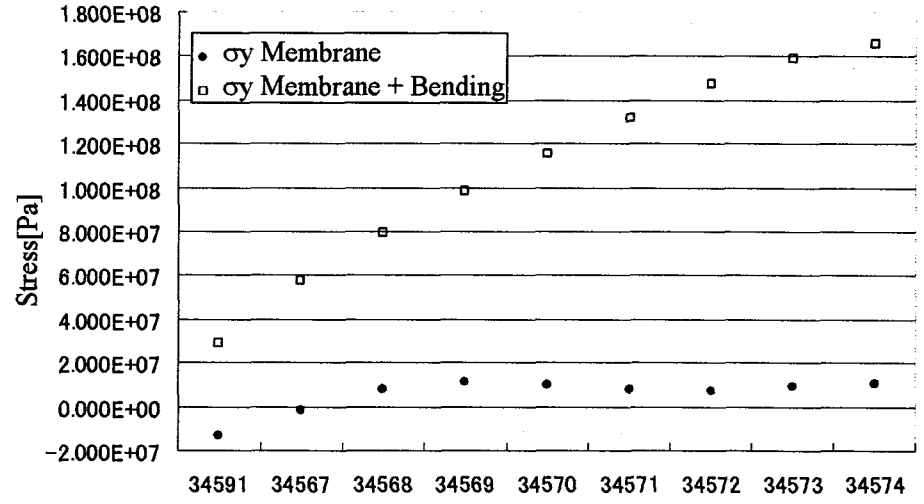

Toroidal rib I1-T-L1-0-1

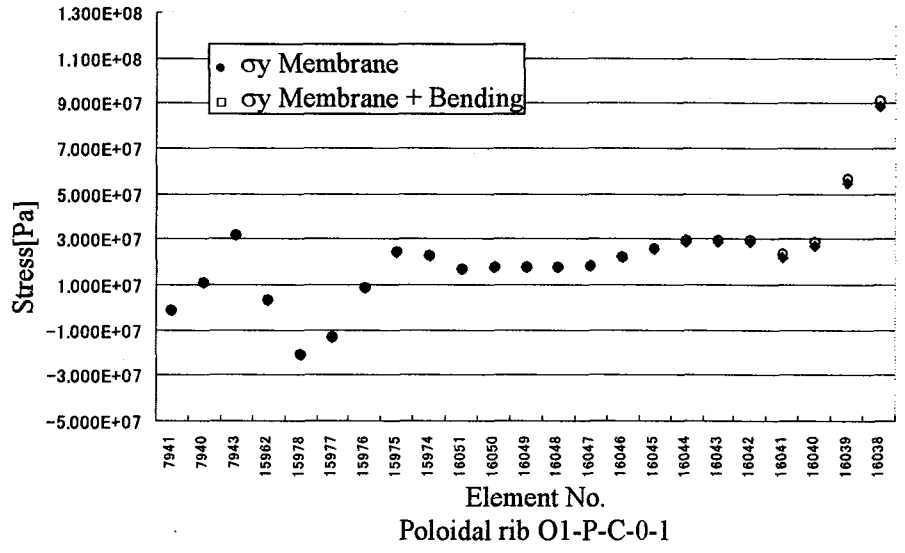

Poloidal rib O1-P-C-0-1

Fig.5.2-4(1/6) Stress distribution : VDE II Fast downward disruption + coolant pressure

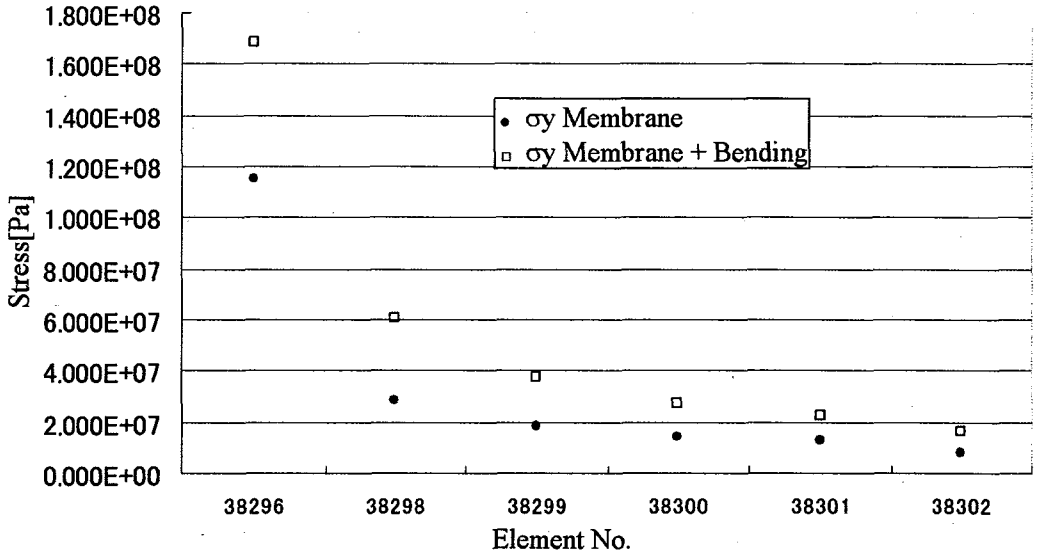

Toroidal rib 04-T-L1-0-1

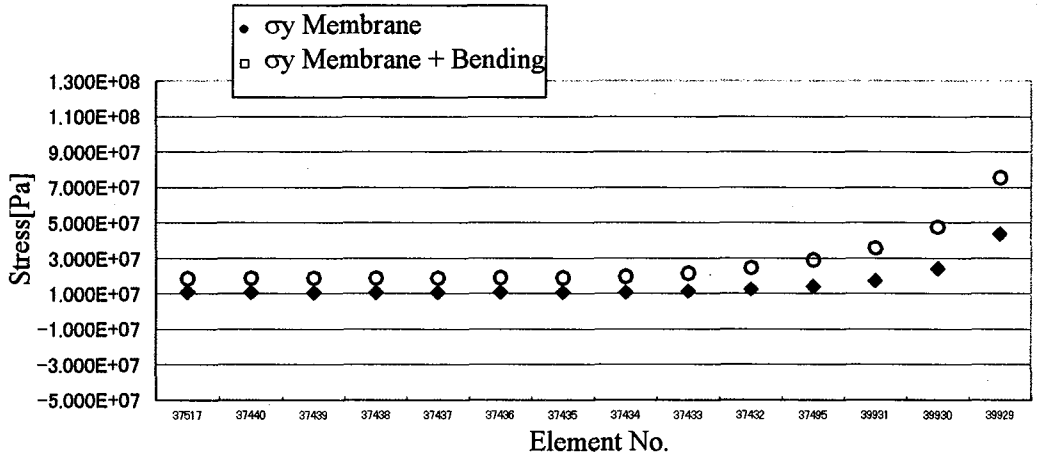

Poloidal rib O2-P-L2-0-1

Fig. 5.2-4(2/6) Stress distribution : VDE II Slow downward disruption + coolant pressure

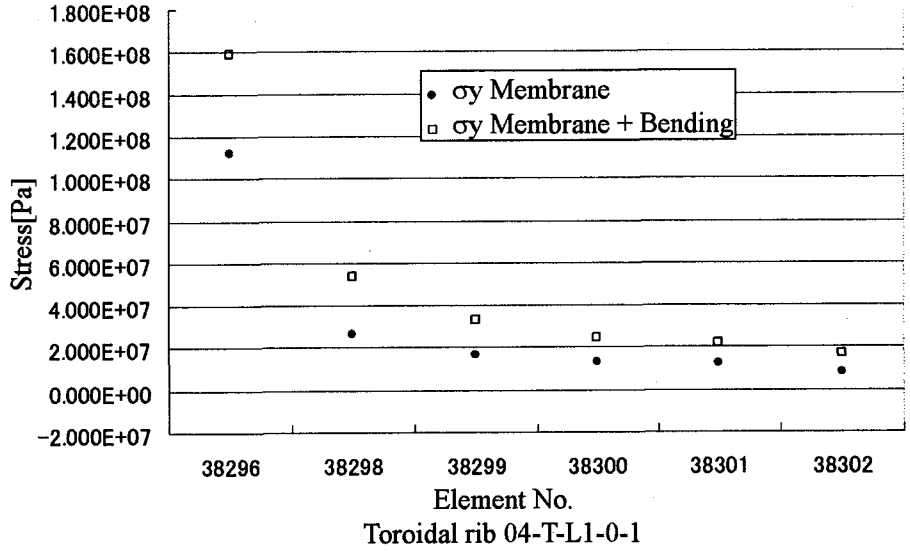

Toroidal rib 04-T-L1-0-1

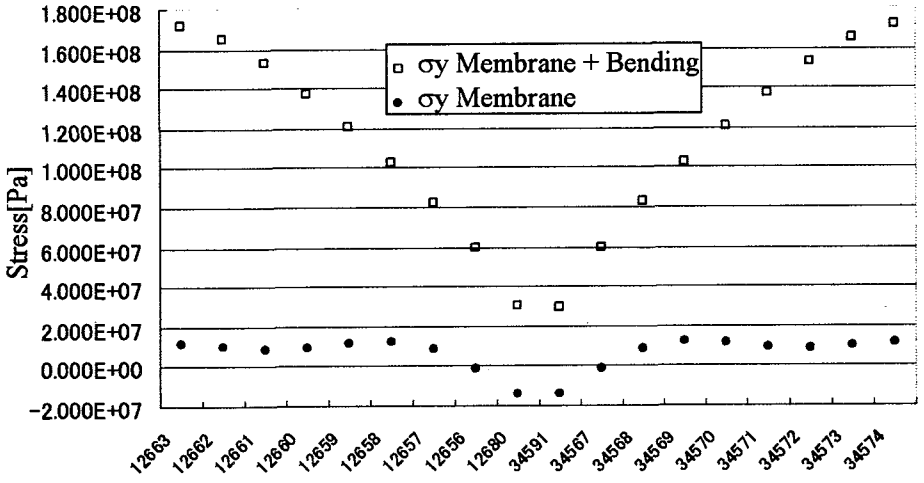

Toroidal rib
I1-T-L1-0-1, I1-T-R1-0-1

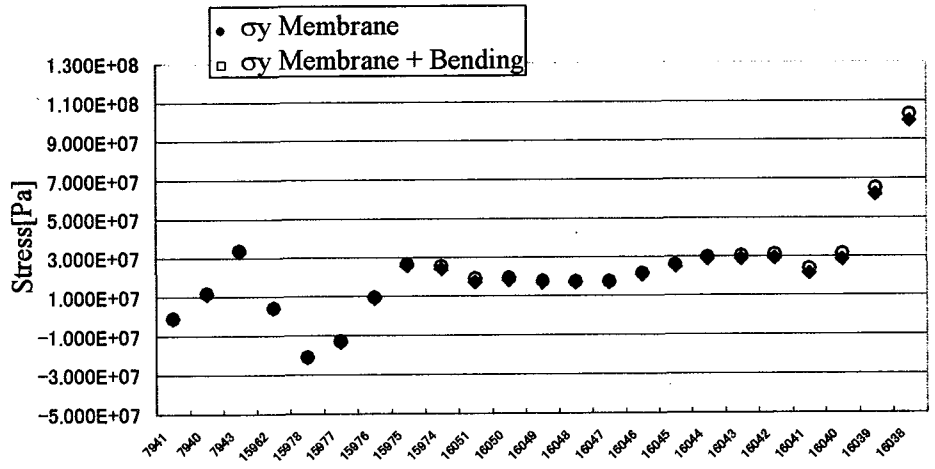

Poloidal rib O1-P-C-0-1

Fig. 5.2-4(3/6) Stress distribution : VDE II Fast downward disruption + TFCFD + coolant pressure

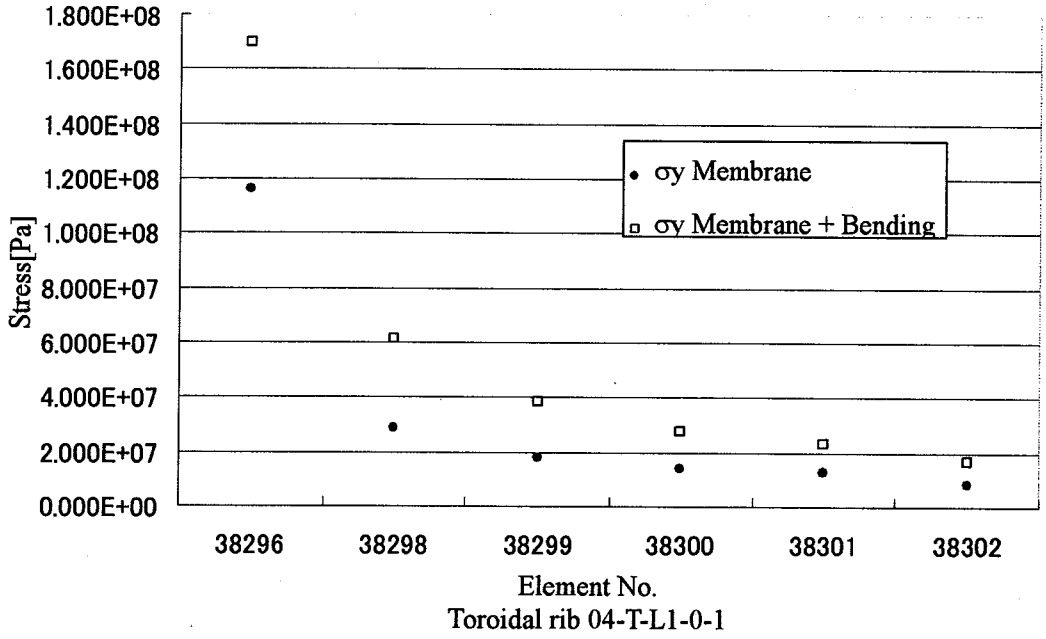

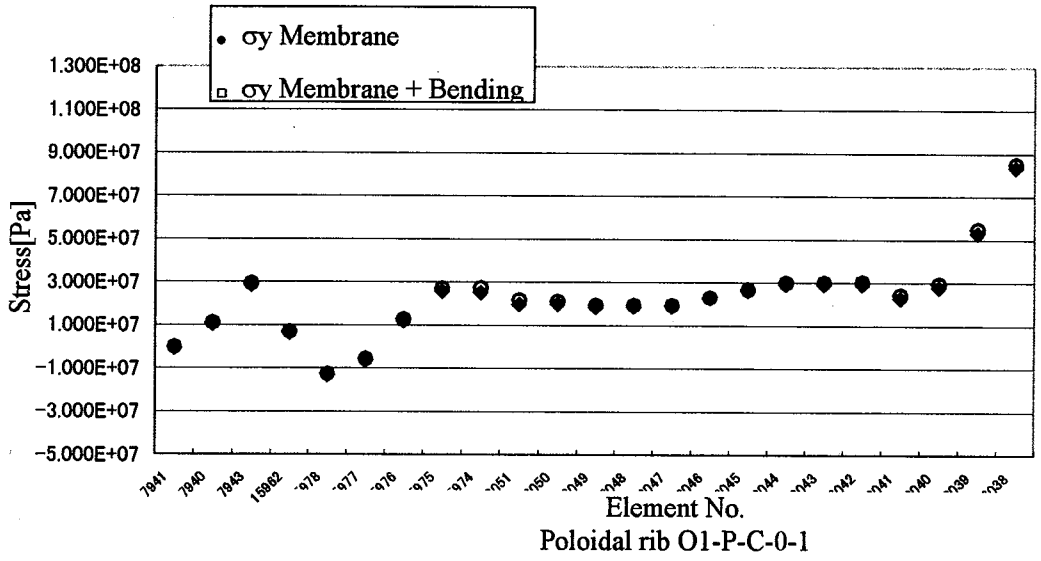

Fig. 5.2-4(4/6) Stress distribution : VDE II Slow downward disruption + TFCFD + coolant pressure

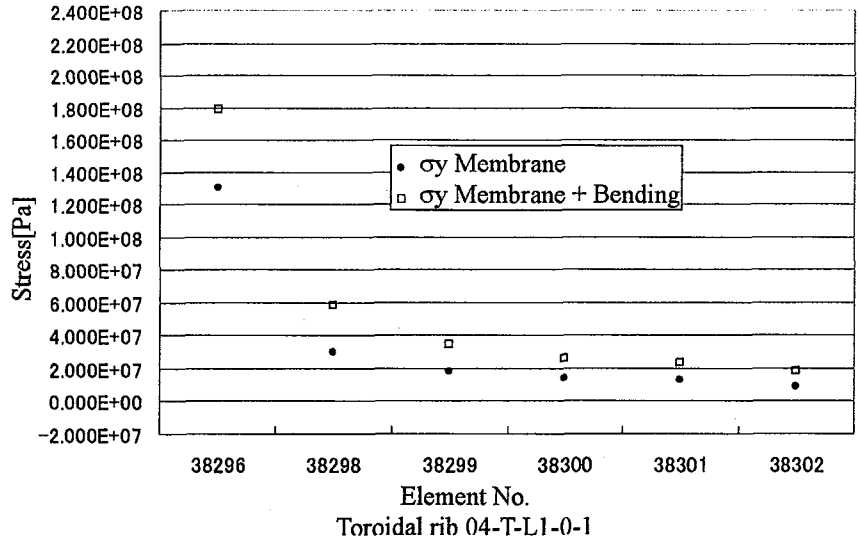

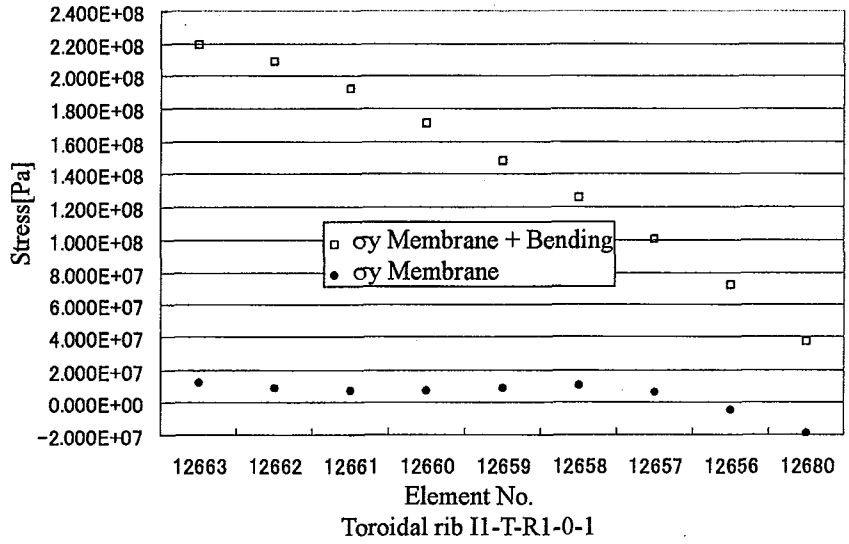

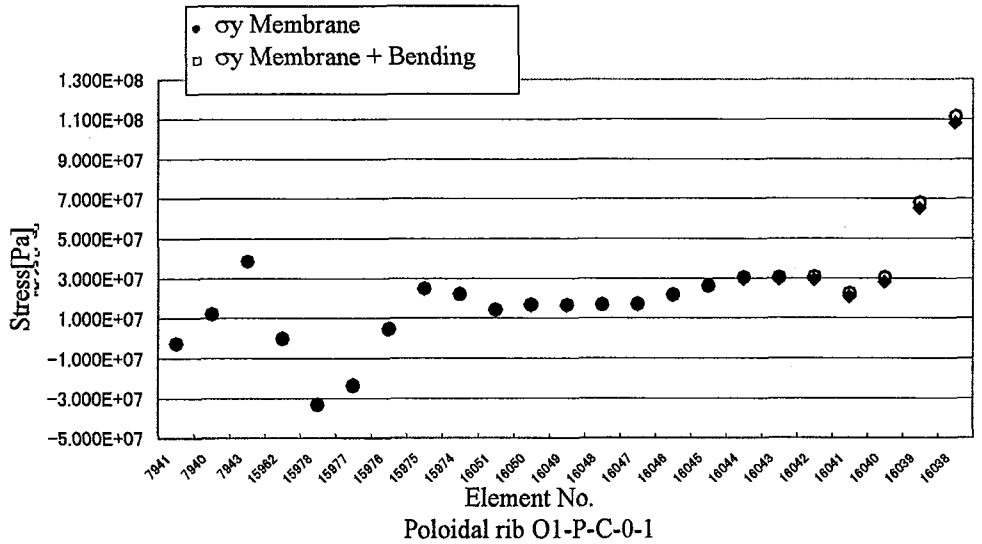

Fig. 5.2-4(5/6) Stress distribution : VDE III Fast downward disruption + coolant pressure

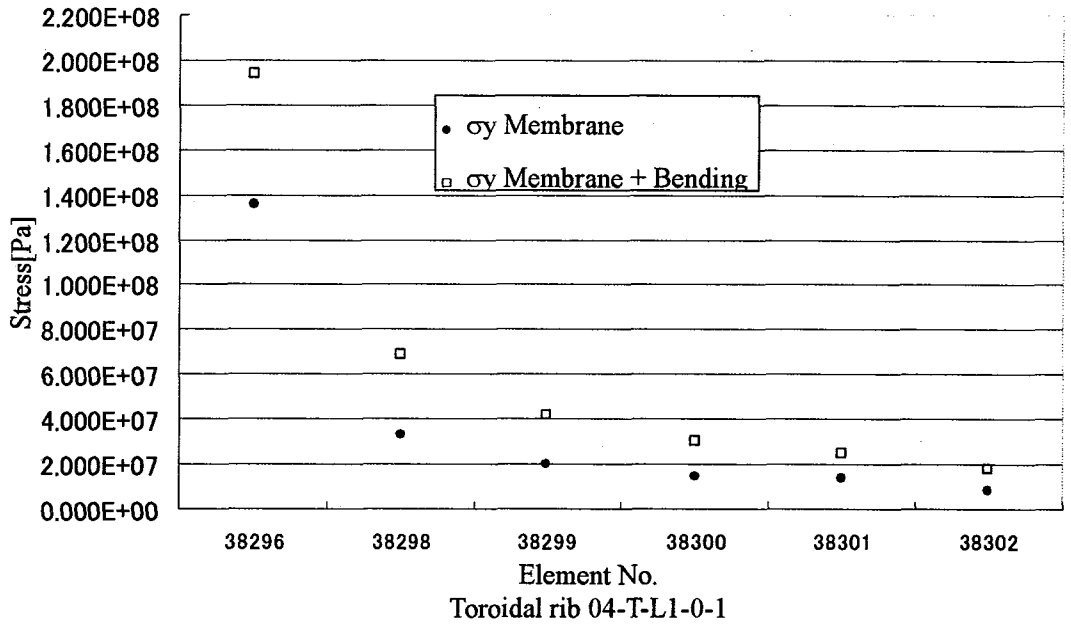

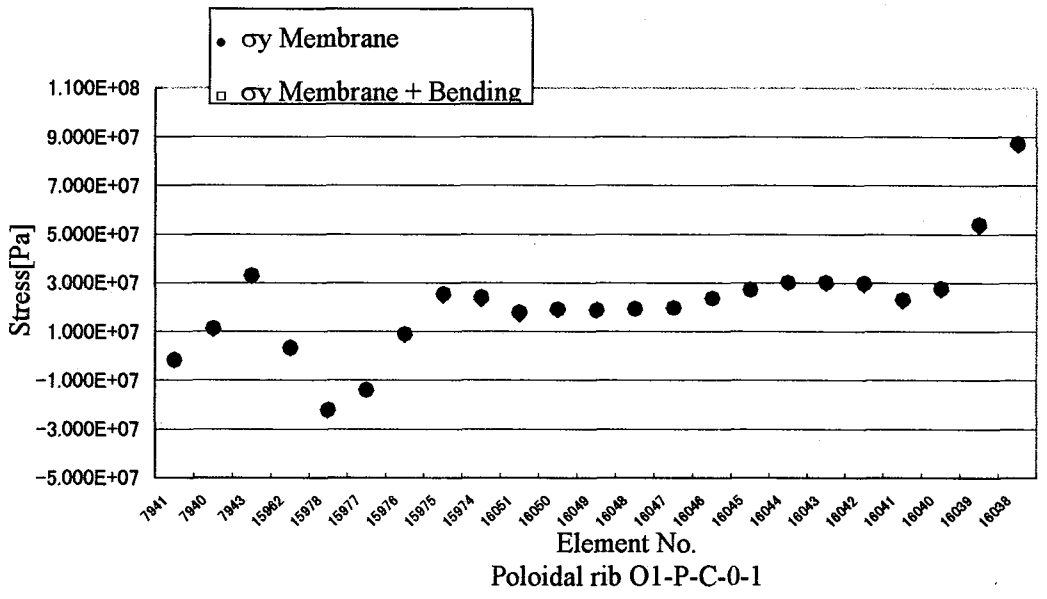

Fig. 5.2-4(6/6) Stress distribution : VDE III slow downward disruption + coolant pressure

6. Crack propagation of typical inboard region

Detail stress and crack propagation analyses have been carried out in order to determine allowable crack lengths. In a typical inboard region, as ribs and housings are successively located, fabricability improvement can be expected by using plug weld. Relatively simple boundary and load conditions can be set for the stress analyses in the typical inboard region.

6.1 Detail stress analyses of typical inboard region

6.1.1 Analysis model

Fig.6.1-1 shows the analysis region of the inboard stress analysis. Two finite element (FE) models are prepared for the stress analyses to apply fine meshes for the weld of housings and that of ribs, respectively. The FE models of housings and ribs in the inboard region are shown in Figs.6.1-2 and 3, respectively. 3-dimensional solid elements are used in the models. Cracks or un-welded areas are not included in the models.

6.1.2 Analysis conditions

(1) Load conditions

Load conditions of the stress analyses are summarized in Table 6.1-1. The loads of coolant pressure, EM loads due to halo currents and TFCFD event, poloidal moments of blanket modules and thermal load are considered for the stress analyses. For EM loads at disruption, loads due to only halo currents are included in the analyses because those due to eddy currents are considered not to be dominant. The load conditions of the stress analyses are shown in Fig.6.1-4 ~6.

(2) Boundary conditions

Boundary conditions are shown in Fig.6.1-7. Symmetric and asymmetric boundary conditions on the nodes on the vertical boundary planes have been applied depending on the load conditions. The load cases of coolant pressure and EM load pressure have symmetric boundary conditions. That of poloidal moments for housing has asymmetric boundary conditions.

For all cases the two horizontal boundary planes are symmetric. All nodes on the z=0 are restrained in vertical direction. The nodes on the other horizontal boundary plane are coupled in z direction in order to give a free expansion keeping the plane horizontal.

(3) Material properties

Young's modulus and Poisson ratio of the VV structure material are 200GPa and 0.29, respectively. Thermal conductivity is 15.1W/mK. The thermal transfer coefficient in cooling sides of VV shells is 500W/m^{2}K.

6.1.3 Analysis results

Deformations for each load case are shown in Figs. 6.1-8~11. The temperature distributions are shown in Figs 6.1-12 and 6.1-13. The maximum temperature of inner shell is 220°C. The maximum temperature point is the gap between blanket modules on the inner shell. The temperature rise is limited in the inner shell surface. The maximum temperature of housing is 123°C. The deformation due to thermal load is shown in Fig6.1-14.

Tresca stress distributions for each load case are shown in Figs.6.1-15~29. The analyzed load cases are as flows;

(1) Coolant pressure of 1.3MPa (Figs.6.1-15,16,17)

The stresses of the connection between the VV shell and housing/ribs are concentrated at the connection corner. Tresca stresses of the plug weld region are around 40 -50 MPa.

(2) TFCFD event (Inner shell: 0.73MPa, Outer shell: 0.87MPa, Figs.6.1-18,19,20)

Stress concentrations are produced at the connection between VV shells and housings/ribs. Tresca stresses of the plug weld region are around 120 MPa for housing and 40MPa for ribs..

(3) EM forces due to halo current in VDE III (Slow VDE, Inner shell: 2.1MPa, Outer shell: 1.8MPa, Figs.6.1-21,22,23)

The EM force is a pressure from inner shell to outer shell sides. The stress concentrates at the plug weld region to be around 290MPa.

(4) Poloidal moment of blanket at VDEIII (±500kN, Figs.6.1-24,25,26)

Bending stresses due to poloidal moments are produced at the connection between housing and VV shells.

(5) Thermal load due to nuclear heating (Figs.6.1-27,28,29)

Thermal stresses are limited in inner shell. The stresses of the plug weld region are negligible.

Table 6.1-1 Load Conditions of Typical Inboard Region

	Inboard region			
1.Coolant Water Pressure	1.3MPa			
2. MD II Electromagnetic Force by Eddy Current	not to be considered			
Electromagnetic Force by Halo Current	Inner Shell 0.13MPa			
	Outer Shell 0.11MPa			
3. VDE Direction of the VDE	Downward VDE			
Electromagnetic Force by Eddy Current	not to be considered			
Electromagnetic Force by Halo Current	Slow VDE		Fast VDE	
	Inner shell	Outer shell	Inner shell	Outer shell
VDE III	2.1MPa	1.8MPa	2.1MPa×0.6	1.8MPa×0.6
VDE II	2.1MPa×0.75	1.8MPa×0.75	2.1MPa×0.45	1.8MPa×0.45
4. TFCFD Electromagnetic force	Inner shell 0.73MPa Outer shell 0.87MPa			
5. Electromagnetic force from Blanket Housing	Slow VDE		Fast VDE	
VDE III	± 500kN			
VDE II	± 500kN×0.75			
MD II	± 500kN			
6. Nuclear heating Nuclear heating	$H(x,y,z)=Homax \cdot \exp(-ax) \cdot [\exp(-\lambda y^2)+\exp(-\lambda z^2)]$ x:Distance by Outer shell direction from V/V Inner shell(mm) y:Distance by Poloidal direction(mm) z:Distance by Toloidal direction(mm) $Homax:6.6\times10^{-4}(W/mm^3)$ $a:1.28\times10^{-2}(mm^{-1})$ $\lambda:1.08\times10^{-4}(mm^{-2})$ The Housing between Outer Shells in V/V Housing of gap side existing between Blankets $H=13.18\times10^{-5} \cdot \exp(-a1 \cdot x)$ $a1=1.2\times10^{-2}(mm^{-1})$ Housing of Opposite side to the gap existing between Blankets $H=9.45\times10^{-5} \cdot \exp(-a2 \cdot x)$ $a2=1.13\times10^{-2}(mm^{-1})$			

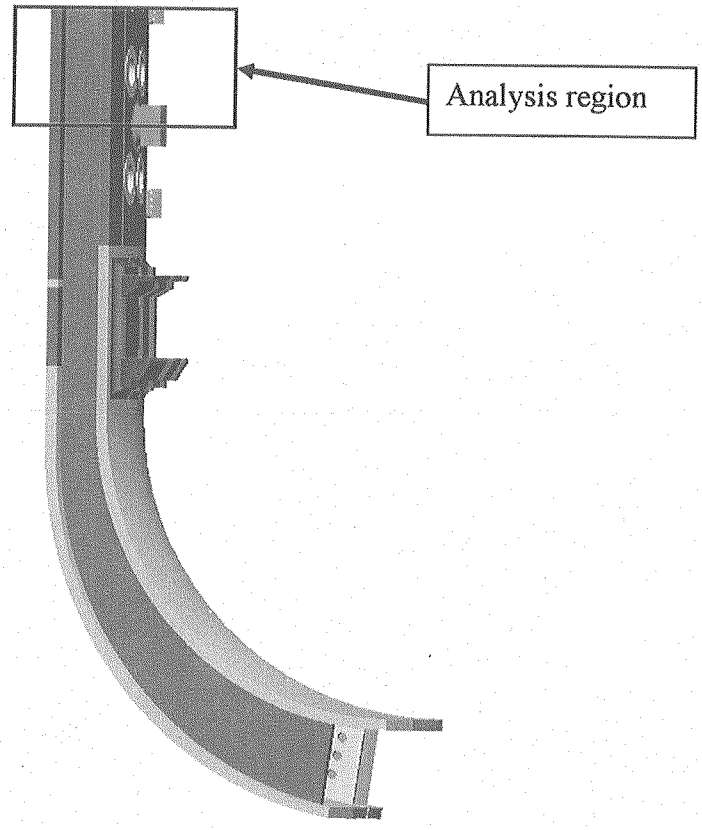

Fig.6.1-1 Analysis region of Typical Inboard Region

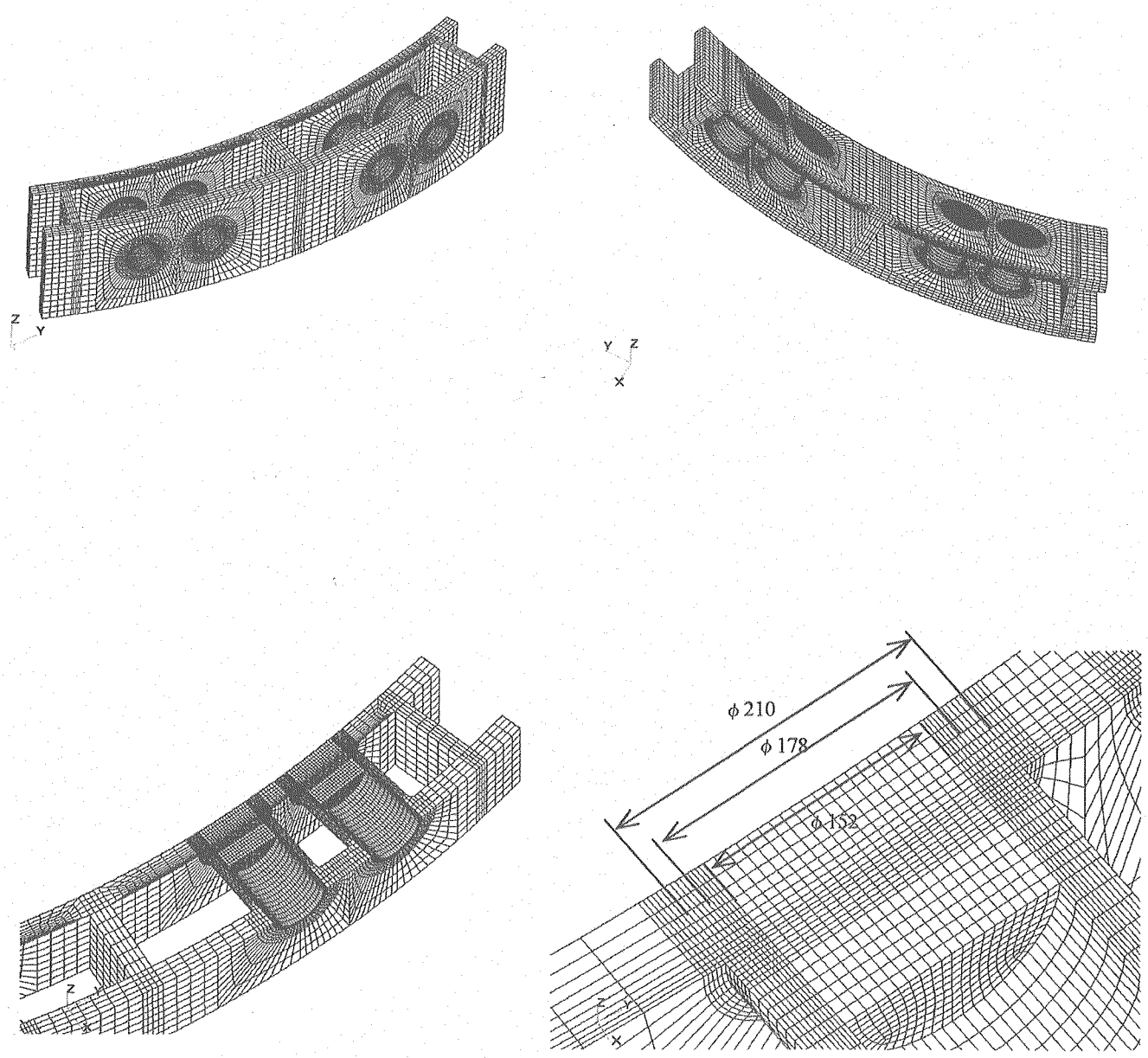

Fig.6.1-2 FE Model of housings in inboard region

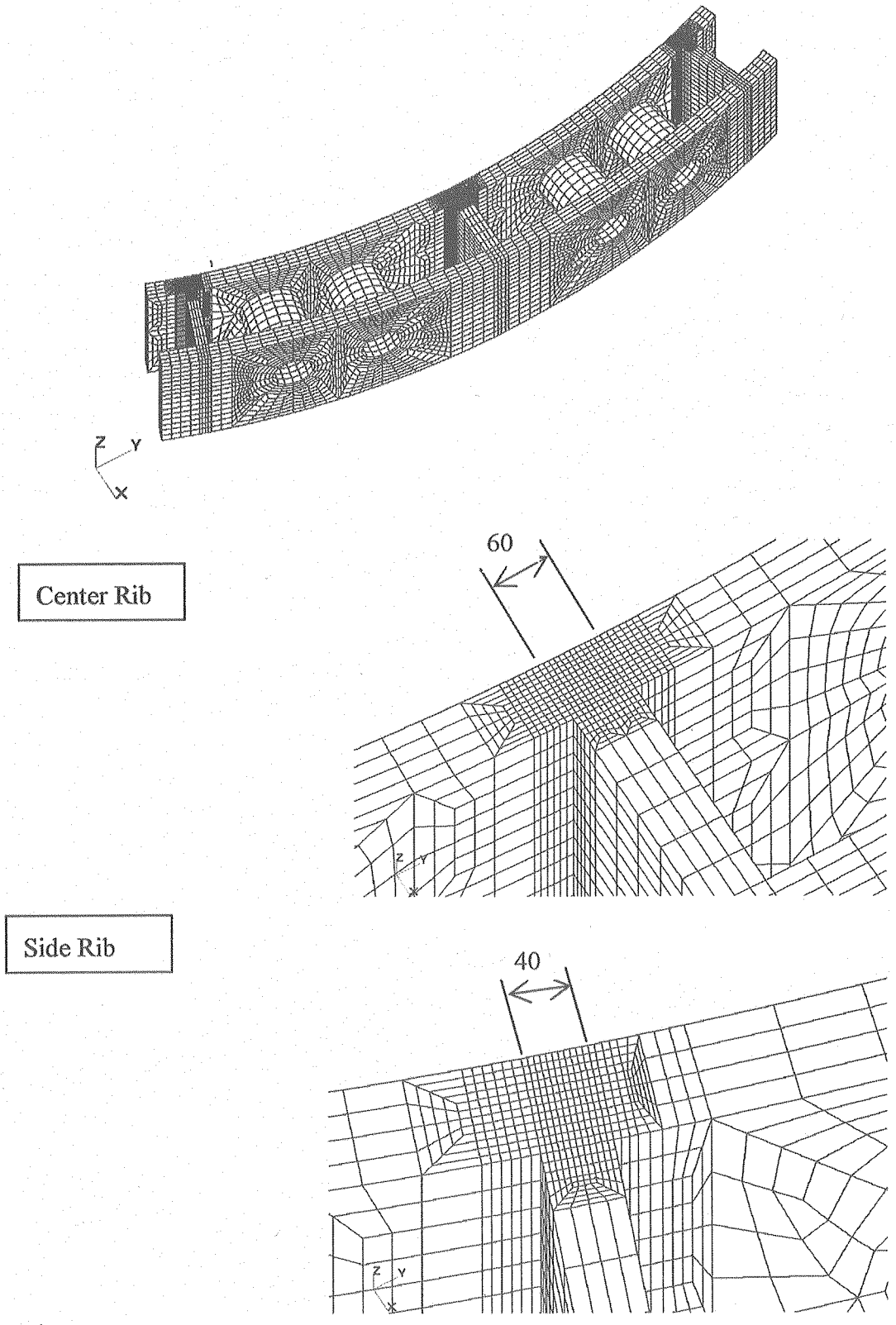

Fig.6.1-3 FE Model of ribs in inboard region

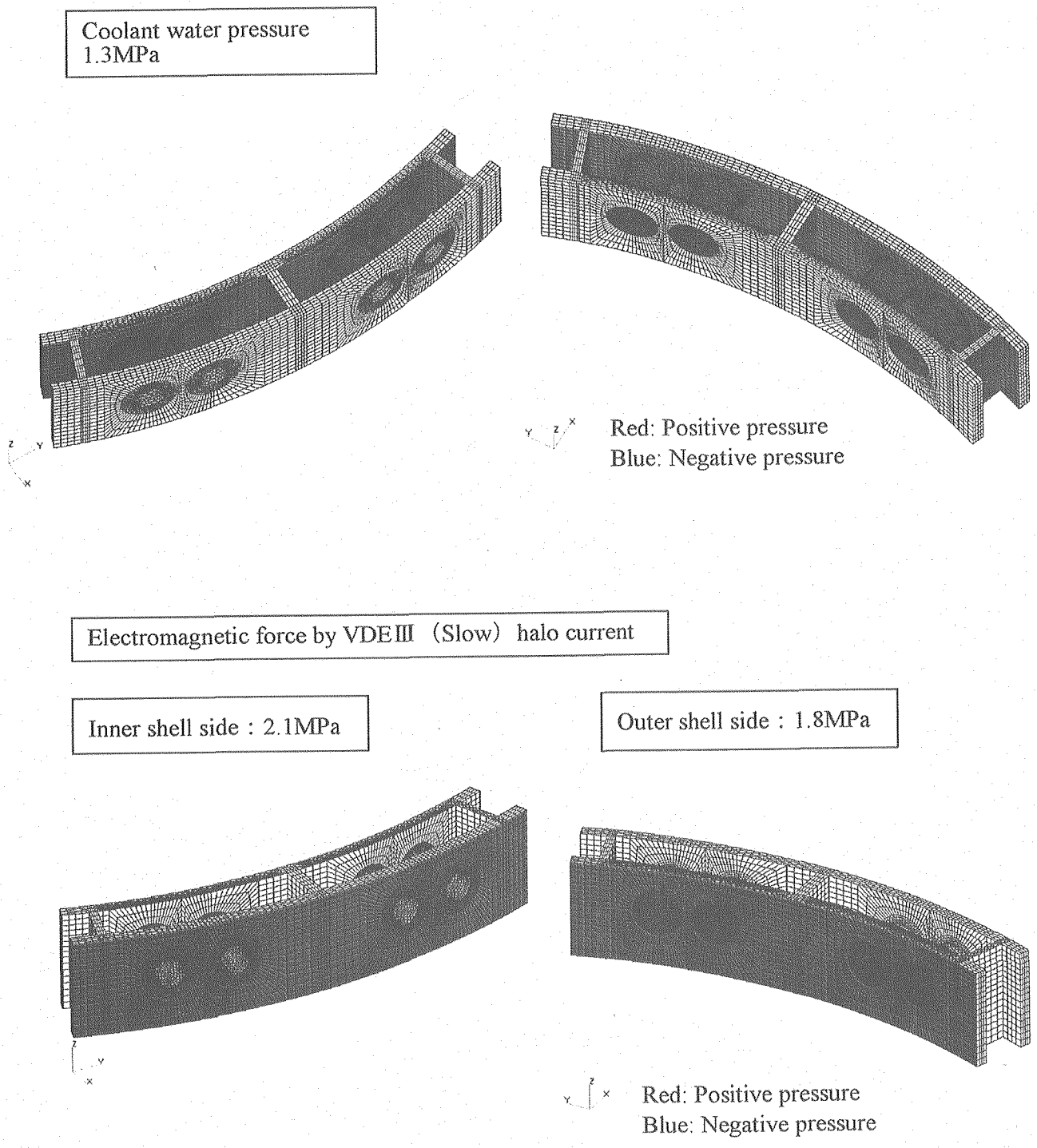

Fig.6.1-4Load condition of inboard model

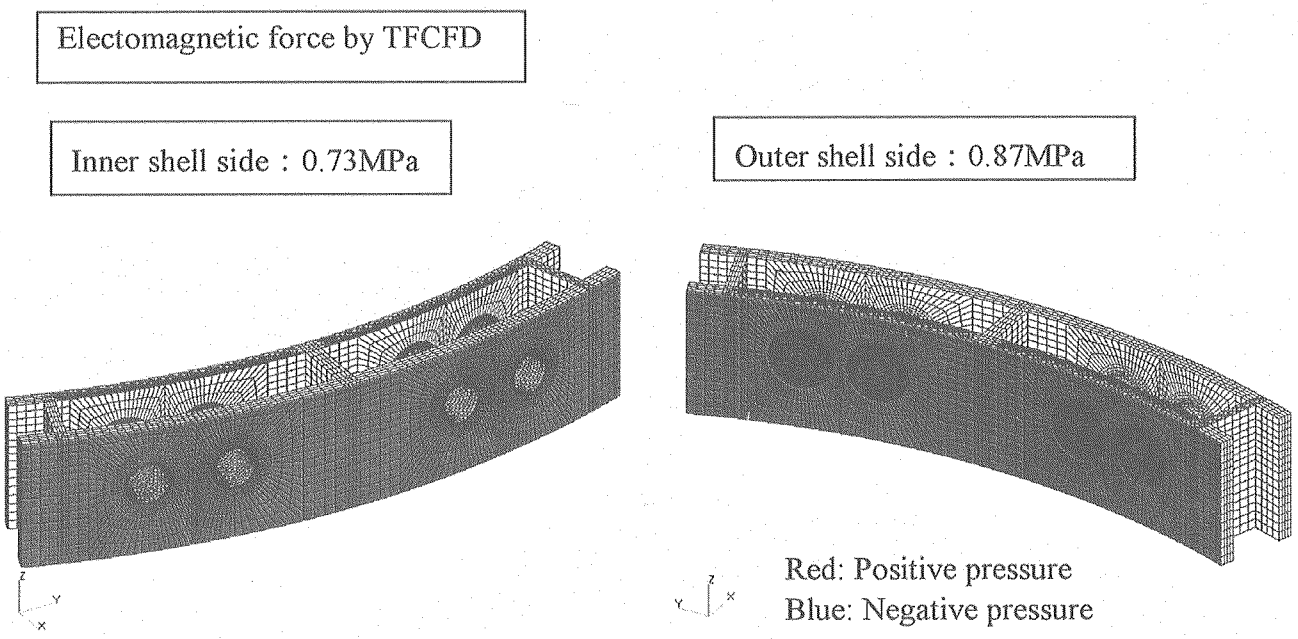

Fig.6.1-5 Load conditions of inboard region

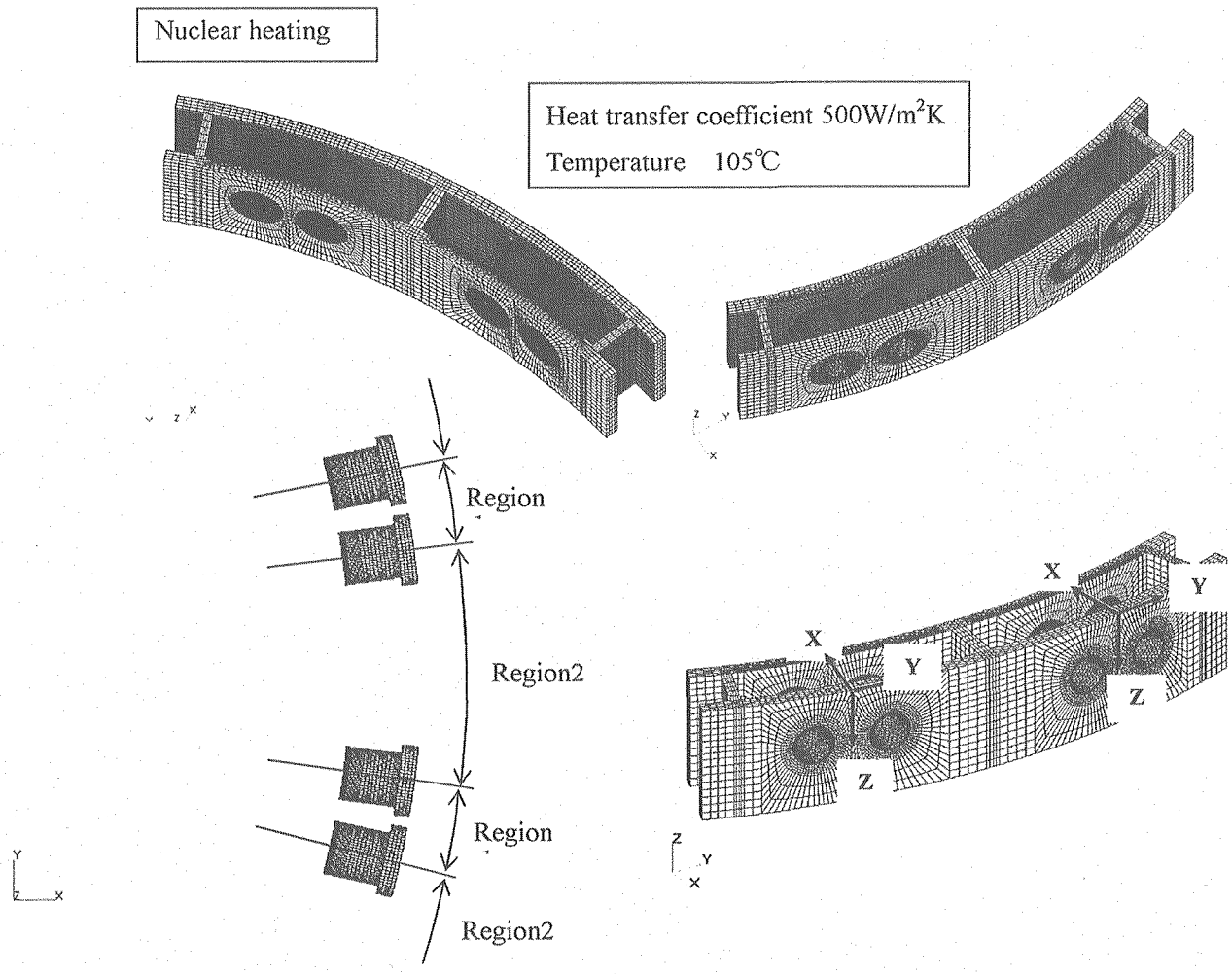

H(x,y,z)=Homax・exp(-ax)・[exp(-λ y²)+exp(-λ z²)]

x: distance by Outer shell direction from VV inner shell (mm)
y: distance by Poloidal direction (mm)
z: distance by Toroidal direction (mm)
Homax: 6.6×10^{-4}(W/mm³)
a: 1.28×10^{-2}(mm⁻¹)
λ: 1.08×10^{-4}(mm⁻²)

The housing between Outer shell and Inner shell in VV
Housing og gap side existing between Blankets(Fig. Region1)
$H=13.18\times10^{-5}\times\exp(-a1\cdot x)$
$a1=1.2\times10^{-5}$(mm⁻¹)
Housing of Opposite side to the gap existing between Blankets(Fig Region2)
$H=9.45\times10^{-5}\times\exp(-a2\cdot x)$
$a2=1.13\times10^{-2}$(mm⁻¹)

Fig.6.1-6 Load conditions of thermal analysis

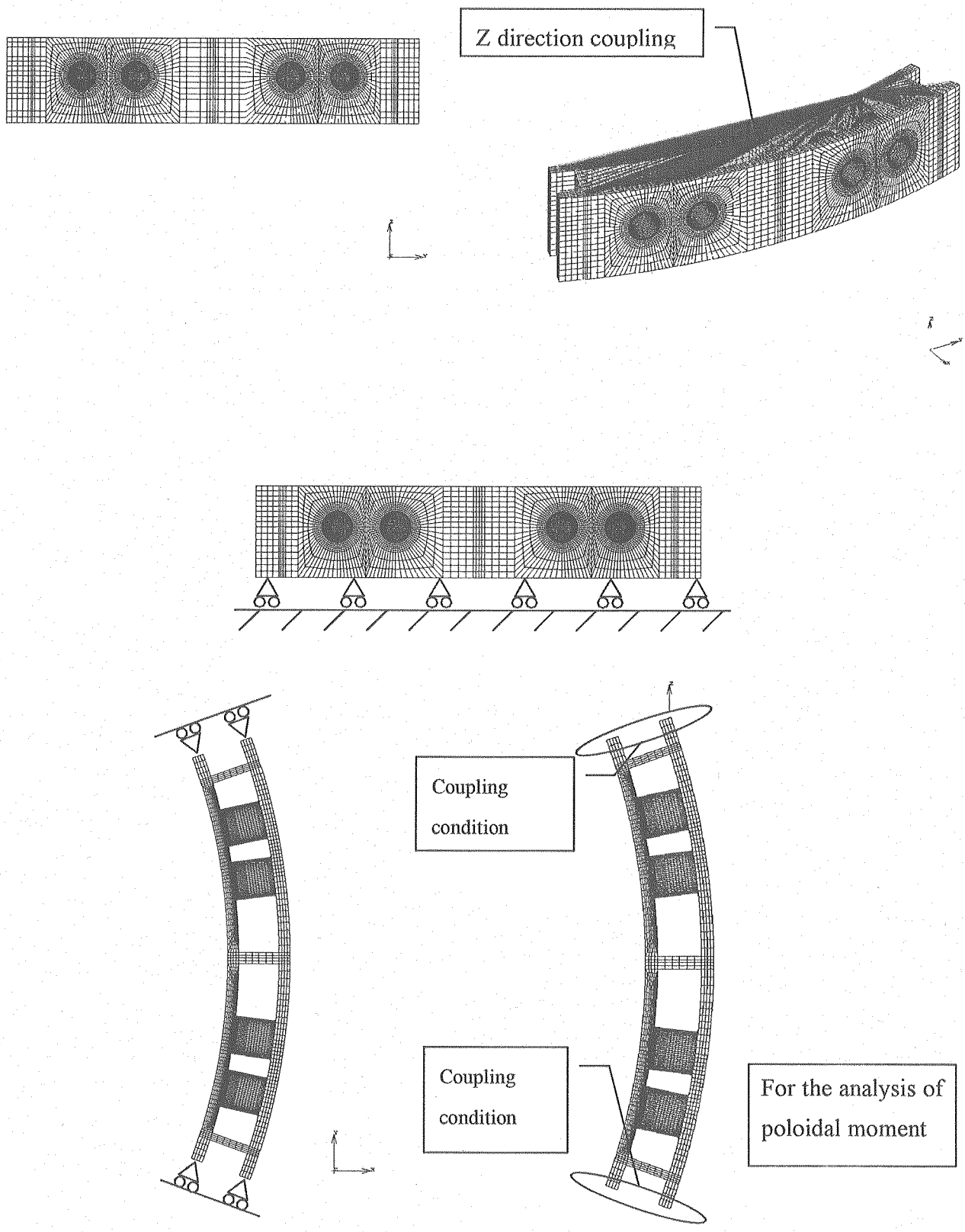

Fig.6.1-7 Boundary conditions of inboard model

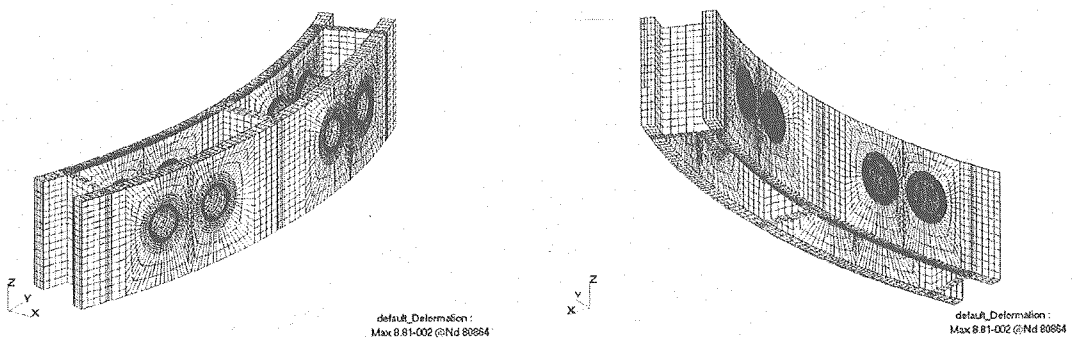

Fig.6.1-8 Deformation due to Coolant Pressure (1.3MPa)

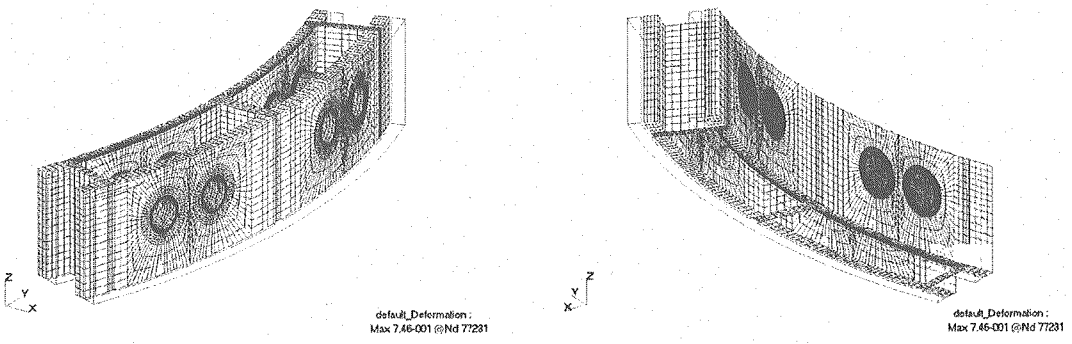

Fig.6.1-9 Deformation in TFCFD event

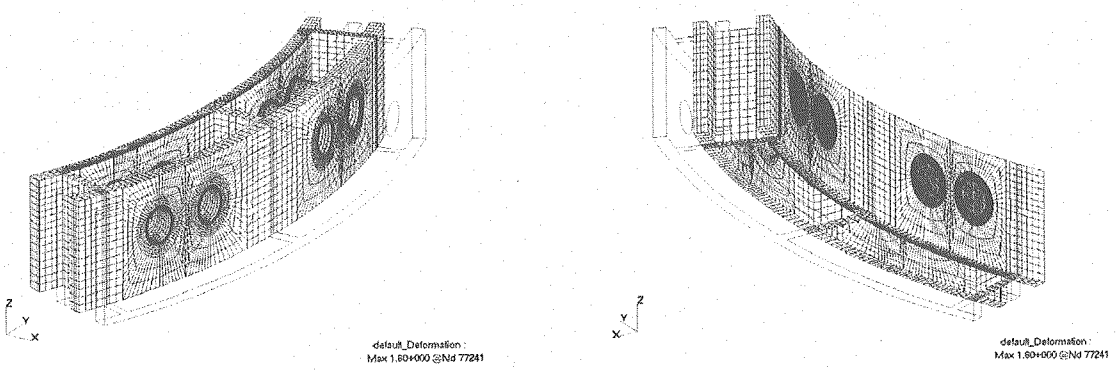

Fig.6.1-10 Deformation due to halo current in VDEIII event (Slow VDE)

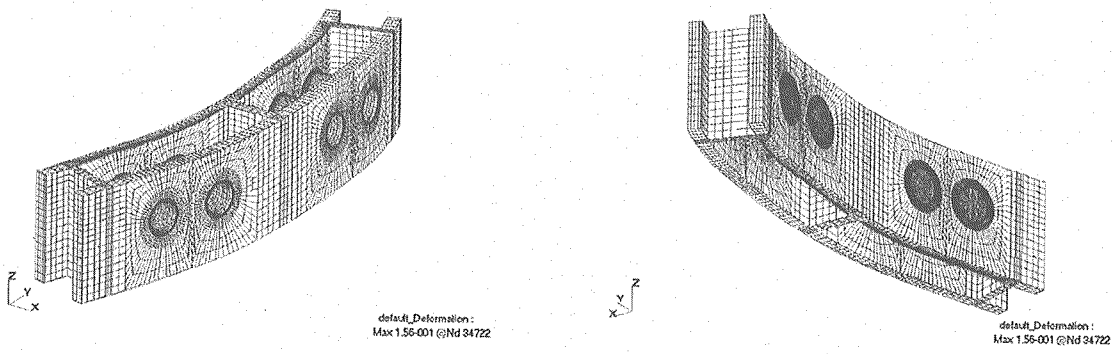

Fig.6.1-11 Deformation due to poloidal moments of blanket (±500kN)

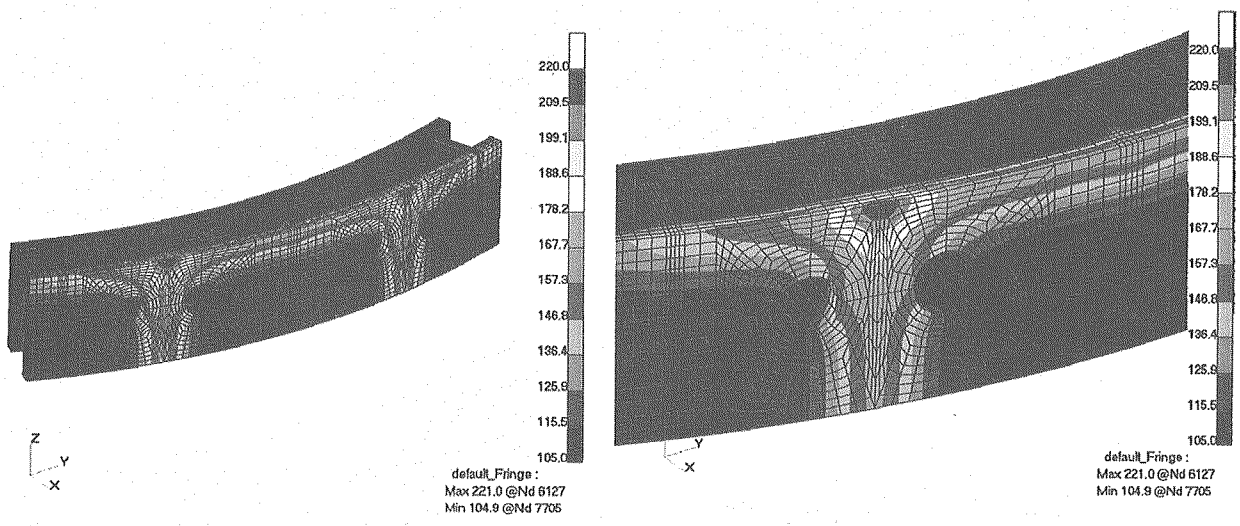

Inner Shell（Plasma side）

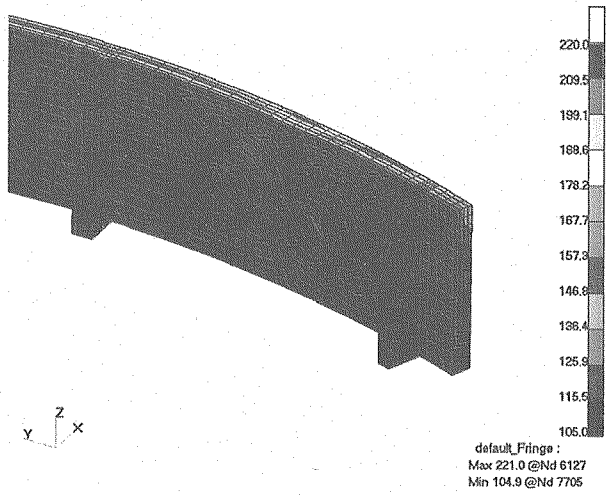

Inner Shell(Back side)

Fig.6.1-12 Temperature distribution of VV

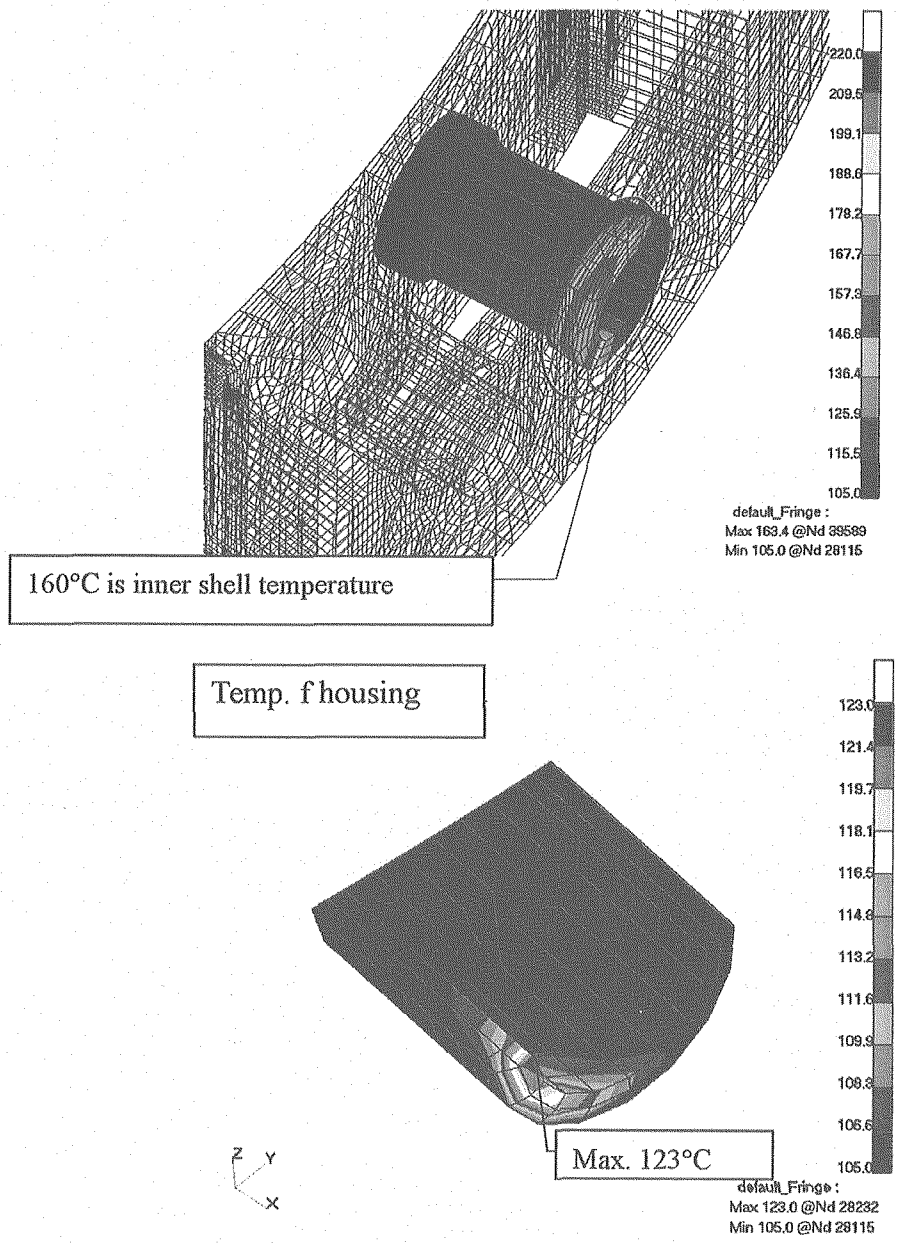

Fig.6.1-13 Temperature distribution of housing

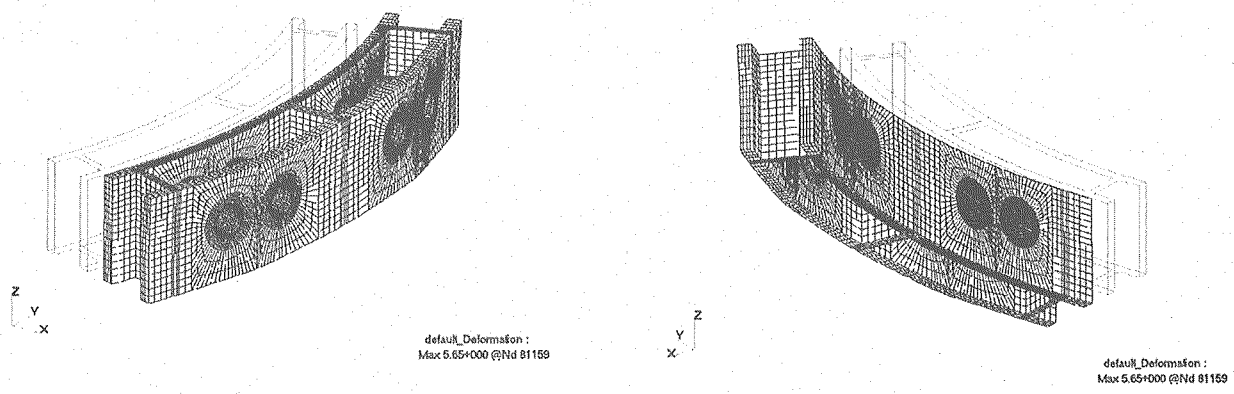

Fig.6.1-14 Deformation due to thermal stress

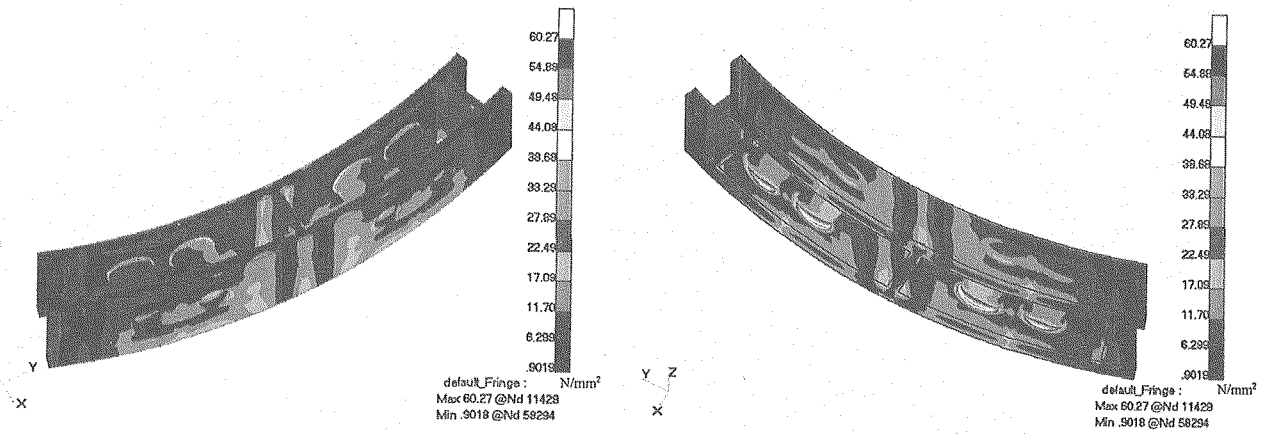

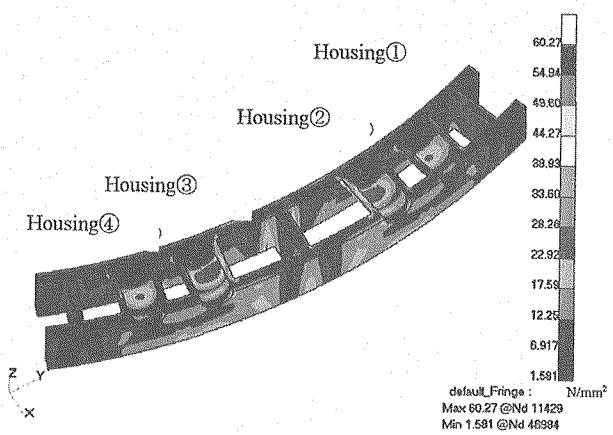

Fig.6.1-15 Tresca stress distribution due to coolant pressure (1.3MPa)

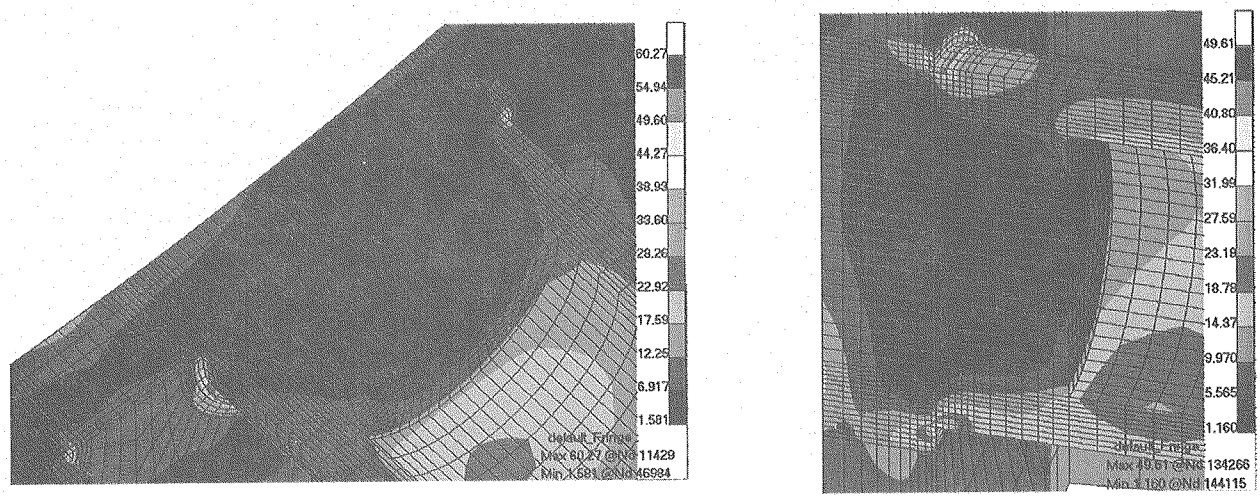

Fig.6.1-16 Tresca stress distributions of housing (1) and outer shell due to coolant pressure (1.3MPa)

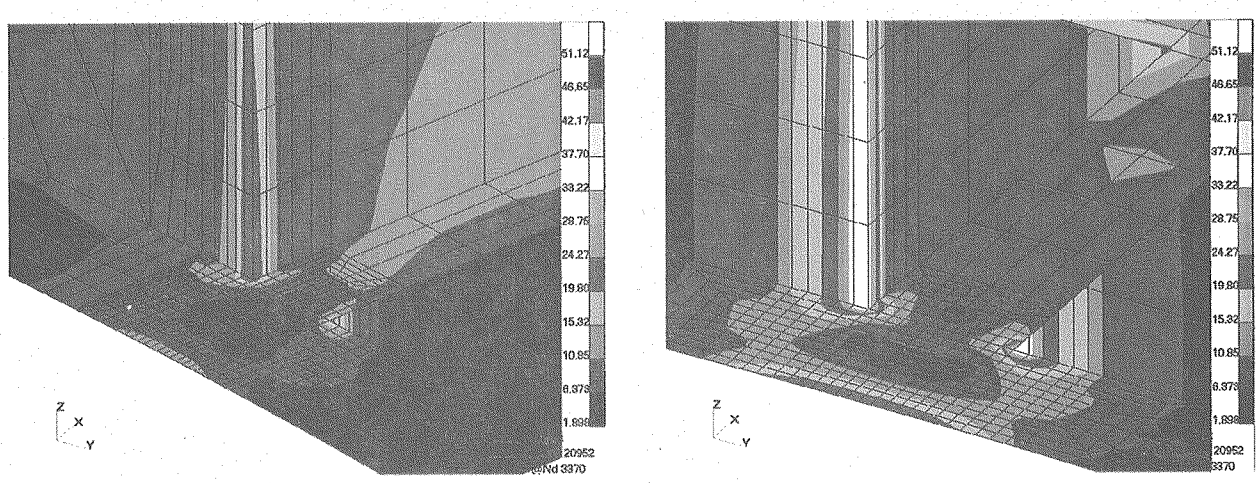

Fig.6.1-17 Tresca stress distributions of poloidal ribs and outer shell due to coolant pressure (1.3MPa)

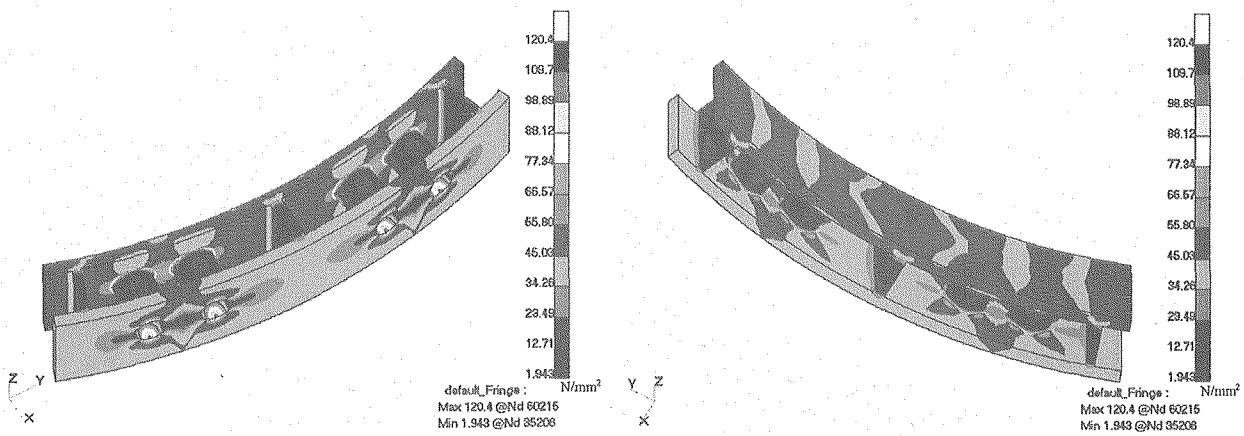

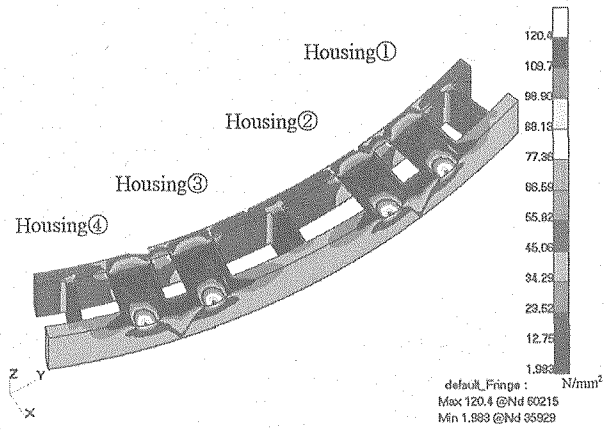

Fig.6.1-18Tresca stress distributions in TFCFD event

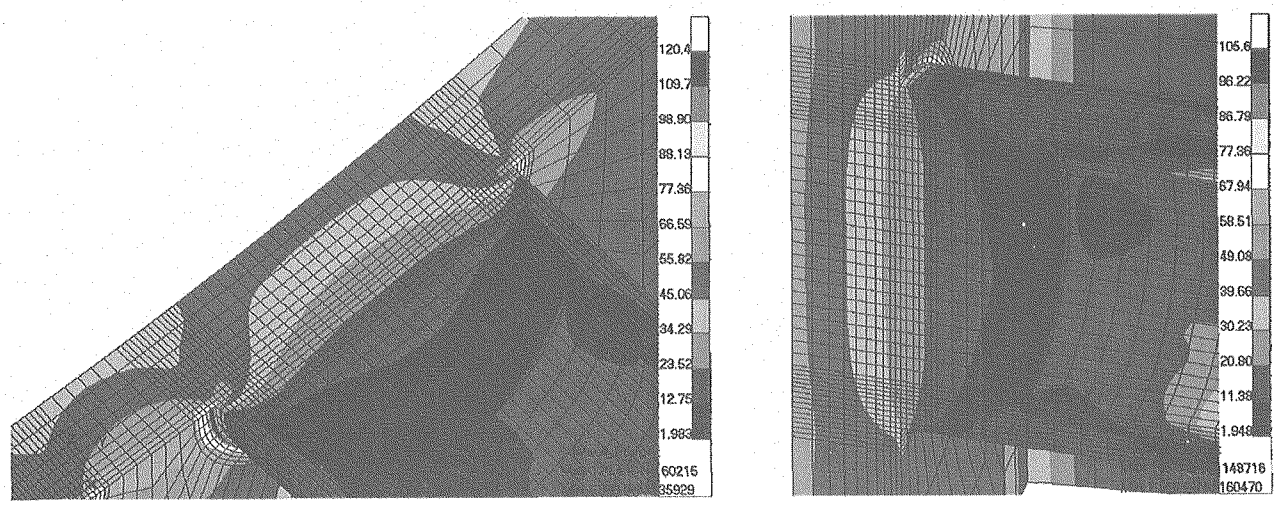

Fig.6.1-19 Tresca stress distributions of housing and outer shell in TFCFD event

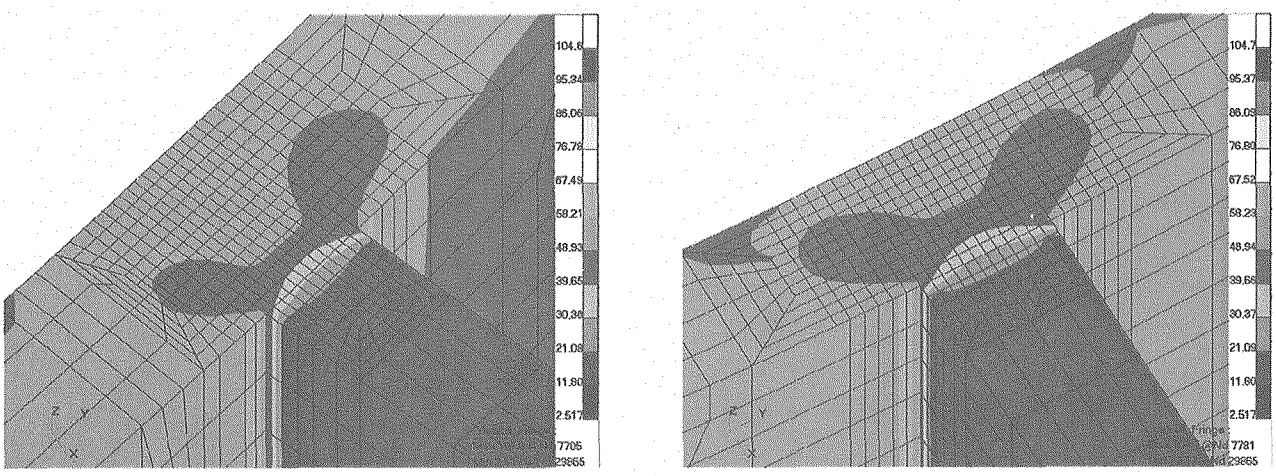

Fig.6.1-20 Tresca stress distributions of poloidal ribs and outer shell in TFCFD event

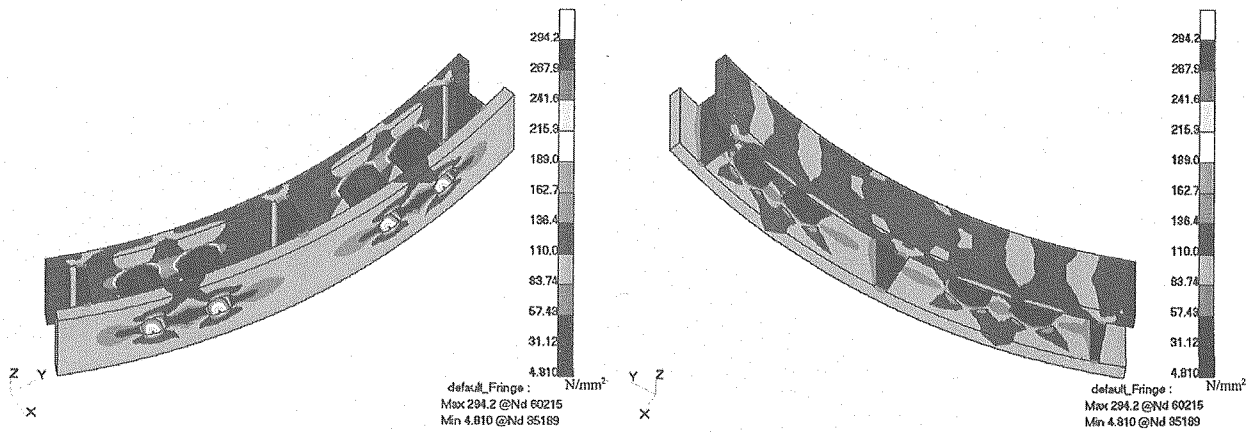

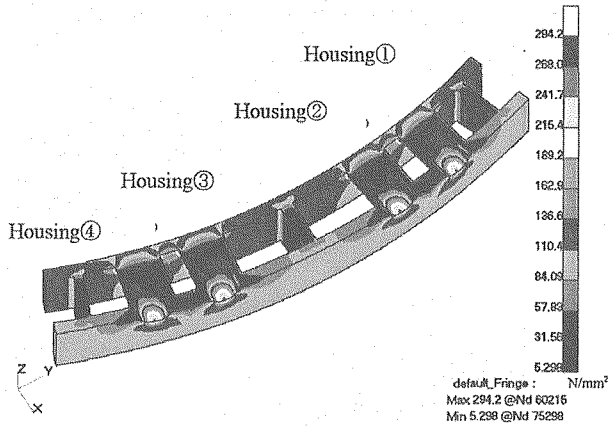

Fig.6.1-21 Tresca stress distribution due to halo current in VDEIII event (Slow VDE)

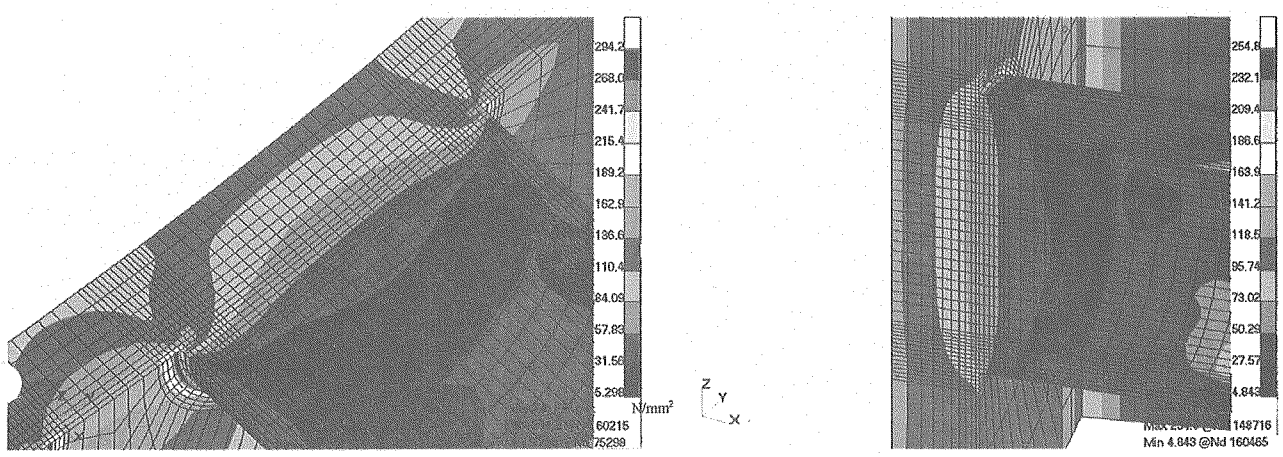

Fig.6.1-22 Tresca stress distributions of housing and outer shell due to halo current in VDEIII event (Slow VDE)

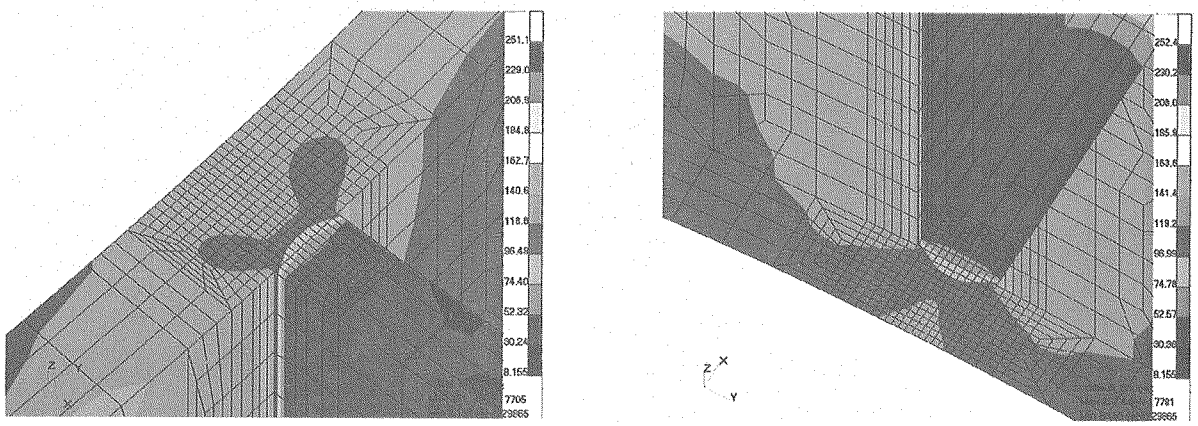

Fig.6.1-23 Tresca stress distributions of ribs and outer shell due to halo current in VDEIII event (Slow VDE)

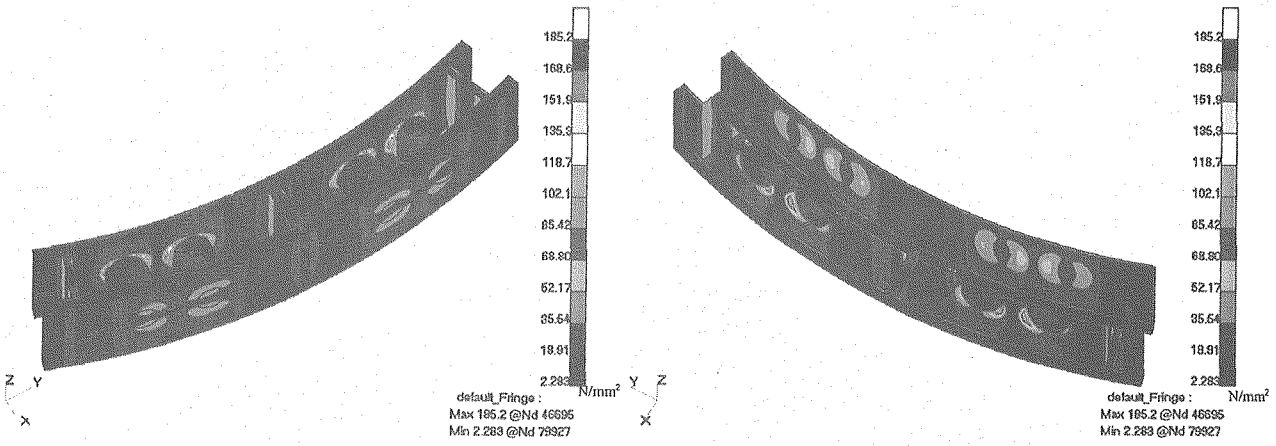

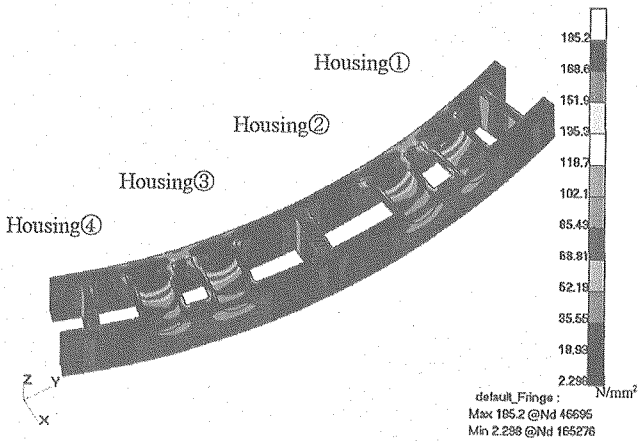

Fig.6.1-24 Tresca stress distribution due to poloidal moments of blankets (±500kN)

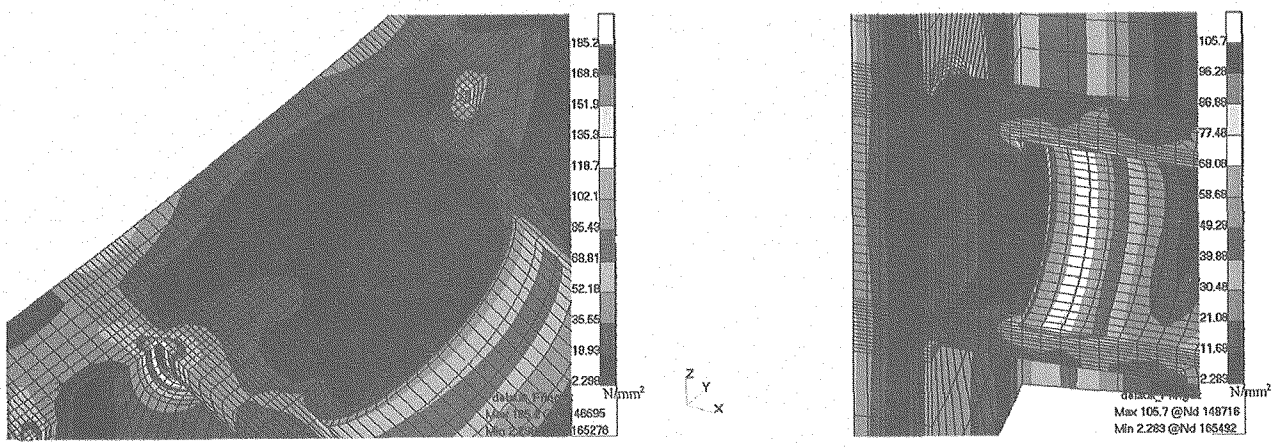

Fig.6.1-25 Tesca stress distribution of housing and outer shell due to poloidal moments of blankets (±500kN)

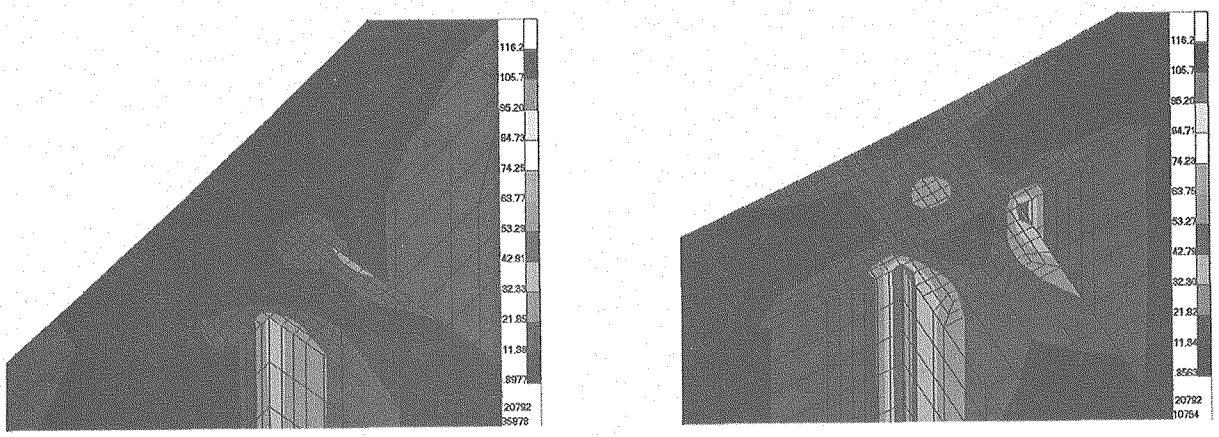

Fig.6.1-26 Tresca stress distribution of ribs and outer shell due to poloidal moments of blankets (±500kN)

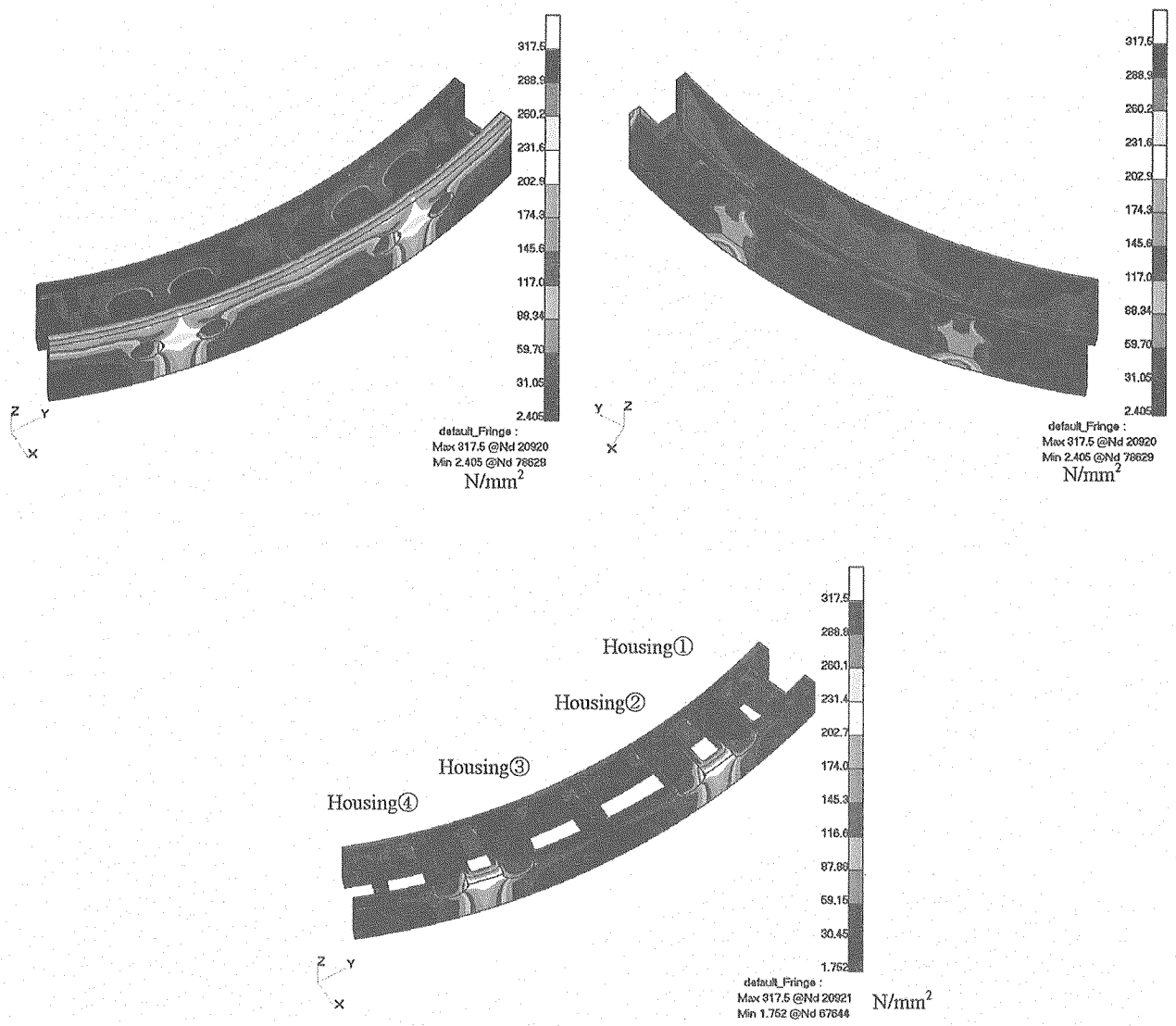

Fig.6.1-27 Tresca stress distribution due to thermal stress

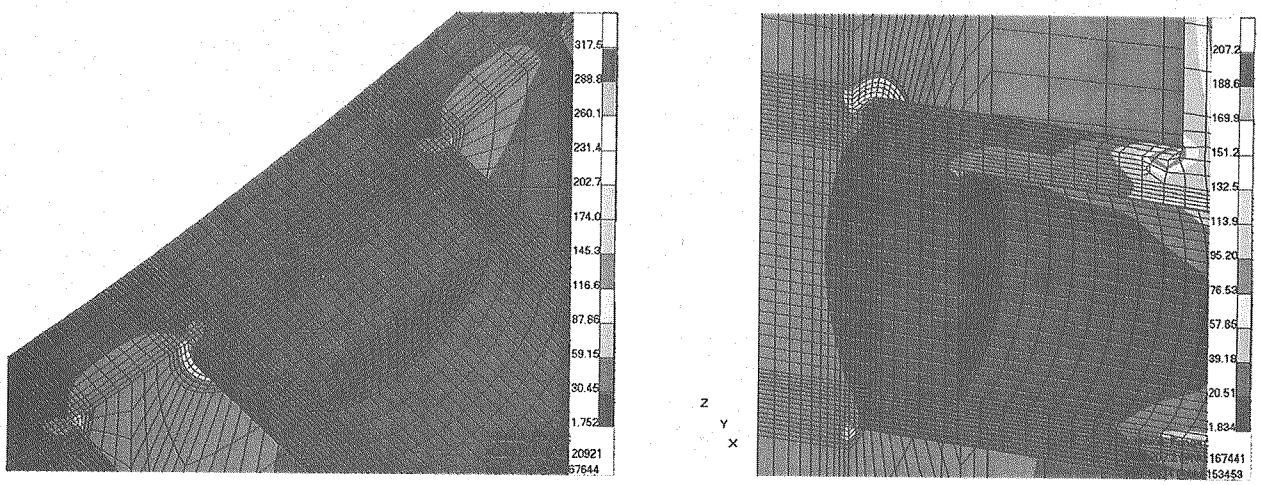

Fig.6.1-28 Tresca stress distributions of housing and outer shell due to thermal stress

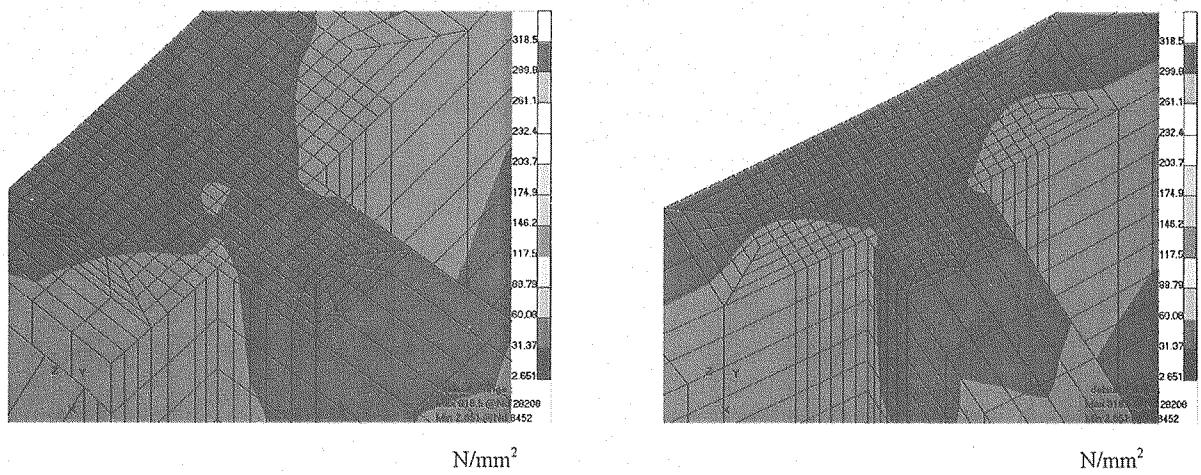

Fig.6.1-29 Tresca stress distributions of ribs and outer shell due to thermal stress

6.2 Allowable crack lengths of plug welds

The allowable un-welded lengths of the plug welds have been estimated by crack propagation analysis in a typical VV inboard region, using membrane and bending stress calculated in the previous section.

6.2.1 Allowable crack lengths of plug welded ribs

Table 6.2-1 shows membrane and bending stresses of ribs for load cycles in the evaluation cross section, shown in Fig.6.2-1. The stresses are obtained by the summation of stress analysis results for each load condition. The stresses in red cells in Table6.2-1 are used to the calculation of critical crack length. Applying 4.3.1(1), (2), the critical crack lengths are calculated, shown in Table6.2-3, where 75 percents of rib thickness is another limit of crack length defined in Rules on Fitness-for-Service for Nuclear Power Plants (JSMES NA1-2002). The limits of 75 percents of rib thickness are smaller than those resulted from collapse loads. Then the critical crack lengths are determined to be the limits of 75 percents of rib thickness.
Assuming initial crack of 0.1mm, crack propagation has been calculated using stress intensity factor of 4.3.5(4) and crack propagation rate of (7). Figs.6.2-4 (a) and (b) show the crack propagation of inboard ribs. The horizontal axis is the multiple number of total design-loading cycles. Though the crack of the center rib propagates fastest, for even the center rib, the multiple number of total design-loading cycles to reach the critical crack length is 132.1 cycles which is fairly large, shown in Fig6.2-4(b). The horizontal axis is the multiple number of total design-loading cycles which are normalized to be one for the total load cycles during ITER lifetime operation. For example, one total design loading cycle means total load cycles of 333282 (=3180+101+1+30000) during ITER lifetime operation. Allowable crack lengths of ribs are summarized in Table 6.2-5. The allowable crack length is the crack length corresponding to the cycles of total design-loading operation cycles minus one operation cycle. The allowable crack lengths of ribs are estimated to be 8.8mm and 12.7mm for a side rib and a center rib, respectively, considering inspection error of 4.4mm. 4.4mm is based on the report that no crack length which exceeded the lower limit of error distribution (mean-2σ) was found in Verification Test about Flaw Detection and Sizing by UT at Nuclear and Industrial Safety Agency in Japan [6-1]. The allowable crack lengths correspond to the allowable un-welded length of plug weld between outer shell and ribs.

6.2.2 Allowable crack length of plug welded housings

For housing, the estimation procedure is the same as that for ribs. Table 6.2-2 shows membrane and bending stresses of housings for load cycles in the evaluation cross section, shown in Figs.6.2-2 and 6.2-3. The stresses in red cells in Table6.2-2 are used to the calculation of critical crack length. Applying 4.3.2(3), the critical crack lengths are calculated, shown in Table6.2-4, where membrane plus bending stress is considered as membrane stress because of the crack model of circumferentially cracked cylinder.. The limits of 75 percents of rib thickness are larger than those corresponding to collapse loads. Then the critical crack lengths are determined to be the limits of collapse load.

Crack propagation has been calculated using stress intensity factor of 4.3.5(5) and crack propagation rate of (7). Fig.6.2-5 shows the crack propagation of housings. The cracks of the four housings propagate similarly. Allowable crack lengths of housings are summarized in Table 6.2-6. The allowable crack lengths of housings are estimated to be 39.5mm considering inspection error of 4.4mm. This means that housings of plug weld with smaller diameter less than 210mm may be applicable.

6.3 Summary

Allowable cracks for the plug weld between outer shell and ribs/housings have been estimated in a typical inboard region. Following results are obtained;

(1) Plug weld for welding between outer shell and ribs/housings in a typical inboard region would be applicable.

(2) Allowable crack length of plug welded ribs are estimated to be 8.8mm and 12.7mm for side rib and center rib, respectively, considering inspection error of 4.4mm.

(3) Allowable crack length of plug welded housings is estimated to be 39.5mm, considering inspection error of 4.4mm. This means that housings with smaller diameter less than 210mm might be applicable.

Reference

[4-1] Application of UT for inspection of pipes etc. in primary loop recirculation system, Nuclear and Industrial Safety Agency in Japan, July, 2004.

Table 6.2-1 Membrane and bending stresses in the evaluation cross section of ribs [MPa]

Cycle		3180				101		1		30000
Load case		Coolant pr +MD +Moment	Coolant pr +MD −Moment	Coolant pr +VDEII +Moment	Coolant pr +VDEII −Moment	Coolant pr +VDEII +Moment +TFCFD	Coolant pr +VDEII −Moment +TFCFD	Coolant pr +VDEIII +Moment	Coolant pr +VDEIII −Moment	Thermal stress (Nuclear Heat)
Rib 1−3	M	7.40	12.60	6.25	10.15	5.15	5.45	4.90	10.10	11.20
	M+B	34.30	−14.30	28.15	−8.30	29.15	−8.40	34.20	−14.40	13.50
	M+B	−19.60	39.60	−15.80	28.60	−18.90	19.30	−24.60	34.60	9.00
Rib 2−3	M	10.30	10.30	7.58	7.58	5.98	0.38	6.50	6.50	11.20
	M+B	57.50	−36.90	42.98	−27.83	41.38	−35.03	53.70	−40.70	11.20
	M+B	−36.90	57.50	−27.83	42.98	−29.43	35.78	−40.70	53.70	11.20
Rib 3−3	M	12.60	7.40	10.15	6.25	9.05	1.55	10.10	4.90	11.20
	M+B	39.00	−20.20	28.00	−16.40	24.90	−25.70	34.00	−25.20	9.00
	M+B	−13.70	34.90	−7.70	28.75	−6.70	28.65	−13.80	34.80	13.50

*M: Membrane stress, M+B: Membrane and bending stresses

**Moment is the poloidal moment of blanket modules

Table 6.2-2 Membrane and bending stresses in the evaluation cross section of housings [MPa]

Cycle		3180				101		1		30000
Load case		Coolant pr +CD +Moment	Coolant pr +CD −Moment	Coolant pr +VDEII +Moment	Coolant pr +VDEII −Moment	Coolant pr+VDEII +Moment +TFCFD	Coolant pr +VDEII −Moment +TFCFD	Coolant pr +VDEIII +Moment	Coolant pr +VDEIII −Moment	Thermal stress
ハウジング①	M	20.09	−16.65	14.35	−13.21	13.34	−14.21	18.49	−18.24	2.50
	M+B	6.25	−0.12	5.39	0.61	5.38	0.60	6.16	−0.22	−0.30
	M+B	33.93	−33.17	23.31	−27.02	21.35	−28.98	30.83	−36.27	5.30
ハウジング②	M	−14.69	22.06	−10.77	16.79	−11.13	16.42	−15.62	21.12	3.00
	M+B	−34.57	32.34	−27.45	22.73	−28.72	21.46	−36.30	30.62	4.90
	M+B	5.19	11.77	5.92	10.85	6.45	11.39	5.06	11.63	1.10
ハウジング③	M	22.07	−14.66	16.80	−10.75	16.43	−11.12	21.13	−15.60	3.00
	M+B	11.79	5.21	10.86	5.93	11.40	6.46	11.64	5.06	1.10
	M+B	32.34	−34.54	22.73	−27.43	21.46	−28.70	30.61	−36.27	4.90
ハウジング④	M	−16.65	20.09	−13.20	14.35	−14.21	13.35	−18.24	18.50	2.50
	M+B	−33.18	33.93	−27.02	23.31	−28.98	21.36	−36.27	30.84	5.30
	M+B	−0.13	6.25	0.61	5.39	0.57	5.35	−0.21	6.17	−0.30
ハウジング⑤	M	5.50	6.69	4.77	5.67	4.54	5.43	4.29	5.47	3.60
	M+B	1.07	5.07	0.87	3.88	0.55	3.56	0.10	4.11	5.50
	M+B	9.93	8.31	8.68	7.46	8.52	7.30	8.47	6.84	1.70
ハウジング⑥	M	8.22	6.07	6.90	5.29	6.60	4.98	6.76	4.61	4.00
	M+B	5.94	0.81	4.45	0.60	4.01	0.16	4.76	−0.37	6.40
	M+B	10.50	11.33	9.35	9.97	9.18	9.81	8.76	9.59	1.50
ハウジング⑦	M	6.07	8.22	5.29	6.90	4.98	6.60	4.61	6.76	4.00
	M+B	0.81	5.94	0.60	4.45	0.16	4.01	−0.37	4.76	6.40
	M+B	11.33	10.50	9.97	9.35	9.81	9.18	9.59	8.76	1.50
ハウジング⑧	M	6.69	5.50	5.67	4.77	5.43	4.54	5.47	4.29	3.60
	M+B	5.07	1.07	3.88	0.87	3.56	0.55	4.11	0.10	5.50
	M+B	8.31	9.93	7.46	8.68	7.30	8.52	6.84	8.47	1.70

*M: Membrane stress, M+B: Membrane and bending stresses

**Moment is the poloidal moment of blanket module

Table 6.2-3 Critical crack length of ribs

Evaluation cross section of ribs	Rib thickness [mm]	Crack length corresponding to 75% of rib thickness* [mm]	Critical crack length corresponding to collapse load [mm]	Critical crack length [mm]
1-3	40	15	17.4	15
2-3	60	22.5	25.5	22.5
3-3	40	15	17.4	15

*75% of rib thickness is defined as the limit in Rules on Fitness-for-Service for Nuclear Power Plants (JSMES NA1-2002)

Table 6.2-4 Critical crack length of housings

Evaluation cross section of housings	Housing radius [mm]	Crack length corresponding to 75% of housing radius* [mm]	Critical crack length corresponding to collapse load [mm]	Critical crack length [mm]
1	105	78.8	44.0	44.0
2			44.0	44.0
3			44.0	44.0
4			44.0	44.0

*75% of rib thickness is defined as the limit in Rules on Fitness-for-Service for Nuclear Power Plants (JSMES NA1-2002)

Table 6.2-5 Allowable crack length of ribs

Rib		1. Side rib	2. Center rib	3. Side rib
Thickness [mm]		40	60	40
Critical crack	Crack length [mm]	15	22.5	15
	Multiple number of total design loading cycles (MDLC)	303.4	132.1	313.6
Allowable crack	Multiple number of total design loading cycles - 1 (MDLC-1) cycles	302.4	131.1	312.6
	Crack length corresponding to (MDLC-1) cycles [mm]	13.2	17.1	13.2
	Allowable crack length considering inspection error (4.4mm)* [mm]	8.8	12.7	8.8

*4.4mm is based on the report that no crack length which exceeded the lower limit of error distribution (mean-2σ) was found in Verification Test about Flaw Detection and Sizing by UT at Nuclear and Industrial Safety Agency in JA.

Table 6.2-6 Allowable crack length of housings

Housing		1	2	3	4
Radius [mm]		105	105	105	105
Critical crack	Crack length [mm]	44.0	44.0	44.0	44.0
	Multiple number of total design loading cycles (MDLC)	818.4	841.1	844.0	816.4
Allowable crack	Multiple number of total design loading cycles - 1 (MDLC-1) cycles	817.4	840.1	843.0	815.4
	Crack length corresponding to (MDLC-1) cycles [mm]	43.9	43.9	43.9	43.9
	Allowable crack length considering inspection error (4.4mm)* [mm]	39.5	39.5	39.5	39.5

*4.4mm is based on the report that no crack length which exceeded the lower limit of error distribution (mean-2σ) was found in Verification Test about Flaw Detection and Sizing by UT at Nuclear and Industrial Safety Agency in JA.

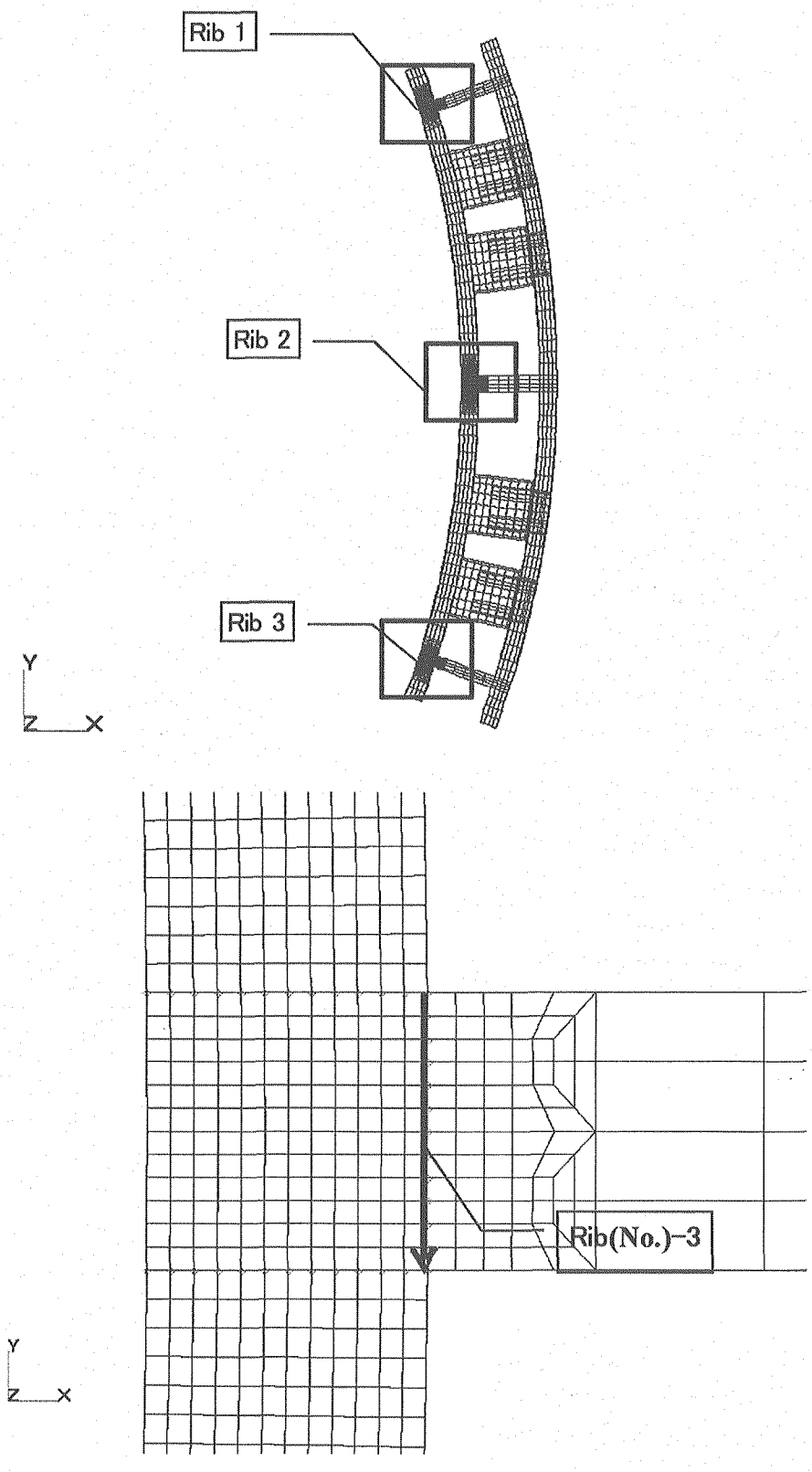

Fig.6.2-1 Evaluation cross section of crack propagation for the rib

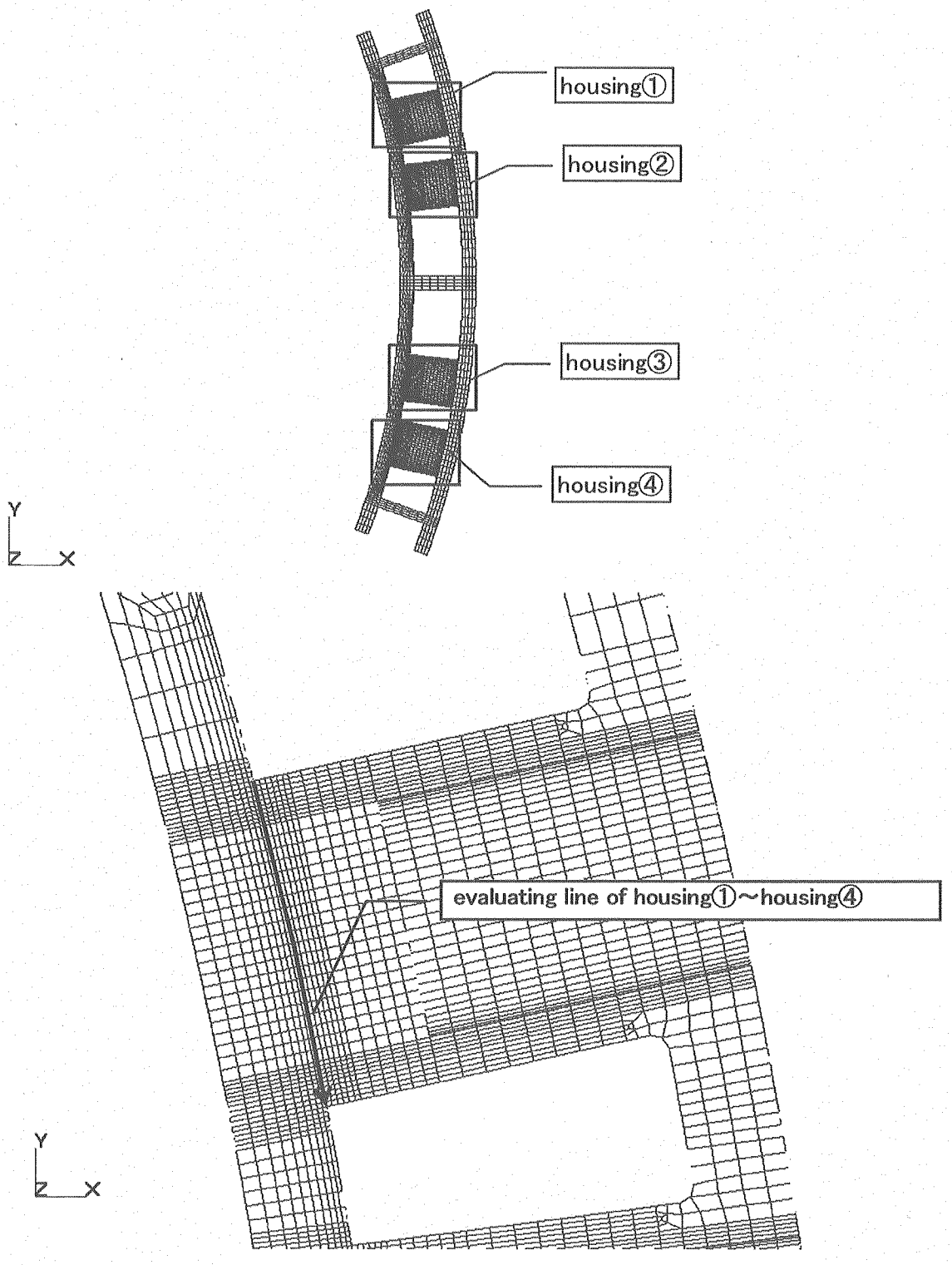

Fig.6.2-2 Evaluation cross section of crack propagation for the housings (Toroidal direction)

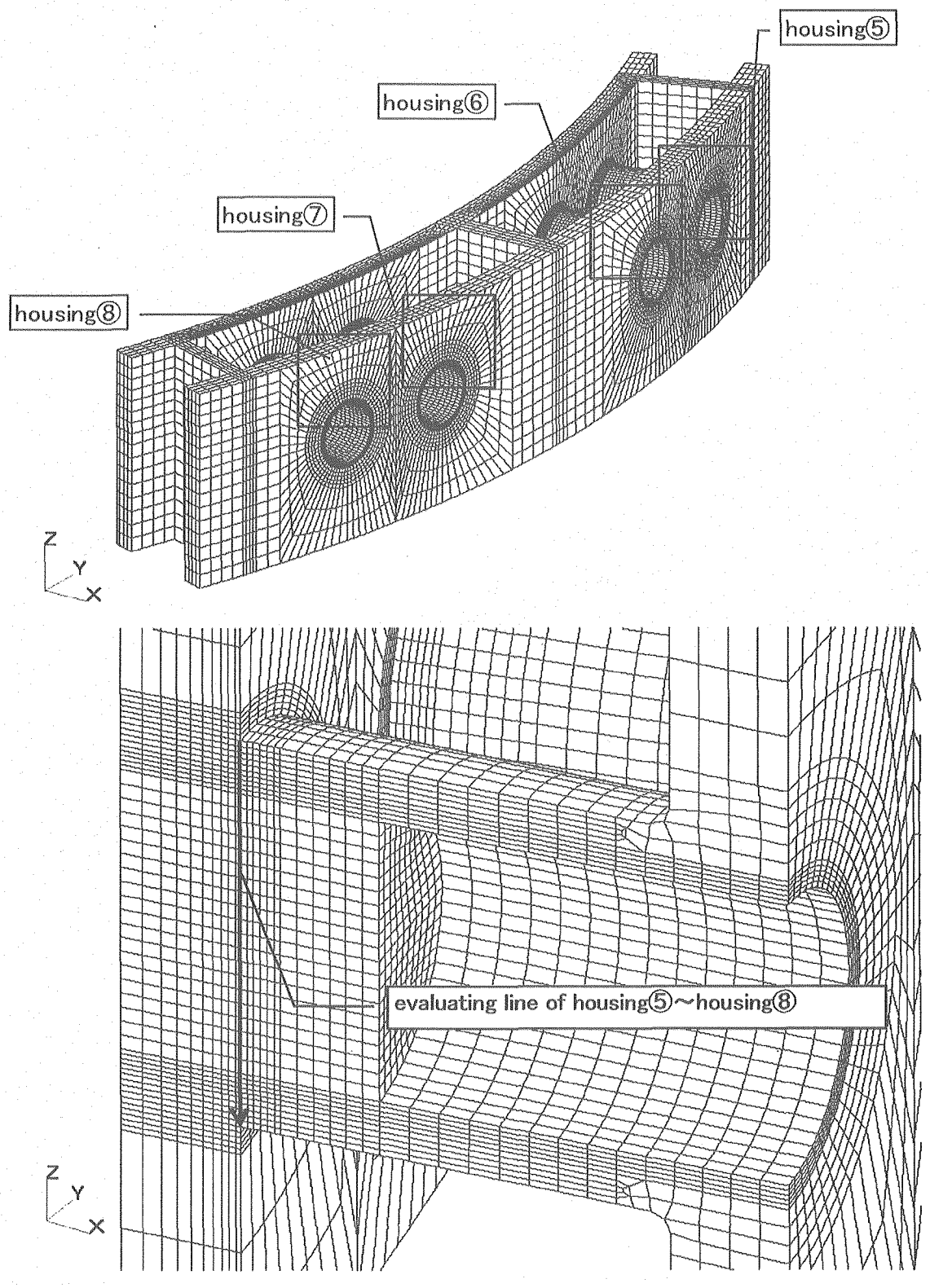

Fig.6.2-3 Evaluation cross section of crack propagation for housing (Vertical direction)

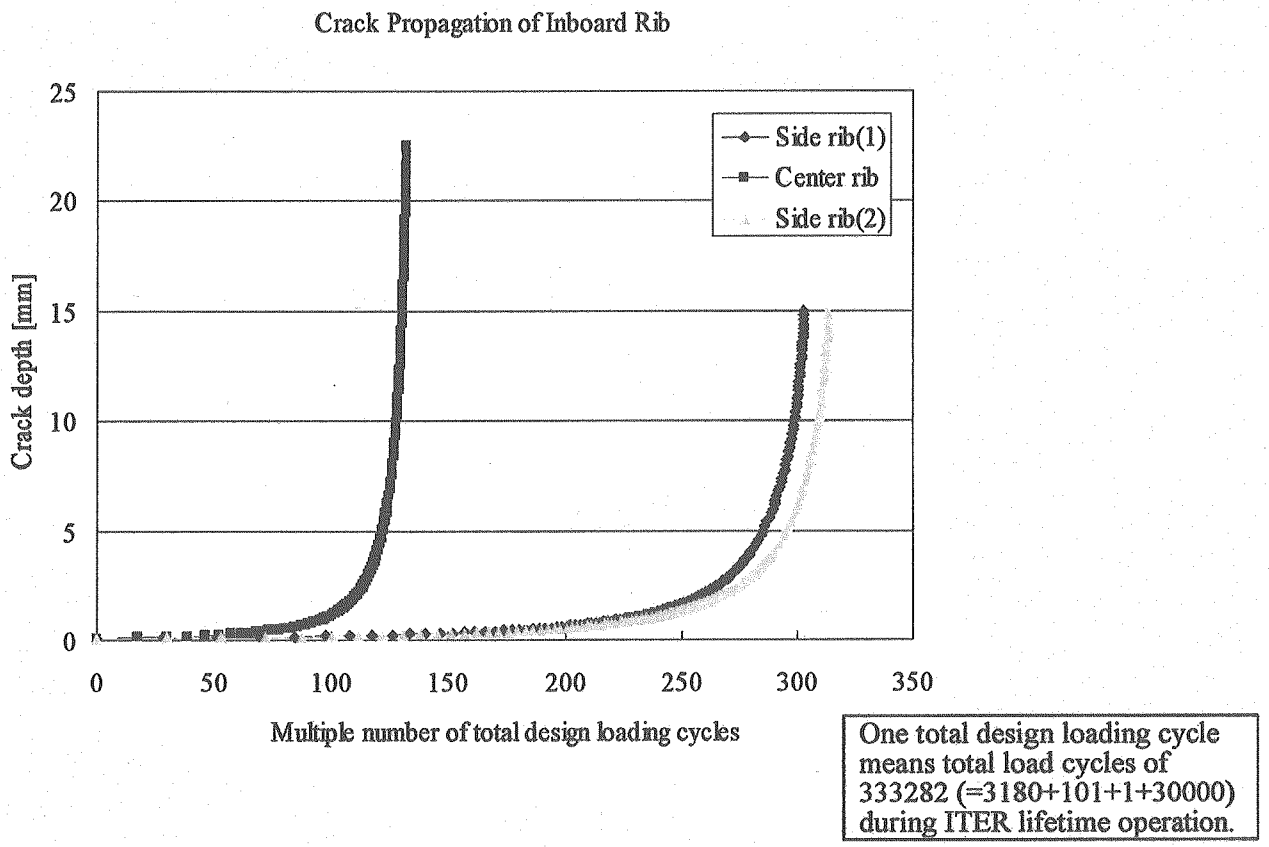

Fig.6.2-4(a) Crack propagation of inboard ribs

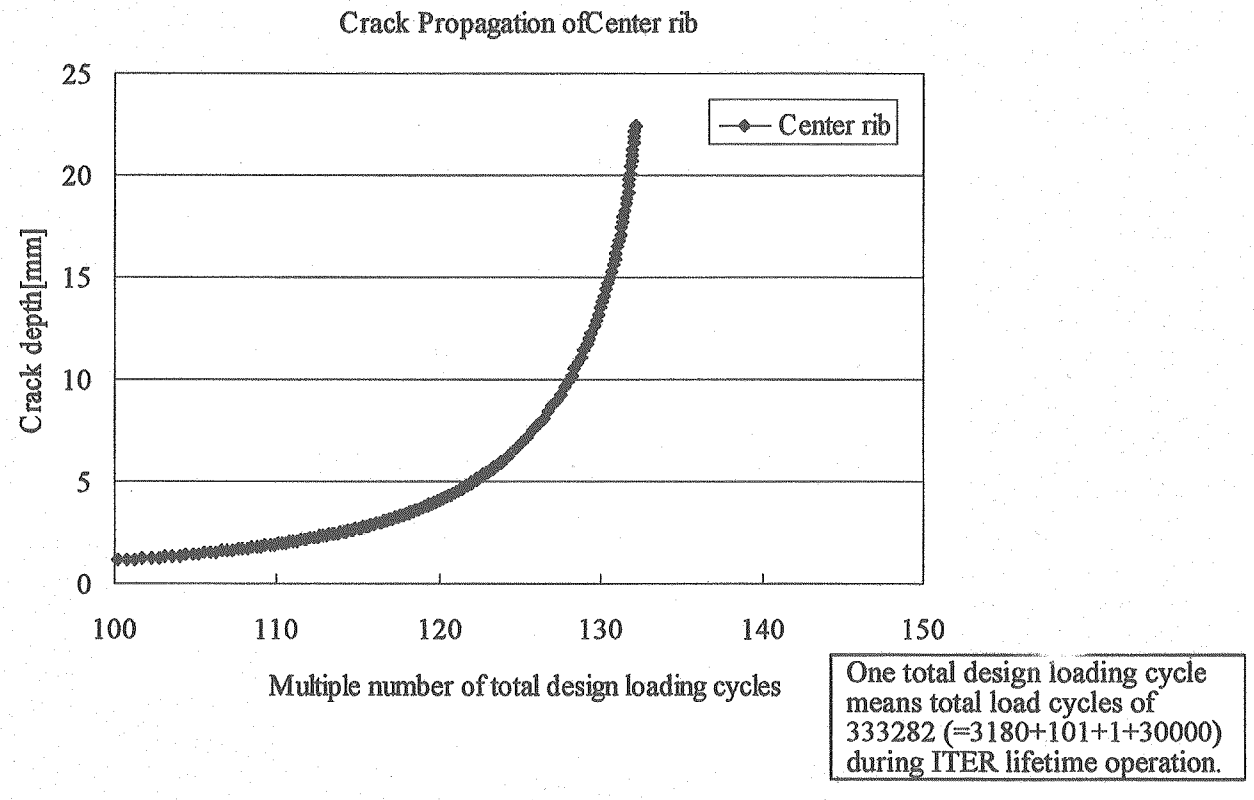

Fig.6.2-4(b) Crack propagation of inboard ribs

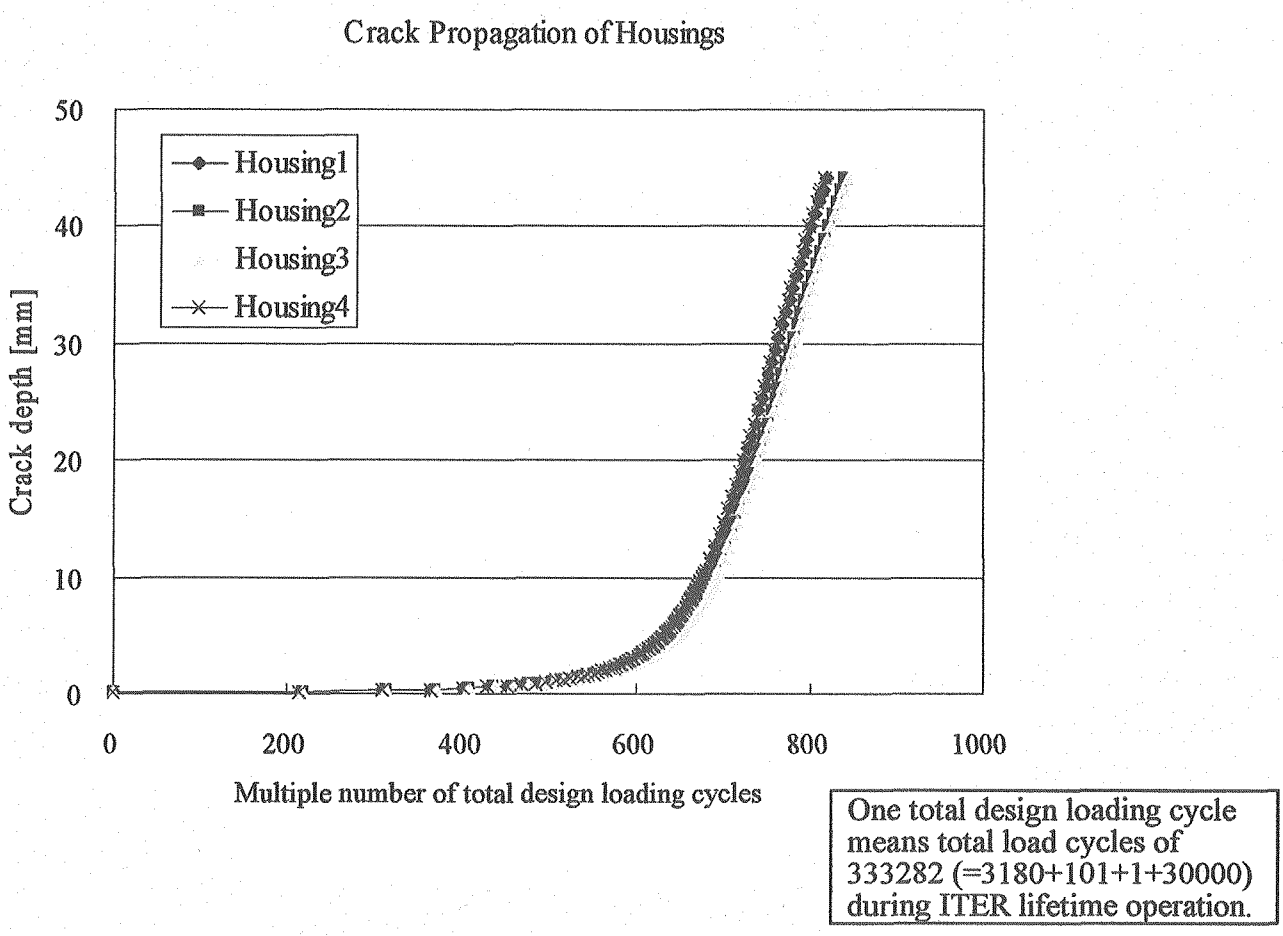

Fig.6.2-5 Crack propagation of inboard housings

7. Crack propagation of inboard upper curved region

From the results of the stress analysis for the whole VV structure in Sec.5.2, high stress regions for toroidal and poloidal ribs are inboard upper region and the lateral side of the lower port. High stresses for housings are produced at No.7 and No.8 blanket housings. Therefore the inboard upper region is selected for detail stress analysis for crack propagation assessment of both ribs and housings.

7.1 Detail stress analyses of inboard curved region

7.1.1 Analysis model

The inboard upper region for detail stress analysis is shown in Figs.7.1.1-1 and 7.1.1-2. The region enclosed blue chain line in Figs.7.1.1-1and 7.1.1-2 is the region of detail stress analysis. The region enclosed bold line is modeled by solid elements and the other regions are by shell elements. Figs.7.1.1-3 and 7.1.1-4 show mesh patterns of the zooming analysis. In solid element region, all of the ribs, housings and VV shells are modeled by solid elements. The connection between of solid and shell elements in the shell-thickness direction is shown in Fig.7.1.1-5. The node of the shell edge has translations and rotations, while those of solid edge have translations only. The solid edge node of thickness center is connected to that of shell edge with regard to all translations. Other solid edge nodes are connected to it with radial and circumferential translations and connected to adjacent nodes by rigid bars, shown in Fig.7.1.1-5.

7.1.2 Analysis conditions

(1) Load conditions

EM loads of solid elements in the detail stress analysis are converged using volume forces of elements as follows, shown in Fig.7.1.2-1

(1) Volume forces of tentative solid elements are calculated from the nodal forces in the global analysis model

(2) The volumetric forces of the elements in the detail analysis are calculated using volume force of tentative solid elements by interpolation

Thermal load is calculated as follows.

(1) For solid element region; thermal analyses have been carried out using nuclear heating condition, shown in Fig7.1.2-2.

(2) For shell element regions, temperatures of integration points of the inner shell are inputted from the results of thermal analyses, shown in Fig7.1.2-3.

(3) For outer shell, ribs and housings, temperature of 105 °C is inputted from the results of thermal analyses, shown in Fig7.1.2-3.

(2) Boundary conditions

Boundary conditions for coolant pressure and EM load are shown in Fig.7.1.2-4. The conditions of the edges in toroidal direction are cyclic symmetry. The results of the global analyses are used for the displacements of the edges in poloidal direction. Fig.7.1.2-5 shows the boundary conditions of thermal analysis. The conditions of the edges in toroidal direction are cyclic symmetry. The conditions of the edge displacements in poloidal direction are sliding.

(3) Material properties

Young's modulus and Poisson ratio of the VV structure material are 200GPa and 0.29, respectively. Thermal conductivity is 15.1W/mK. The thermal transfer coefficient in cooling sides of VV shells is 500W/m^{2}K.

7.1.3 Analysis results

For assessment of the detail stress analyses, following items between the results of global and detail stress analyses are checked;

(1) No difference of the stress distributions

(2) No difference of the displacement distributions

(3) Continuity at the connection between solid and shell elements

From Fig.7.1.3-1 to Fig.7.1.3-5 show the comparison between the results of the global and detail analyses. Mises stresses and displacements of VV structures are compared in the figures. Overall stress and displacement distributions agree with the corresponding stress analysis results. Fig.7.1.3-6 is the temperature distributions for thermal stress analysis. Thermal analysis has been performed for solid element inner shell and uniform temperature of 105 °C is given for ribs, housings and outer shell. Fig.7.1.3-7 shows stress distribution and deformations due to thermal stress. Stresses in outer shell are smaller than those in inner shells. Fig.7.1.3-8 shows the connection between solid and shell elements is effective in the continuity of the element-edge angle.

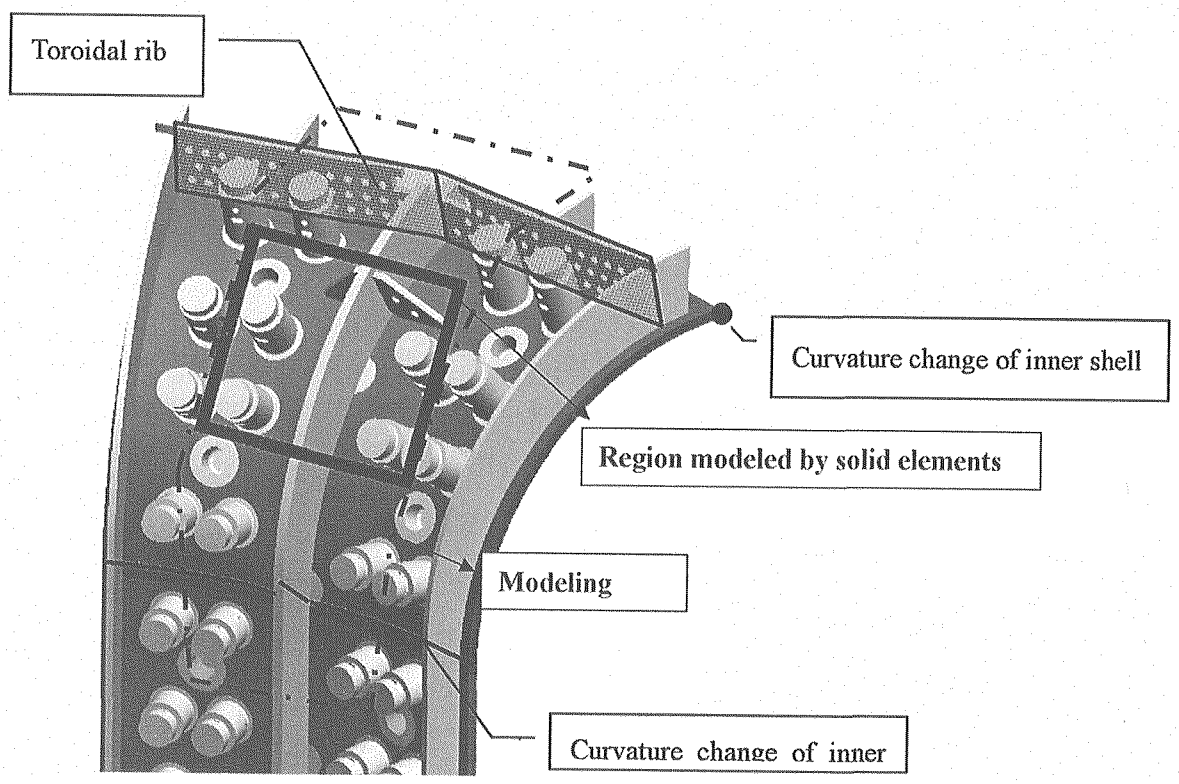

Fig. 7.1.1-1 Region of detail stress analysis

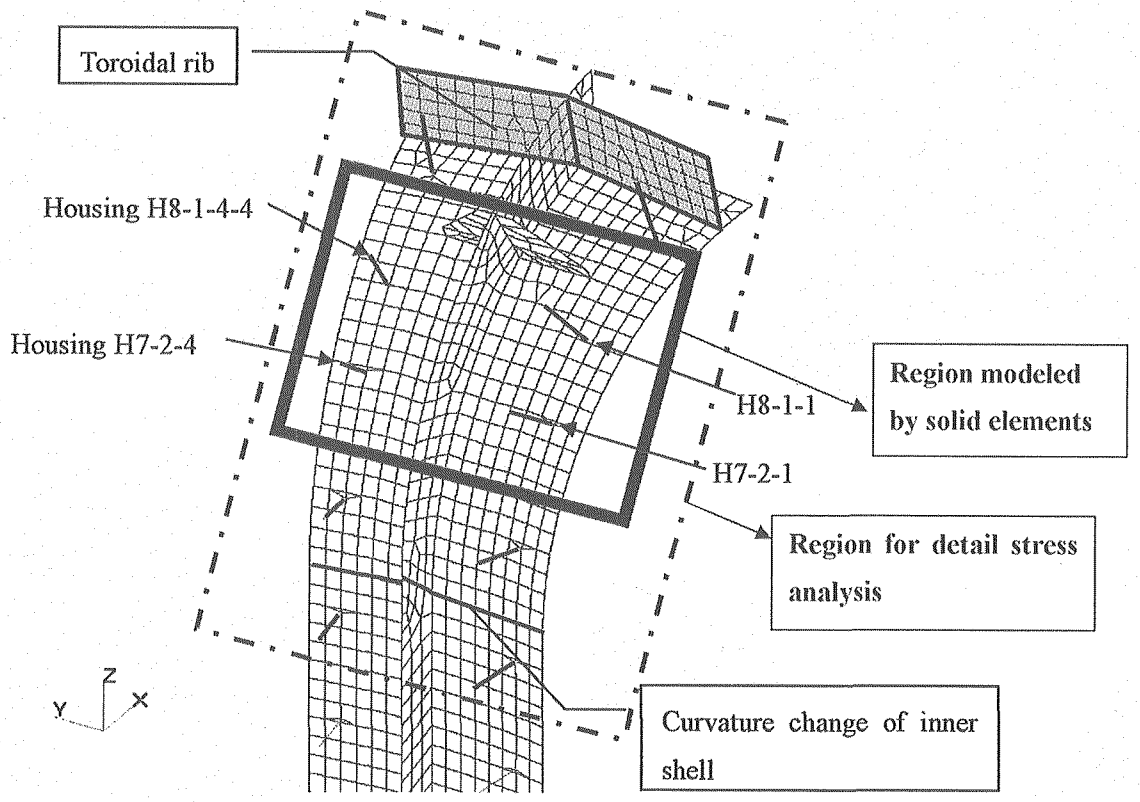

Fig. 7.1.1-2 Region of detail stress analysis

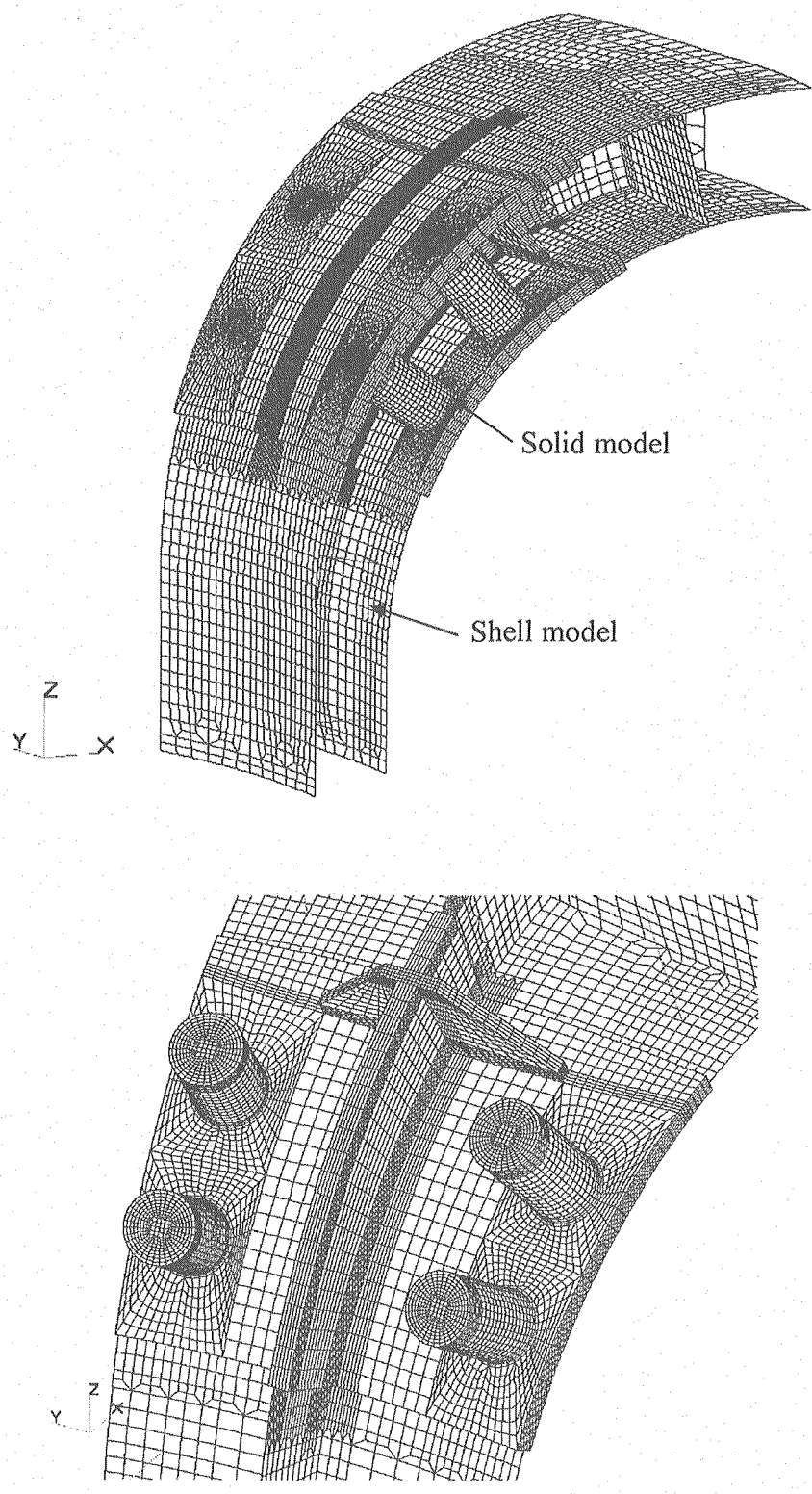

Fig. 7.1.1-3 Mesh pattern of detail stress analysis

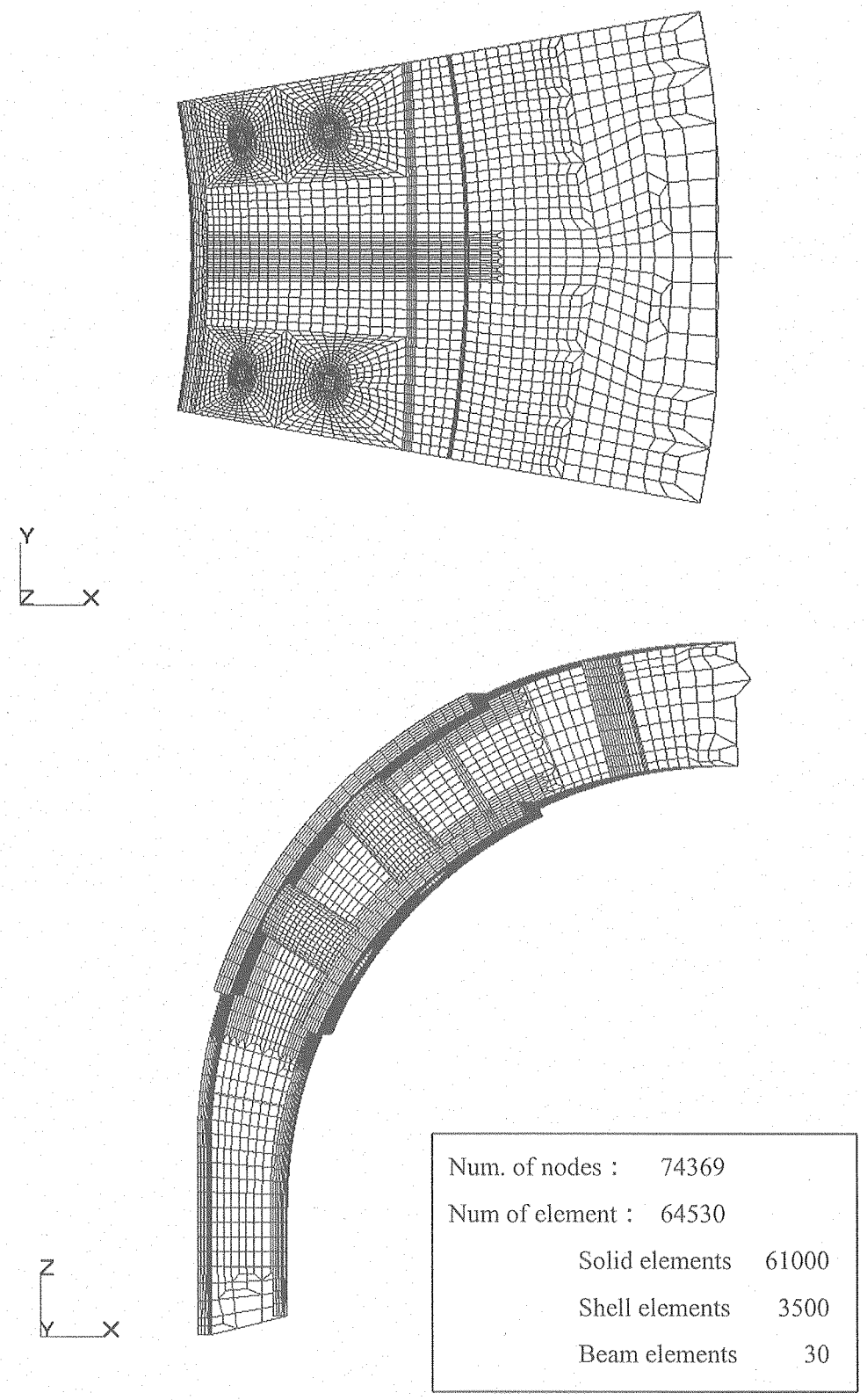

Fig. 7.1.1-4 Mesh pattern of detail stress analysis

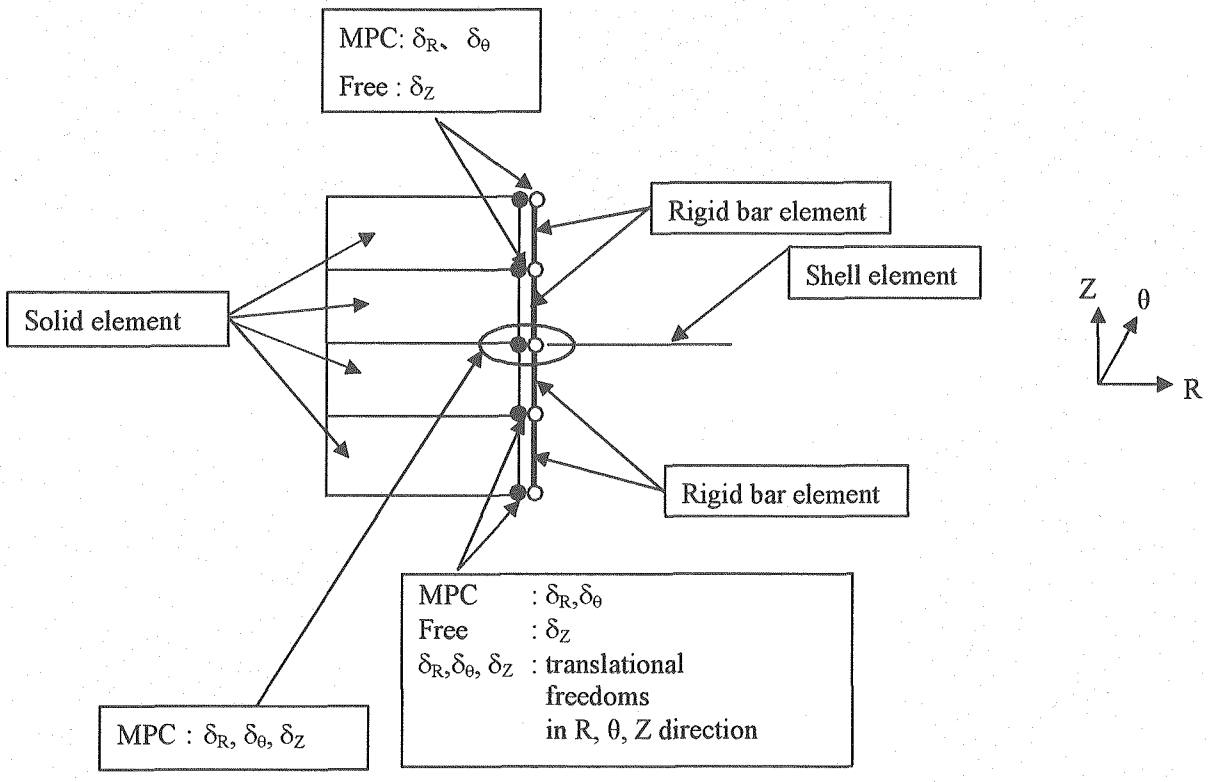

Fig. 7.1.1-5 Connection between solid and shell elements in the shell-thickness direction

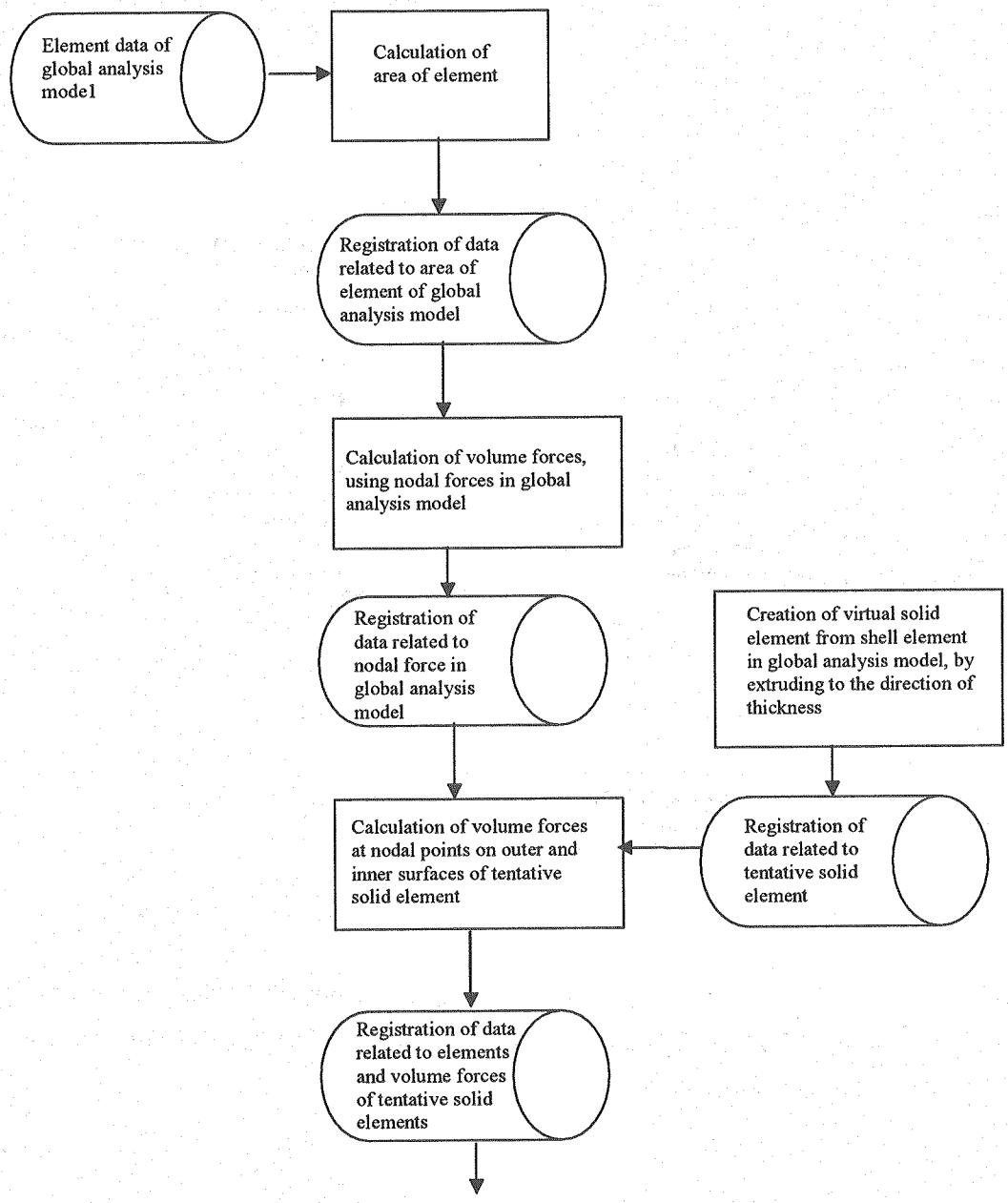

Fig. 7.1.2-1(1/2) Conversion of nodal forces in global analysis model to volume forces in detailed analysis model (Flow chart of model force data conversion)

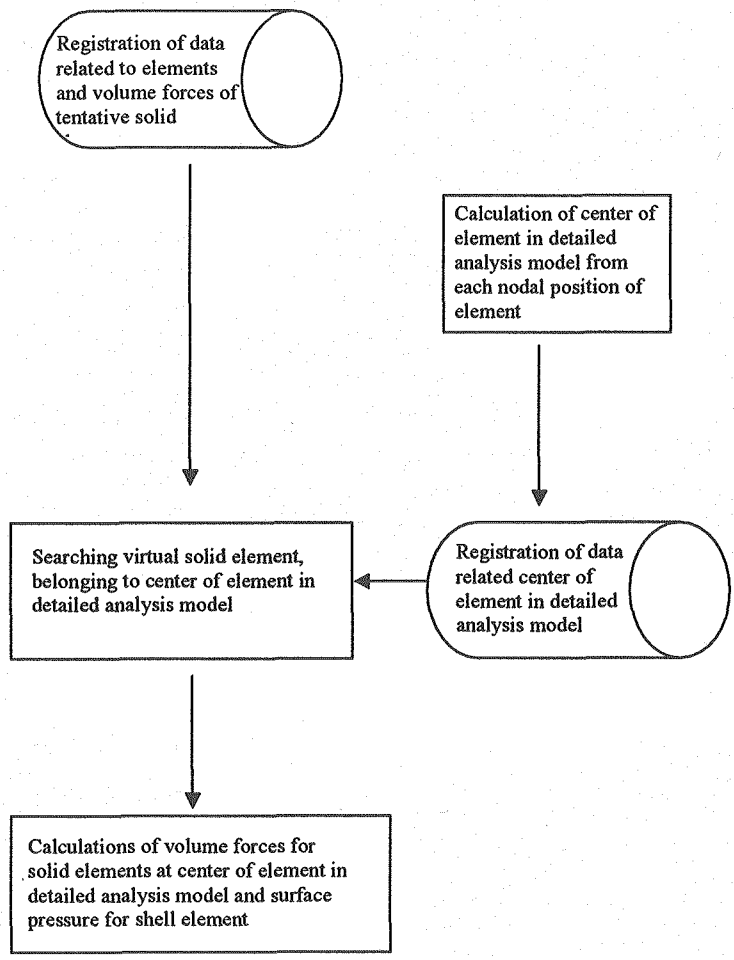

Fig. 7.1.2-1(2/2) Conversion of nodal forces in global analysis model to volume forces in detailed analysis model (User subroutine and special function in MARC used for force data conversion)

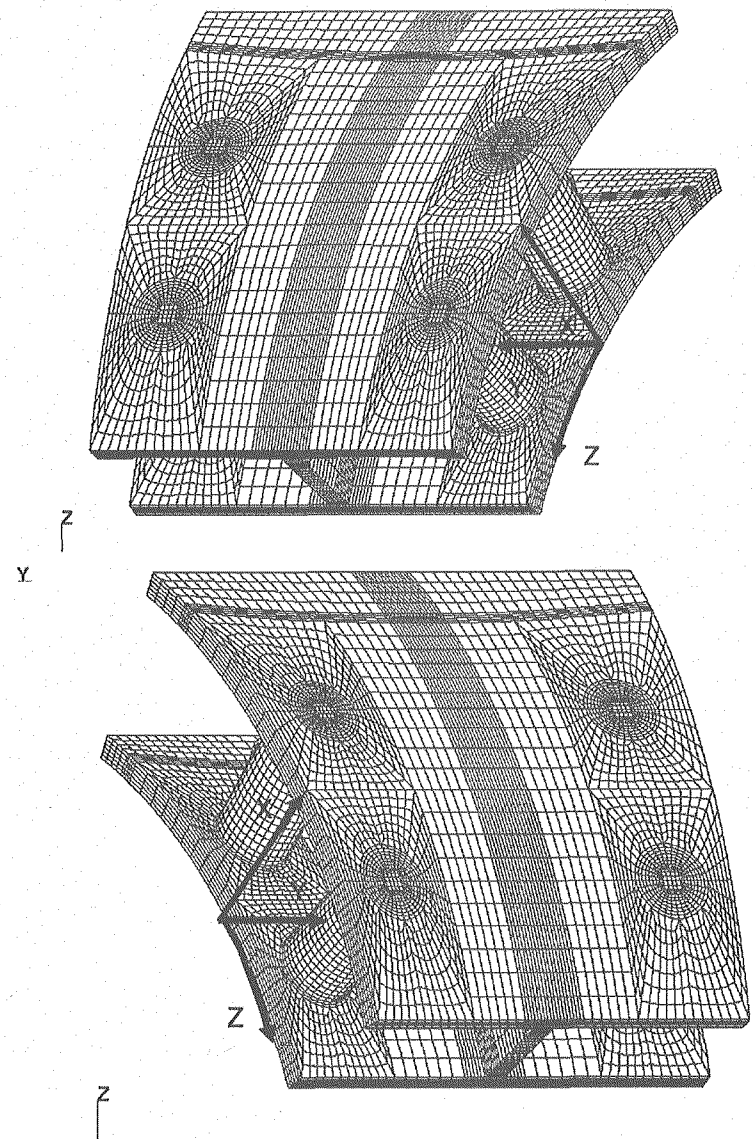

Heat transfer condition between shells and coolant:

- Heat transfer coefficient: 0.005W/mm^{2}K
- Ambient temperature: 105°C

Nuclear heating

$H(X,Y,Z)=H_{0max} \cdot \exp(-ax) \cdot [\exp(-\lambda Y^2) + \exp(-\lambda Z^2)]$

X: Radial distance from inner shell surface [mm]

Y: Poloidal distance from center of crossing gap [mm]

Z: Toroidal distance from center of crossing gap [mm]

H_{0max}: 6.6×10^{-4}[W/mm^3]

a: 1.28×10^{-2}[mm^{-1}]

λ: 1.08×10^{-4}[mm^{-2}]

Nuclear heating of support housing gap side

$H=13.18\times10^{-5} \cdot \exp(-\alpha_1 X)$

Nuclear heating of support housing center of modules side

$H=9.45\times10\text{-}5 \cdot \exp(-\alpha_2 X)$

$\alpha1$: 1.2×10^{-2}[mm^{-1}]

$\alpha2$: 1.13×10^{-2}[mm^{-1}]

Fig. 7.1.2-2 Nuclear heating and heat transfer conditions applied to solid models

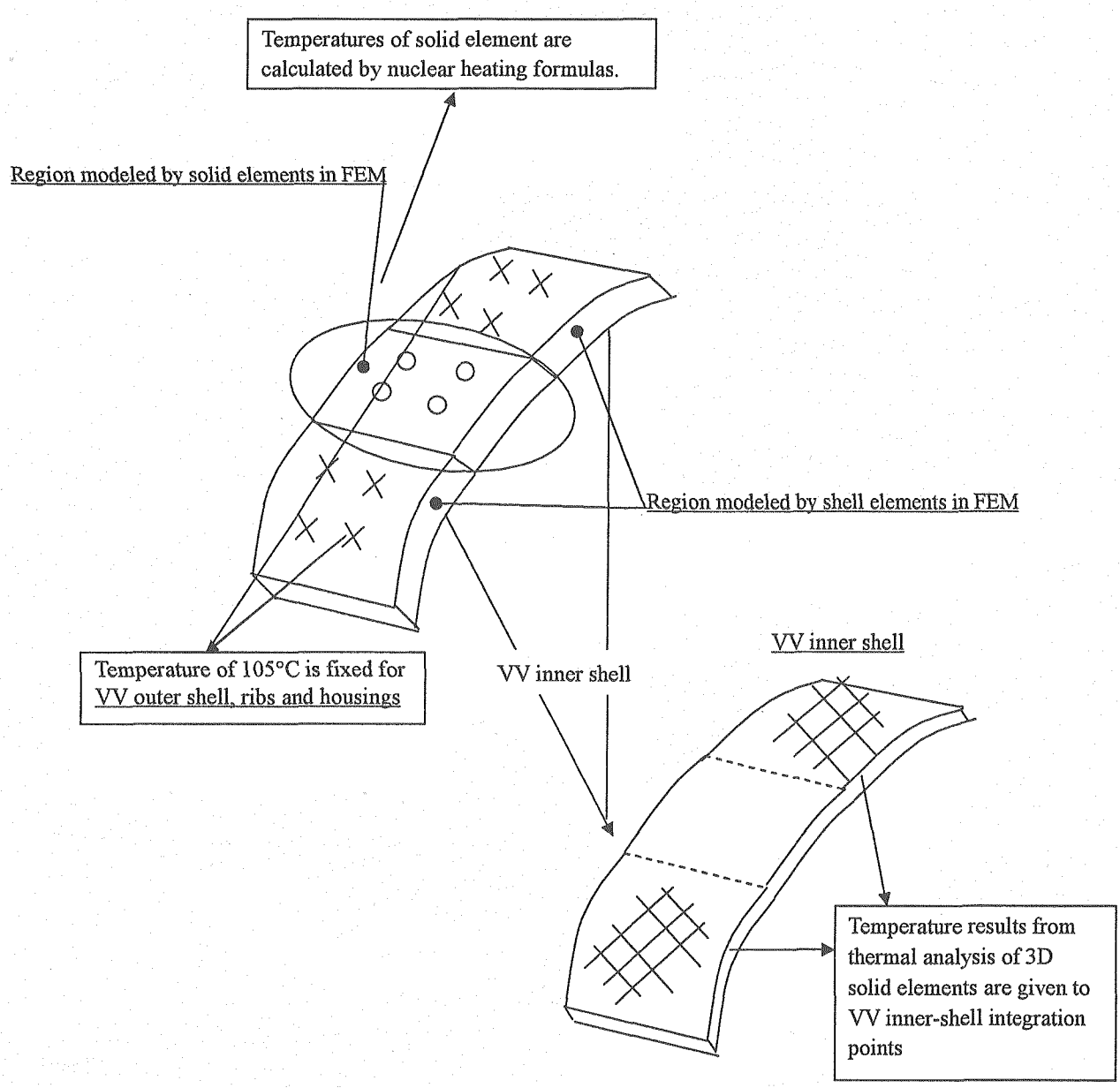

Fig. 7.1.2-3 Temperature loads for the detail stress analysis

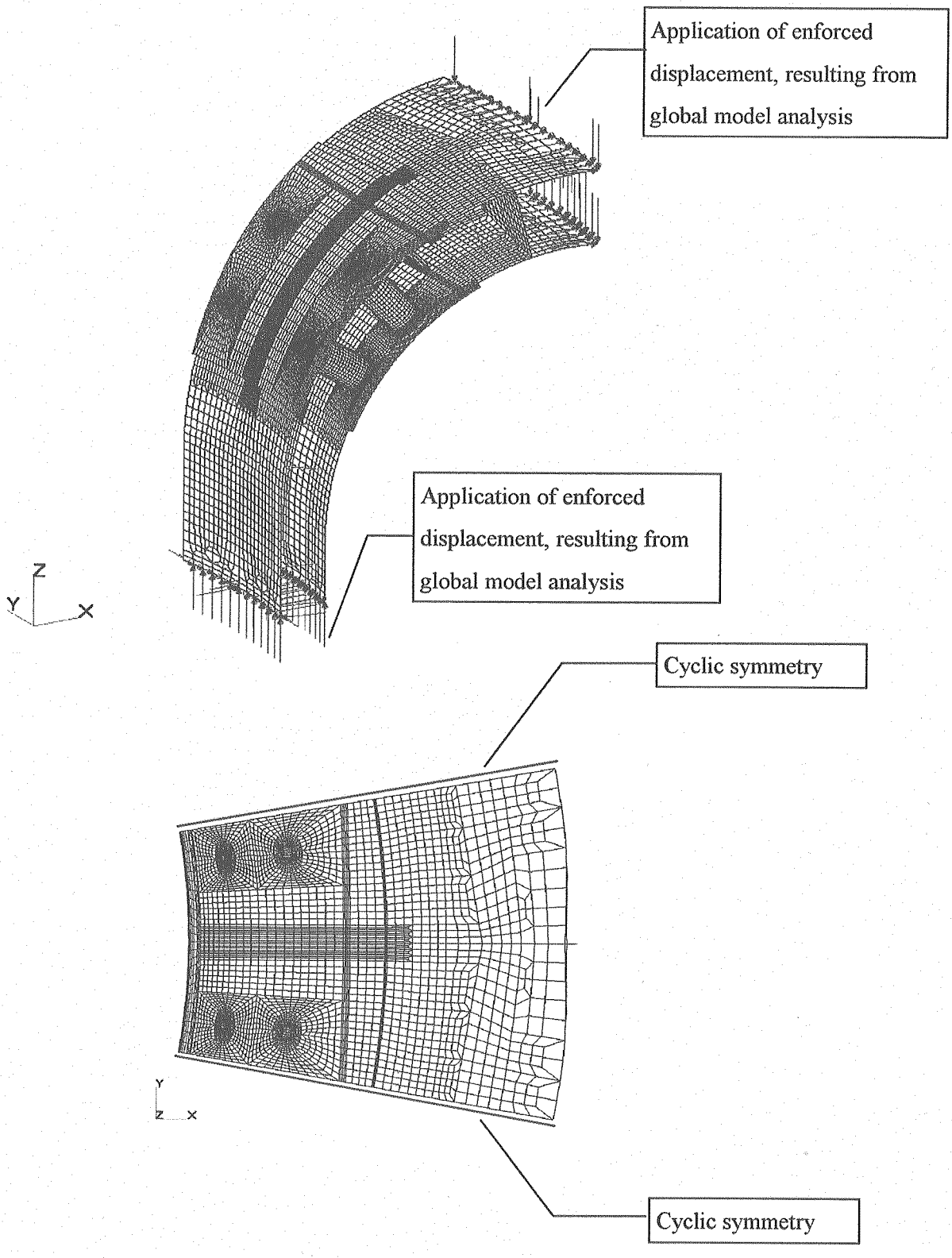

Fig. 7.1.2-4 Boundary conditions: Coolant pressure and EM loads

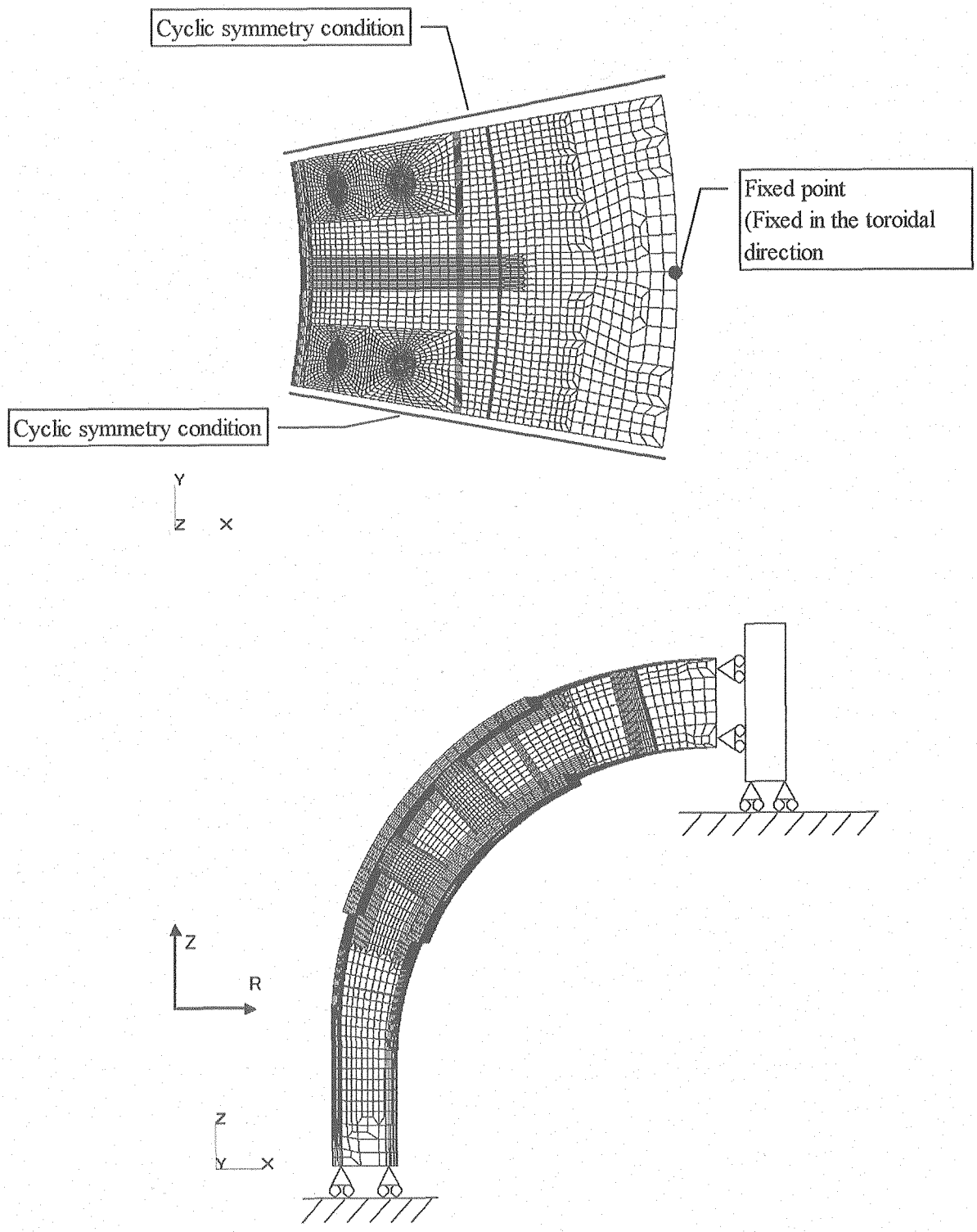

Fig. 7.1.2-5 Boundary conditions applied to thermal stress analysis and stress analysis on EM forces of blanket to housing

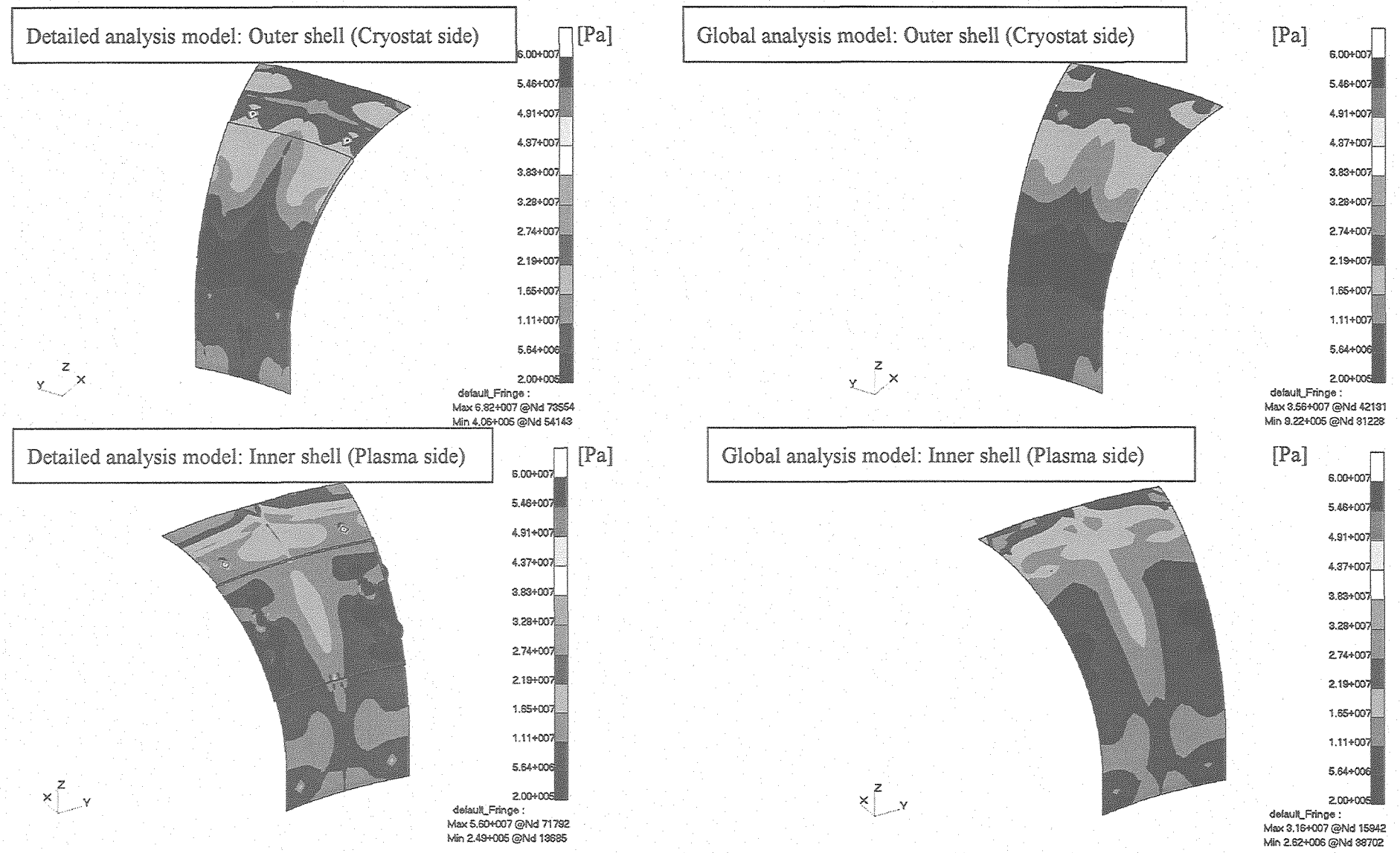

Fig. 7.1.3-1(1/3) Stress distribution (von-Mises stress) in the case of MD

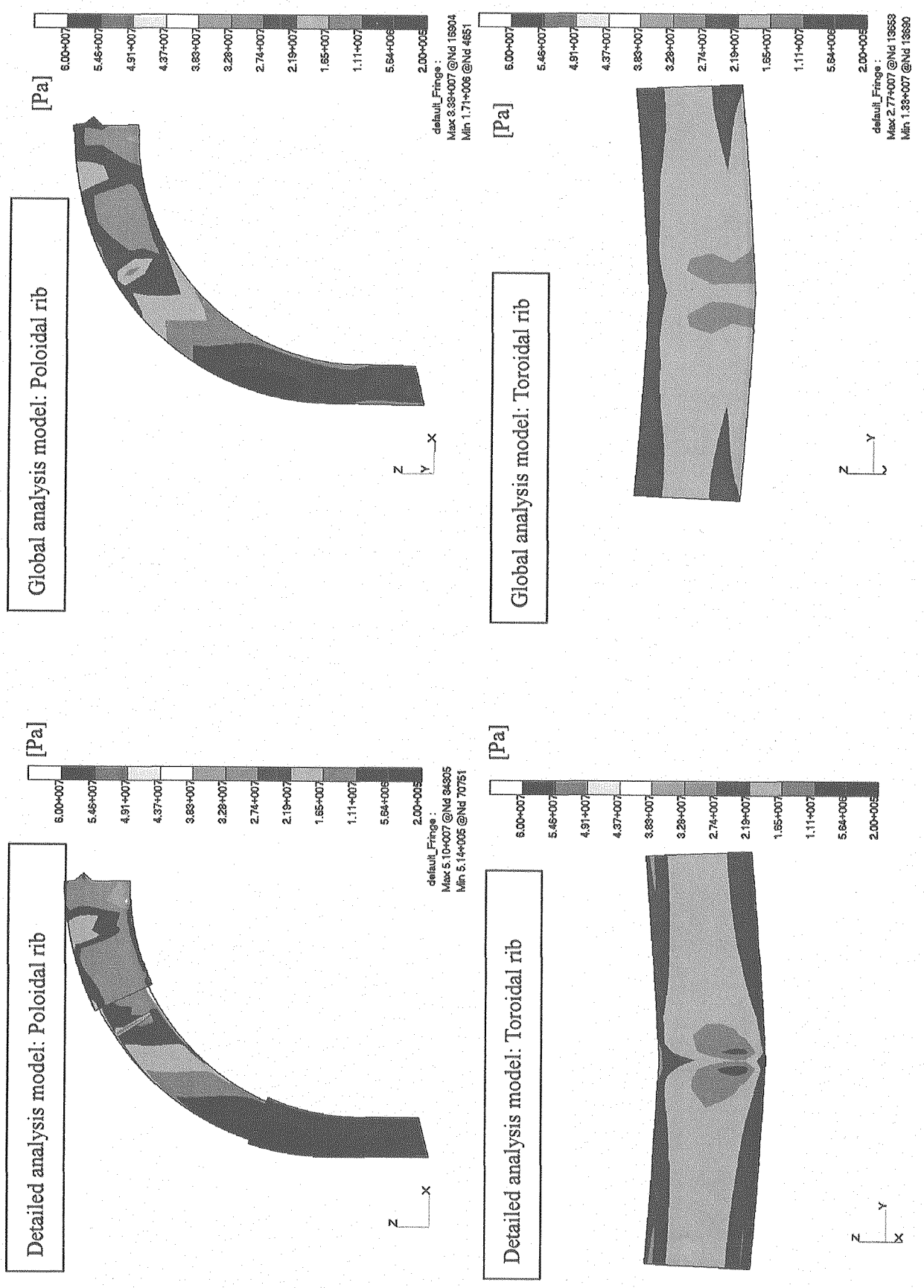

Fig. 7.1.3-1(2/3) Stress distribution (von-Mises stress) in the case of MD

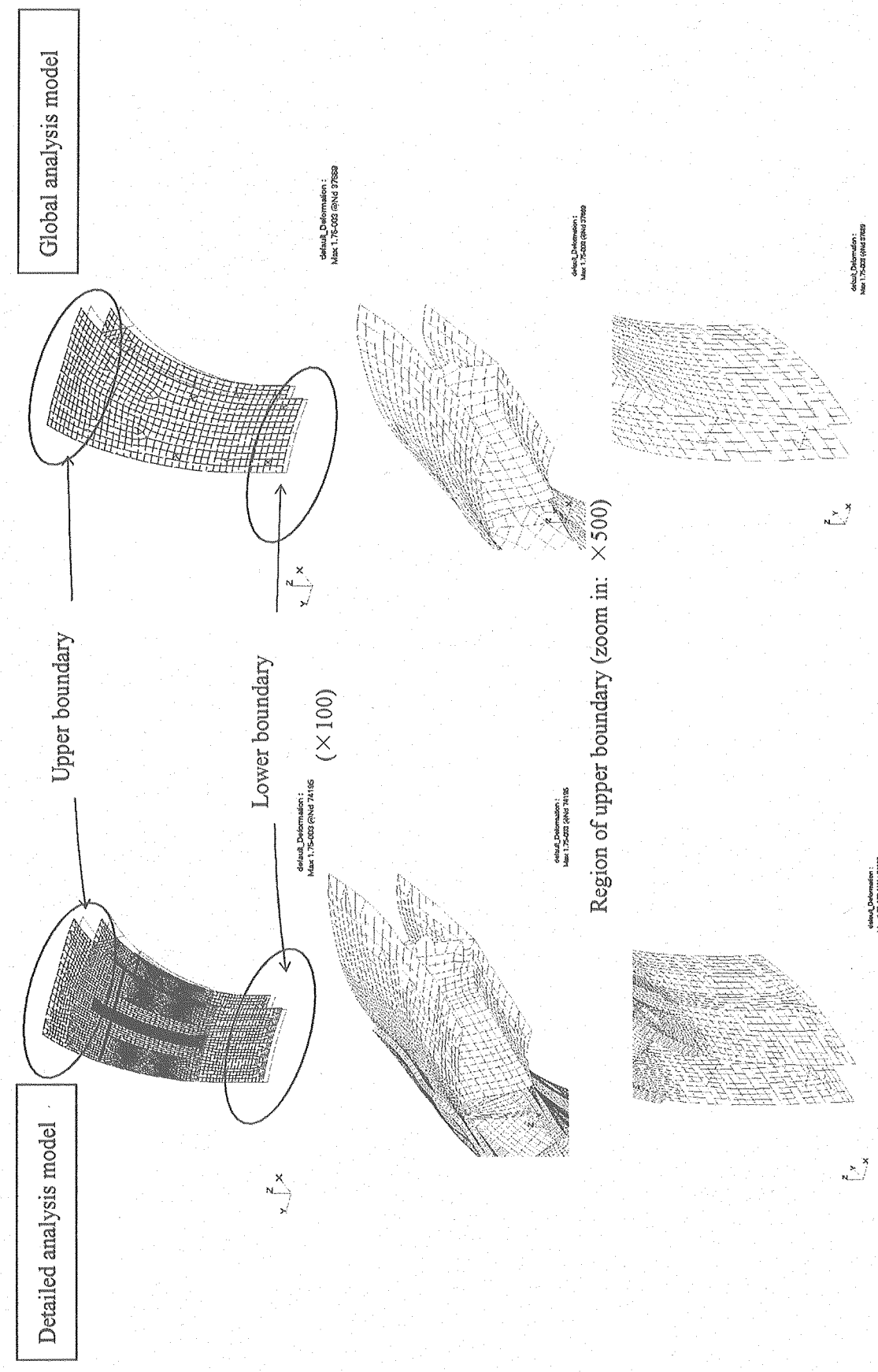

Fig. 7.1.3-1(3/3) Deformation in the case of MD

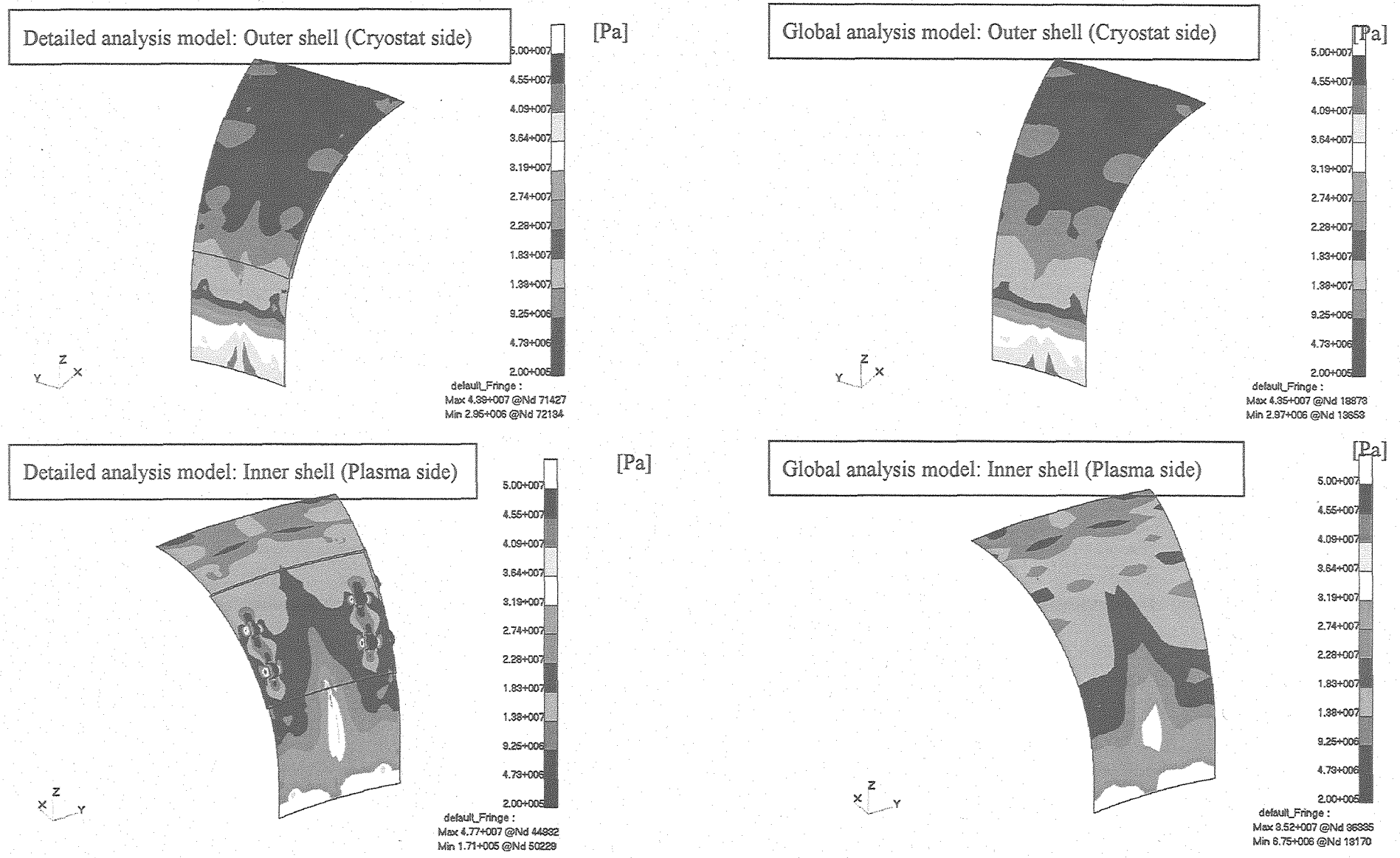

Fig. 7.1.3-2 (1/3) Stress distribution (Von. Mises stress) in the case of TFCFD

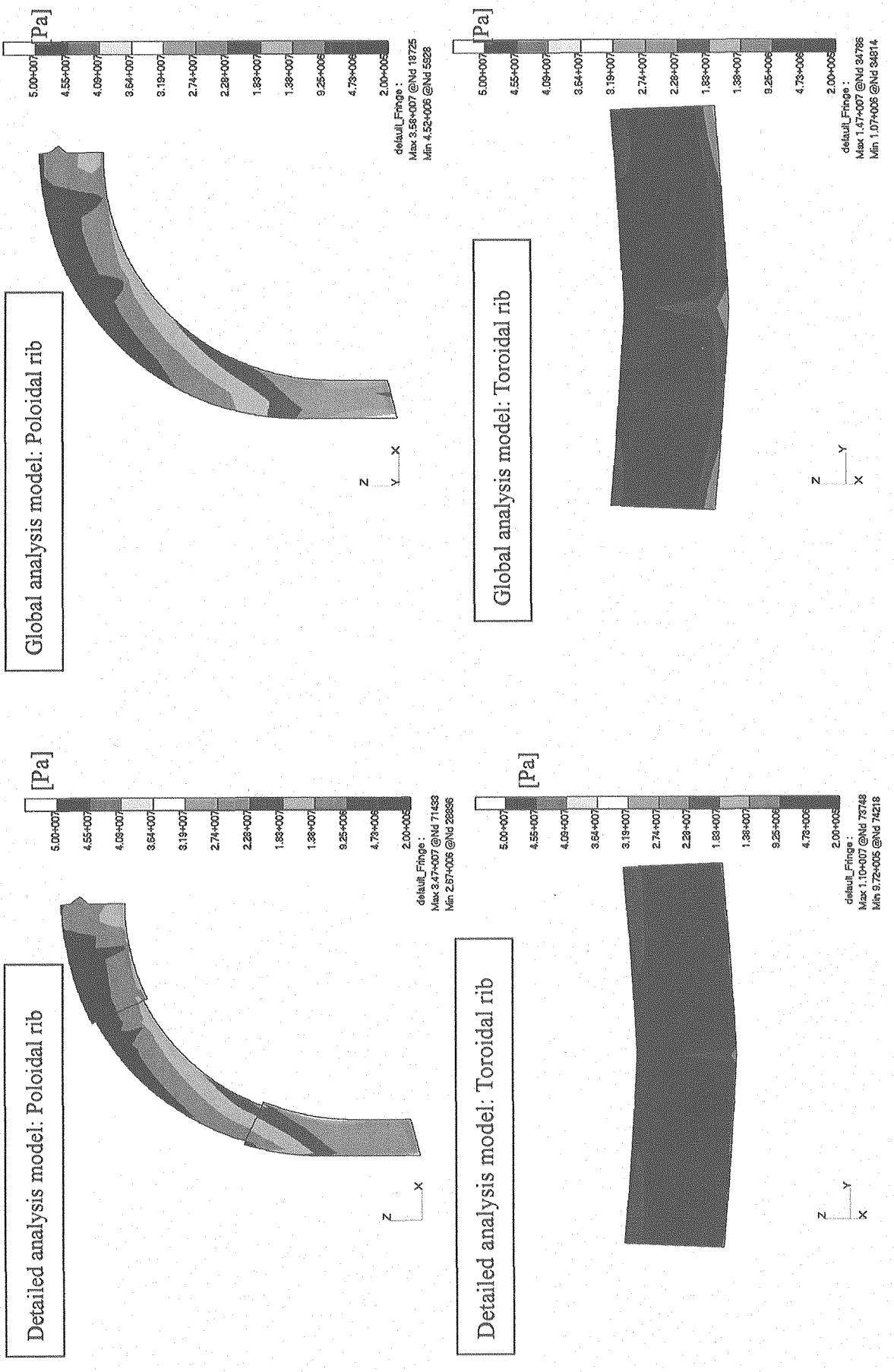

Fig.7.1.3-2 (2/3) Stress distribution (Von. Mises stress) in the case of TFCFD load

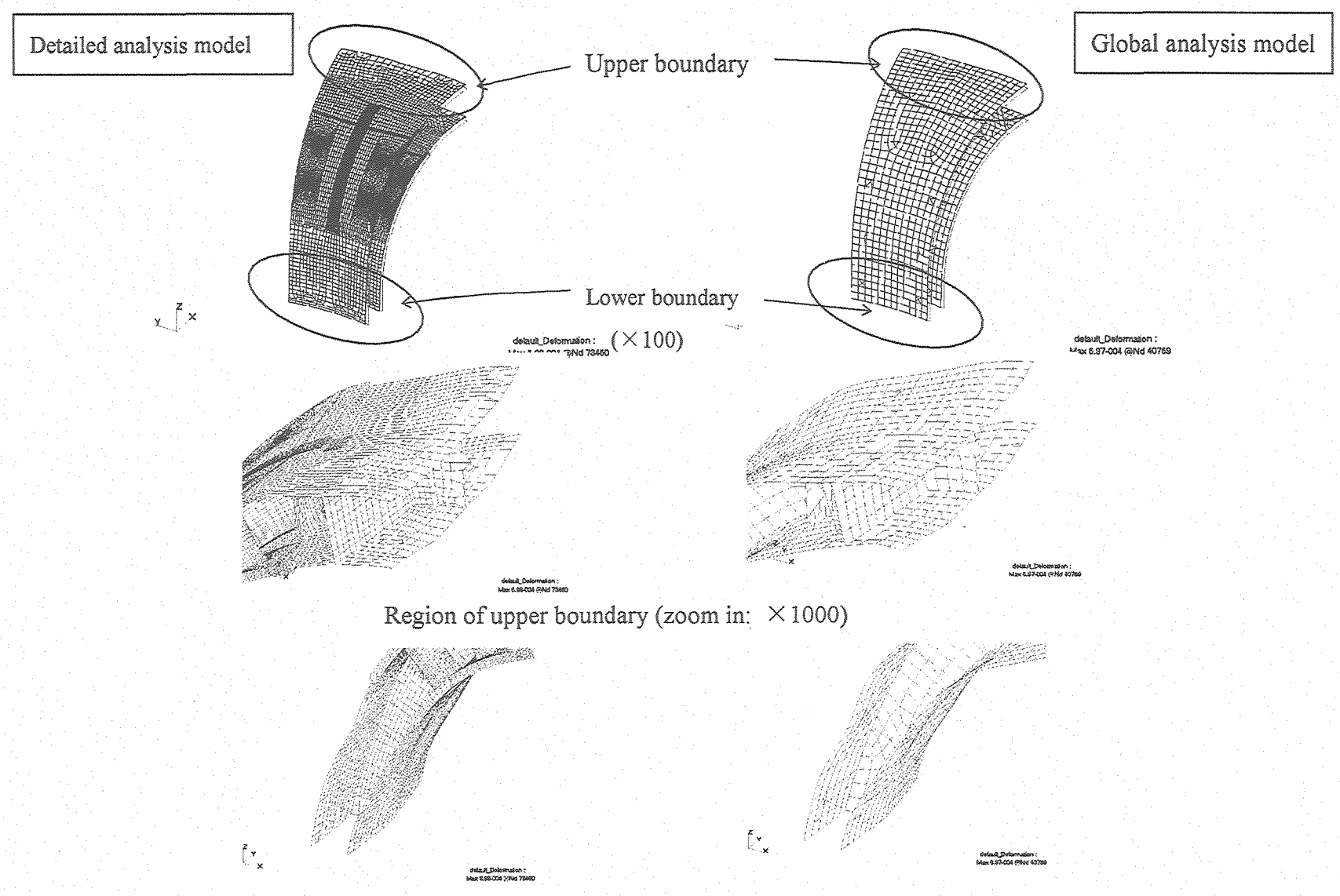

Fig. 7.1.3-2 (3/3) Deformation the case of TFCFD load

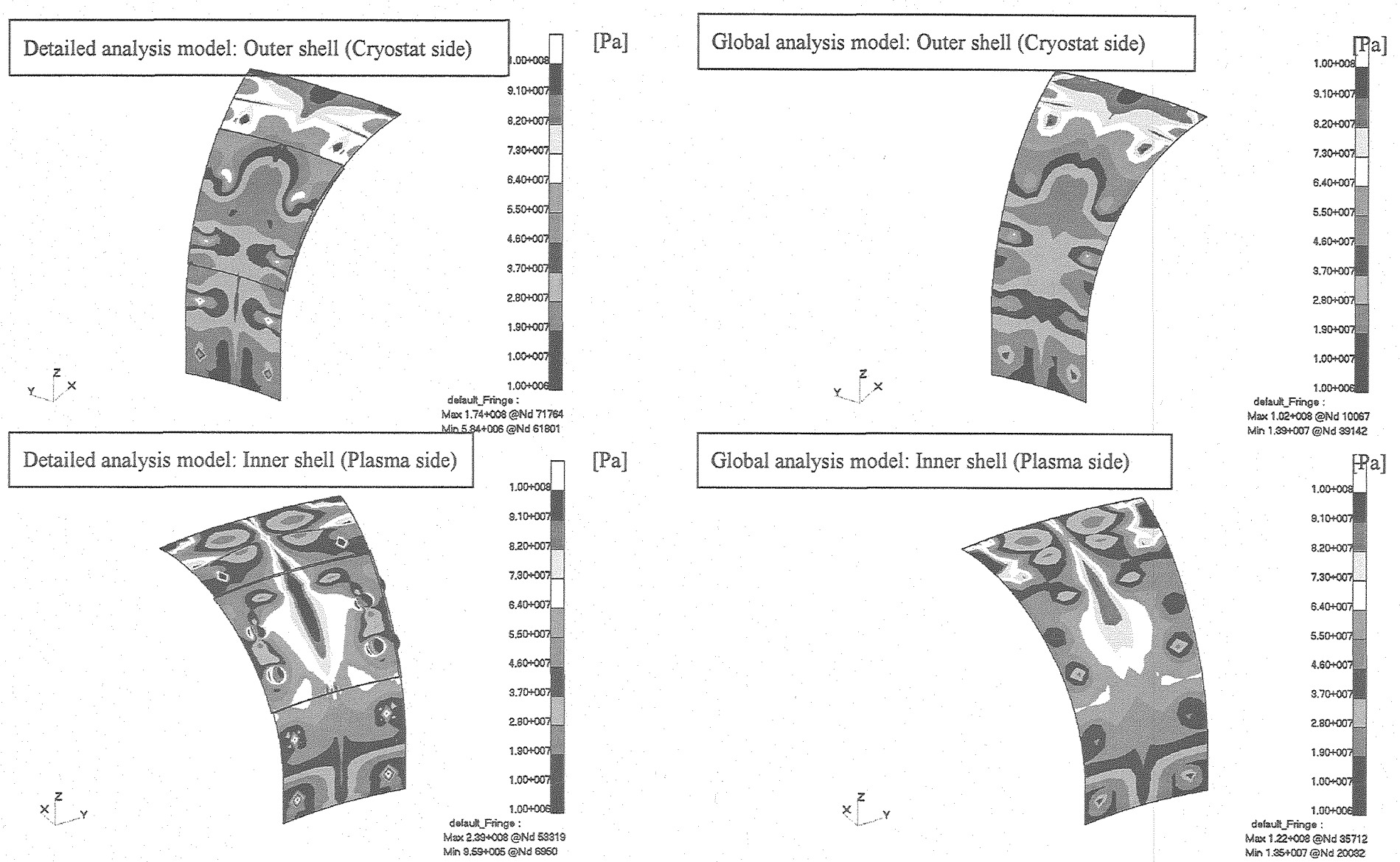

Fig. 7.1.3-3 (1/3) Stress distribution (Von-Mises stress) in the case of VDE III Fast downward disruption (EM force due to Eddy current)

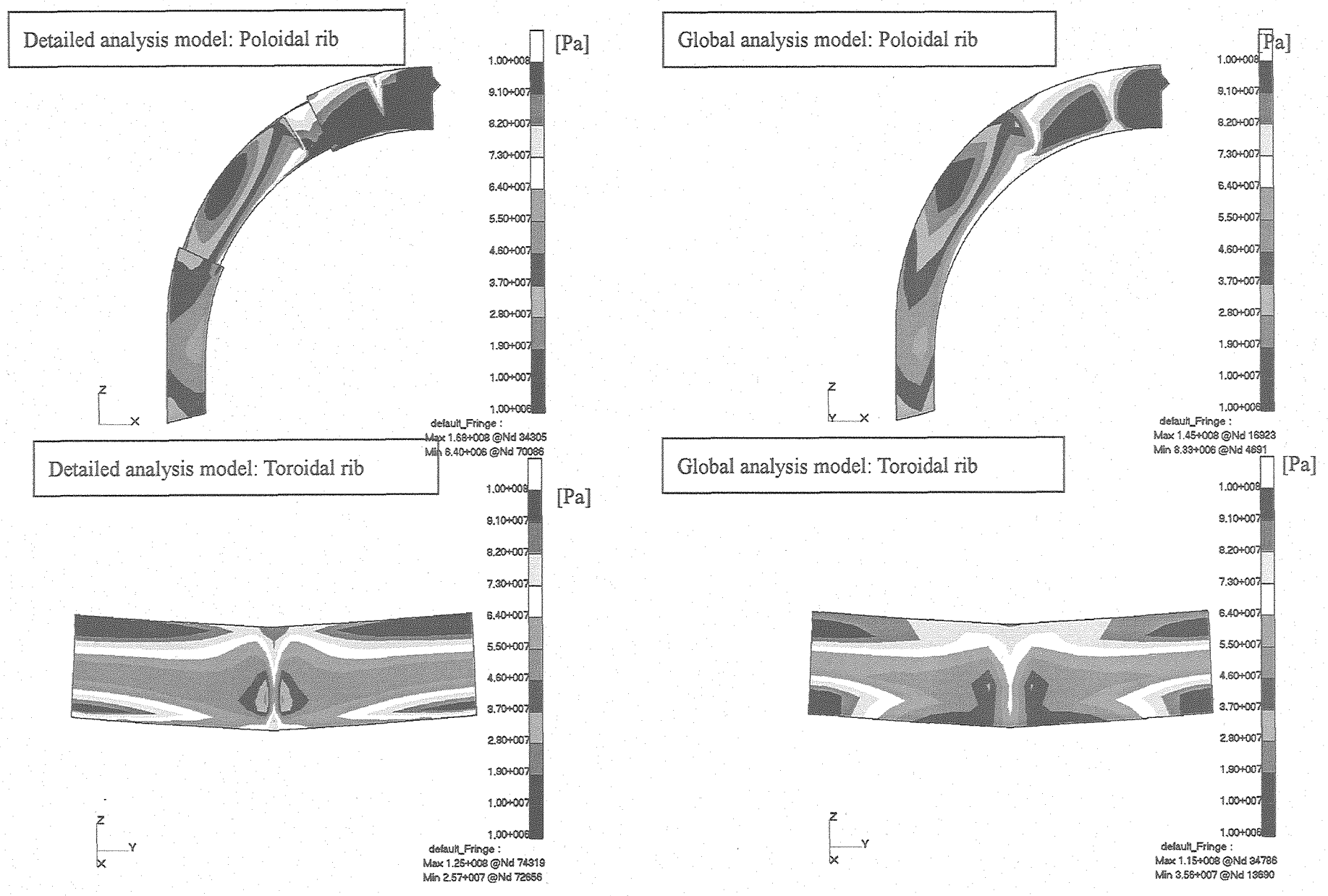

Fig. 7.1.3-3 (2/3) Stress distribution (Von-Mises stress) in the case of VDE III Fast downward disruption (EM force due to Eddy current)

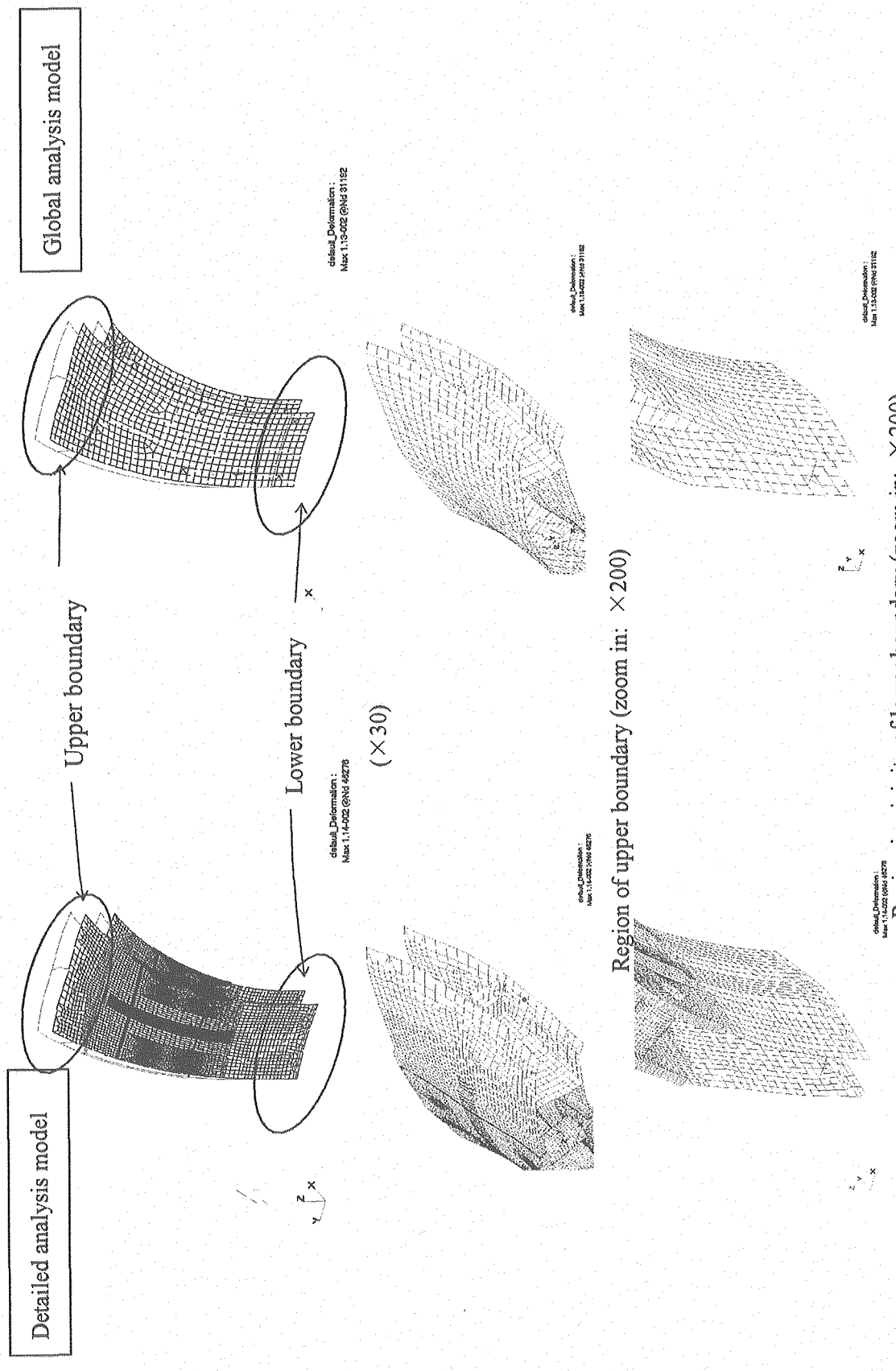

Fig. 7.1.3-3 (3/3) Deformation in the case of VDE III Fast downward disruption (EM force due to Eddy current)

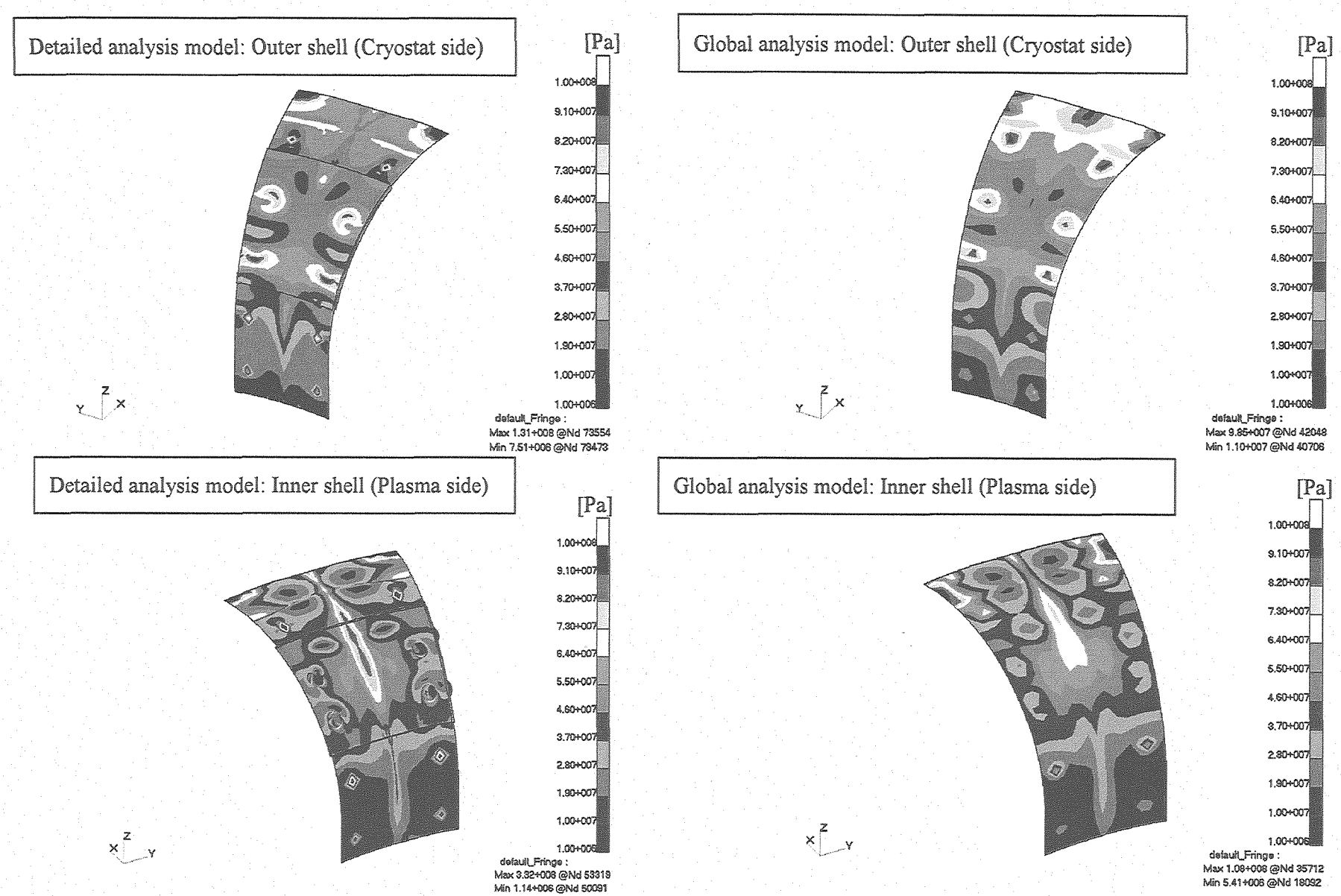

Fig. 7.1.3-4 (1/3) Stress distribution (Von-Mises stress) in the case of VDE III slow downward (EM force due to halo-current)

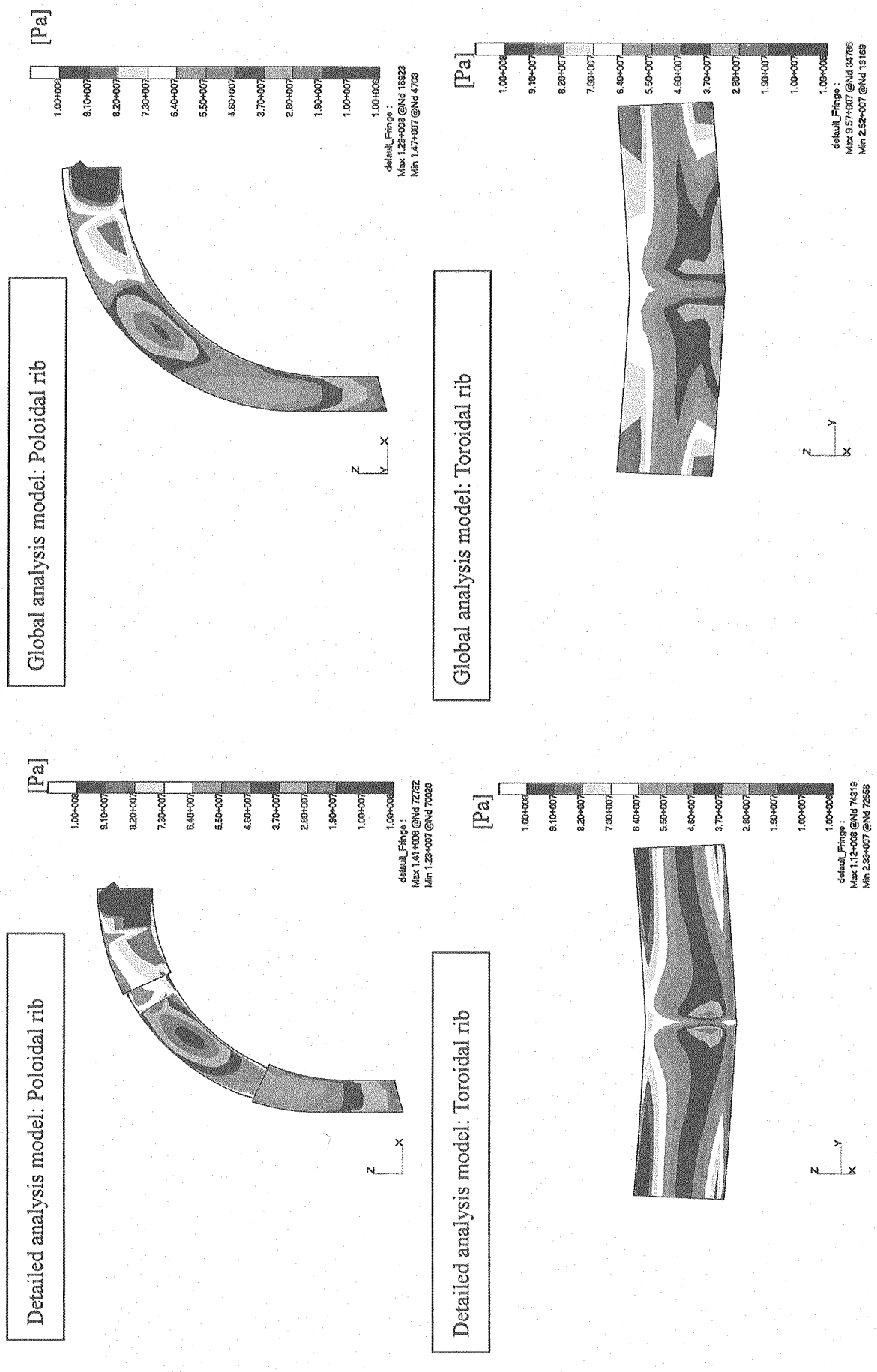

Fig.7.1.3-4 (2/3) Stress distribution (Von-Mises stress) in the case of VDE III slow downward (EM force due to halo-current)

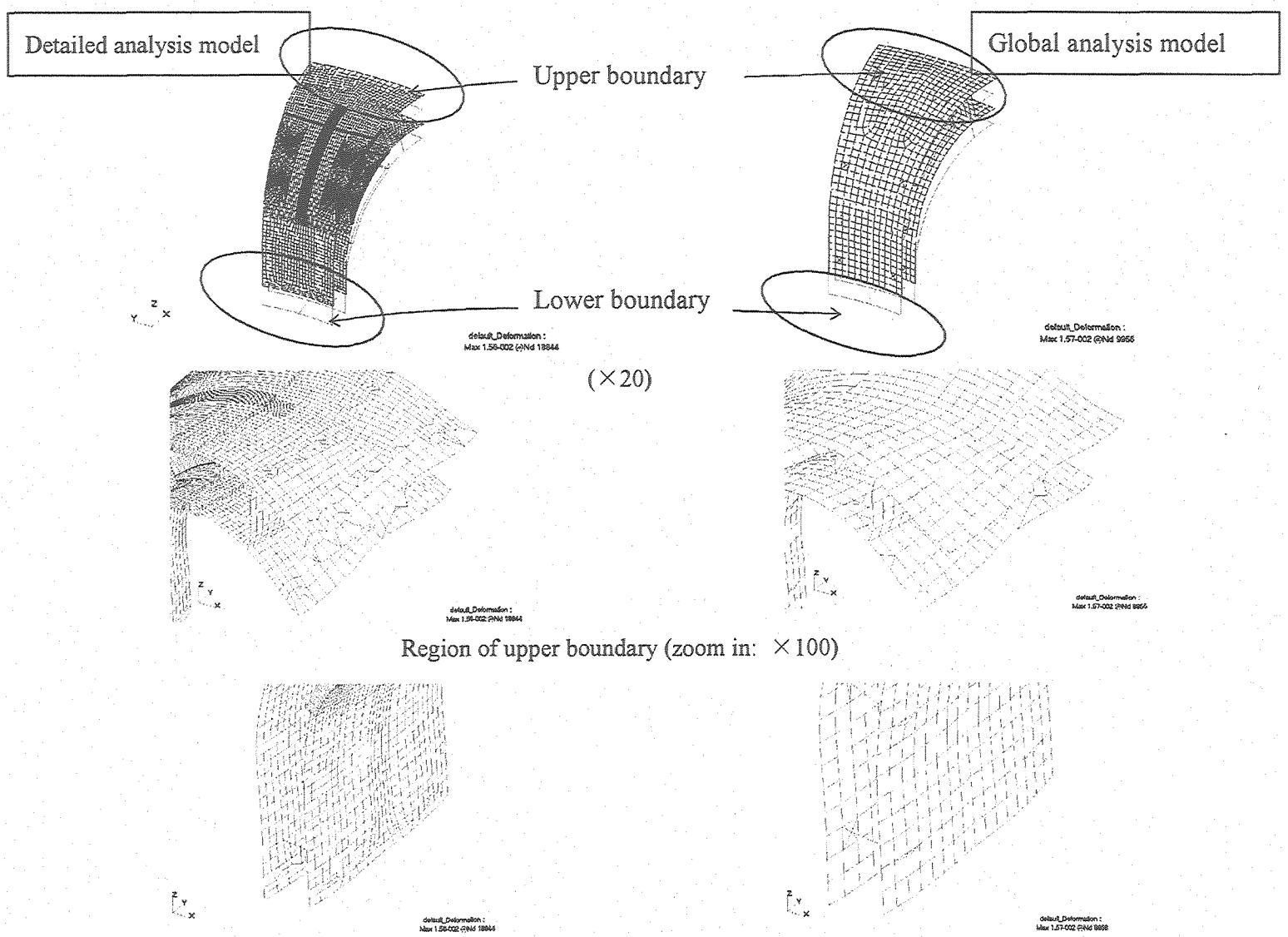

Fig. 7.1.3-4 (3/3) Deformation in the case of VDE III slow downward (EM force due to halo-current)

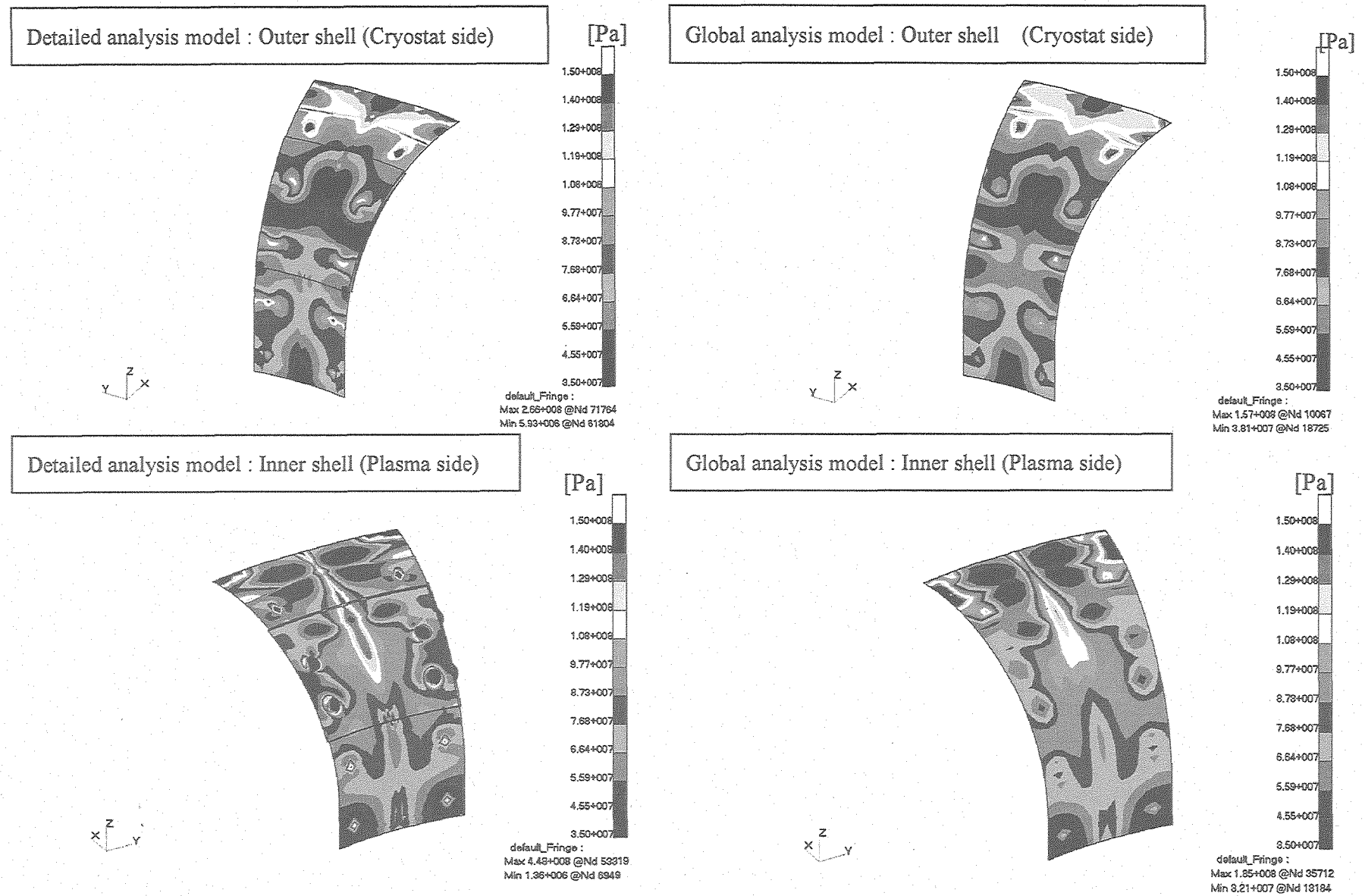

Fig. 7.1.3-5 (1/3) Stress distribution (Von. Mises stress) in the case of VDE III Slow upward disruption (EM force due to halo current)

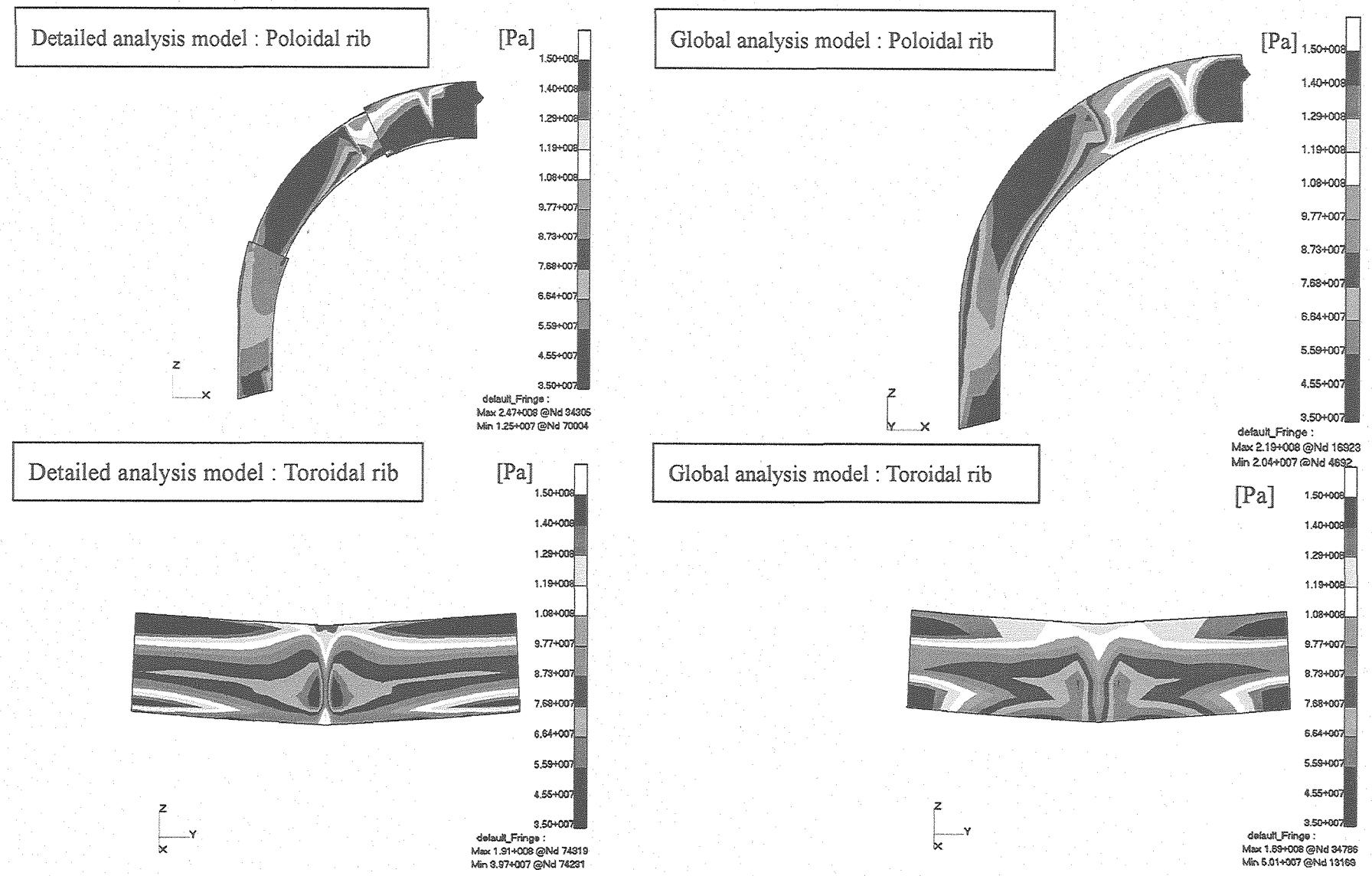

Fig. 7.1.3-5 (2/3) Stress distribution (Von. Mises stress) in the case of VDE III Slow upward disruption (EM force due to halo current)

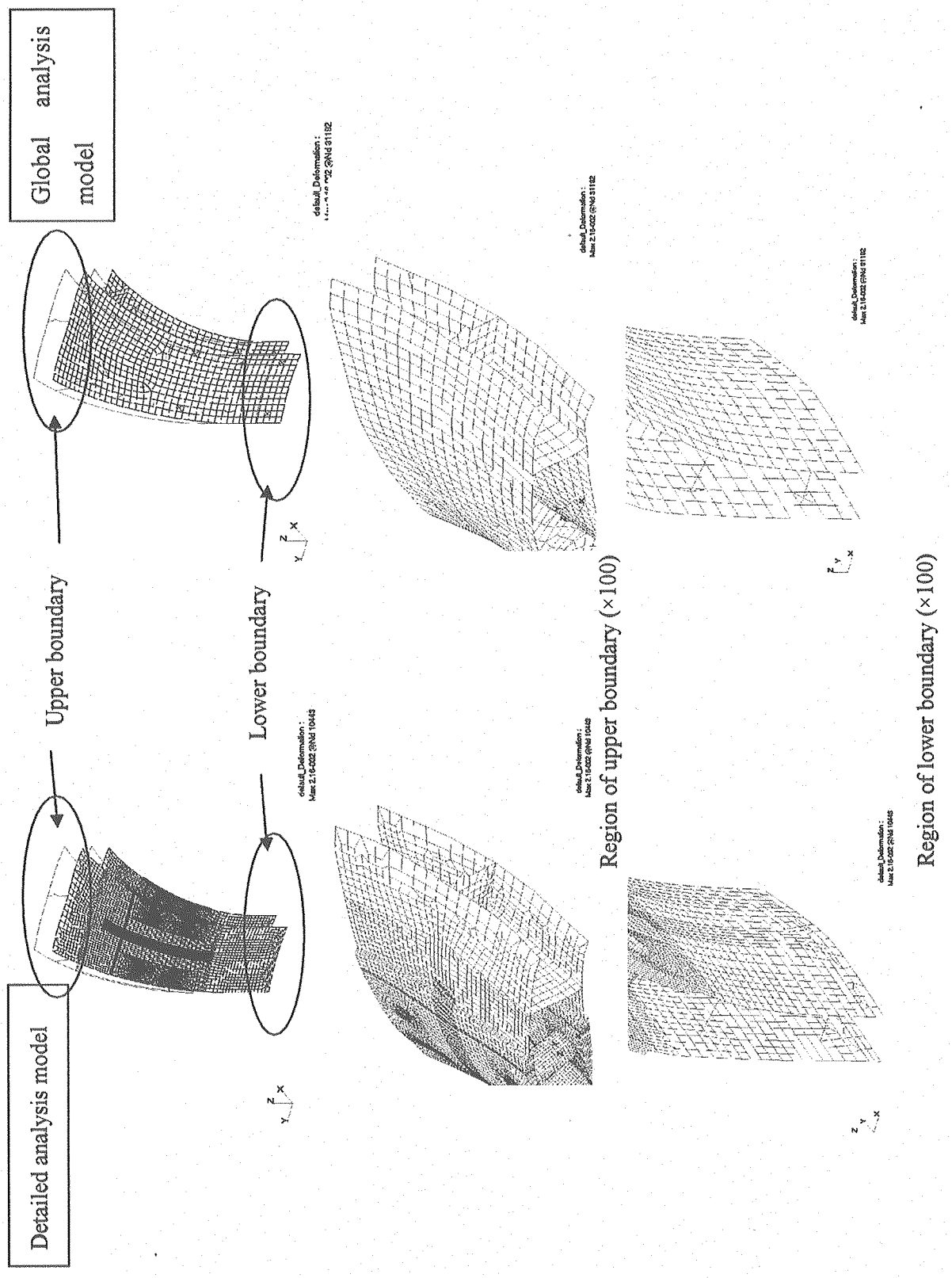

Fig. 7.1.3-5 (3/3) Deformation in the case of VDE III Slow upward disruption (EM force due to halo current)

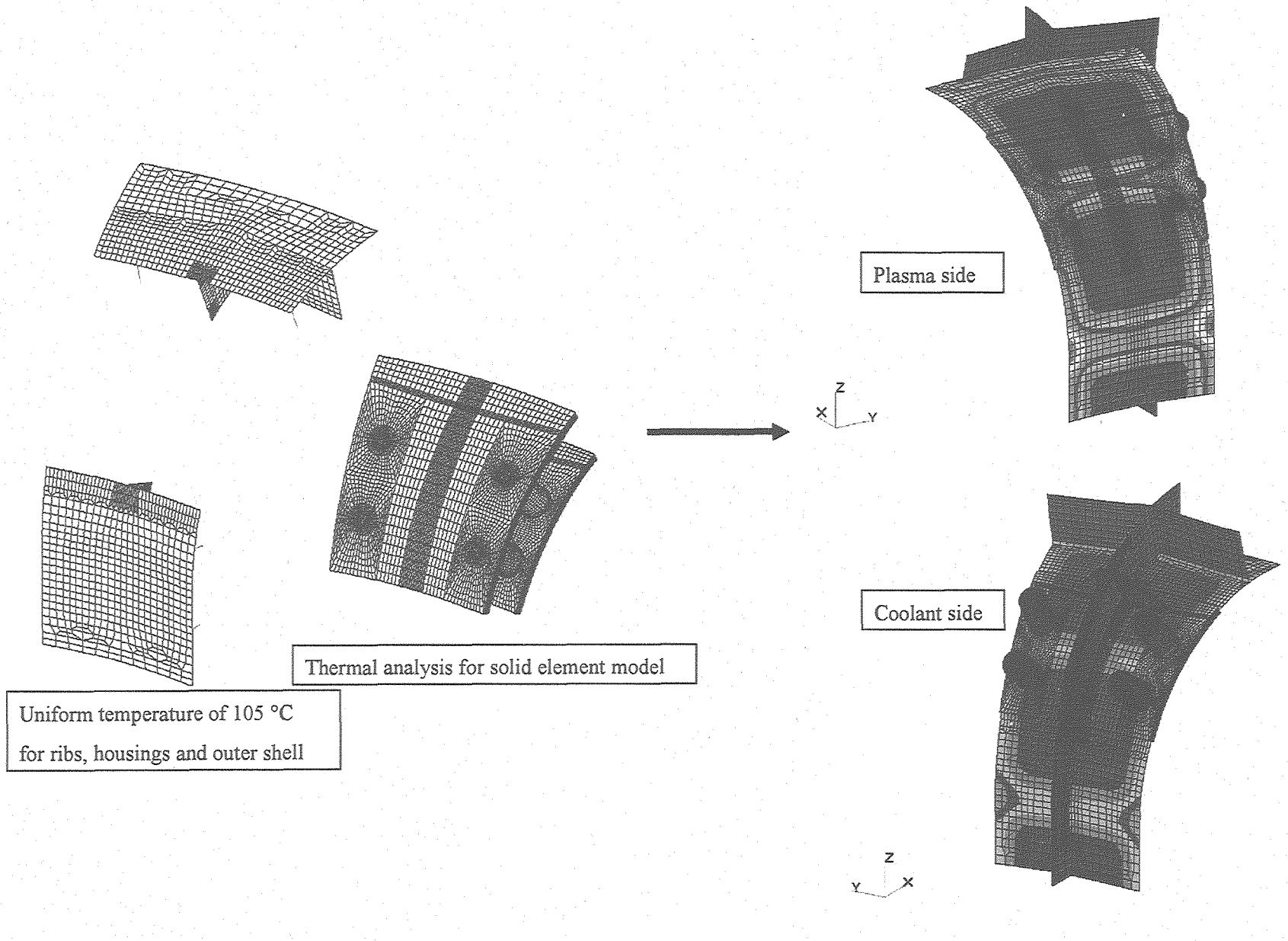

Fig. 7.1.3-6 Temperature distribution for thermal stress analysis

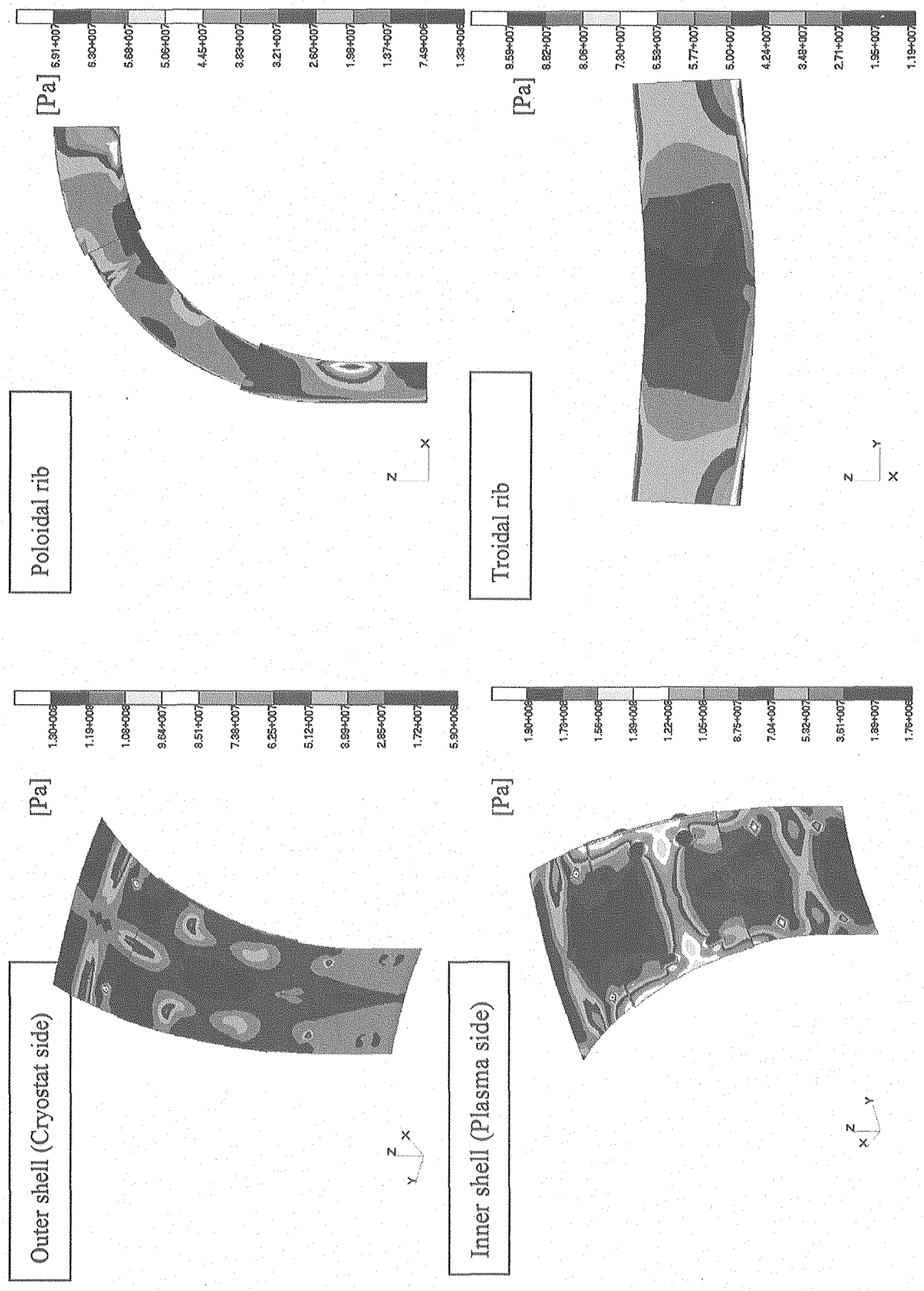

Fig. 7.1.3-7 (1/2) Thermal stress distribution (Von. Mises stress)

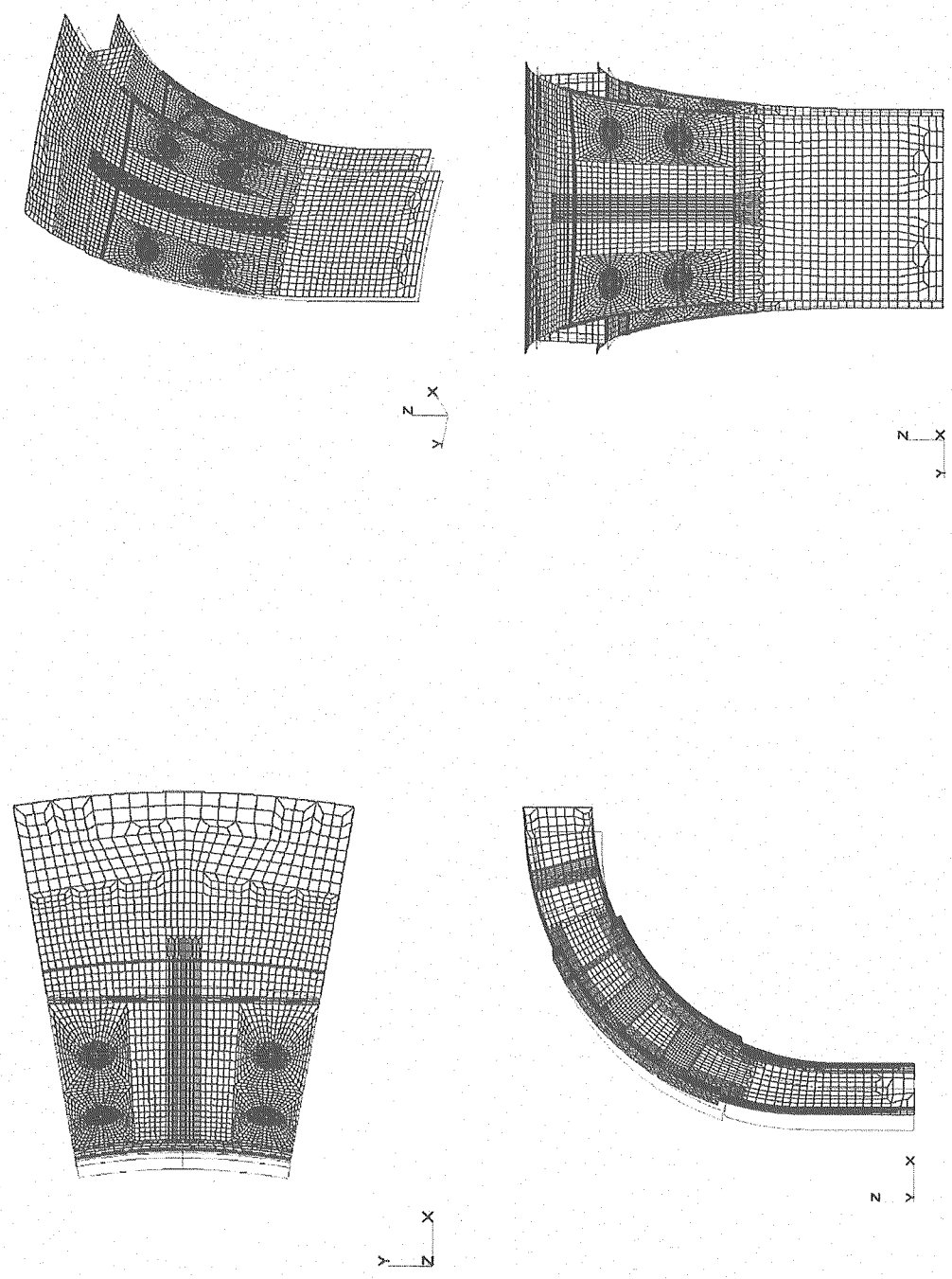

Fig. 7.1.3-7 (2/2) Deformation due to thermal stress

Shell element	Solid element	
Rotation(θ)	Displacement of inner node (u_1)	Displacement of outer node (u_2)
7.670E-04 [rad]	7.363E-05 [m]	1.197E-04 [m]
dR=X· tan (θ) (X=0.06[m])	dR (u_2-u_1)	
4.60E-5 [m]	4.60E-05 [m]	

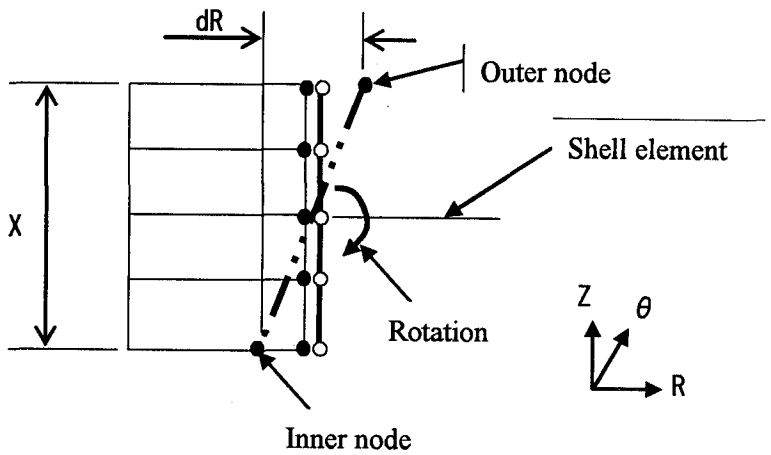

Fig. 7.1.3-8 Assessment of rotational angle at connection between solid element and shell element

7.2 Allowable crack lengths of plug welds

For the inboard upper curved region, allowable crack lengths of the plug welds have been estimated by crack propagation analysis similar to the description in Sec. 6.2. The crack lengths are un-welded lengths of plug welds along outer shell surface.

The estimation procedure of the allowable crack lengths is the same as described in Sec.6.2. The evaluation cross-sections of housing and ribs are shown in Fig.7.2-1. Un-welded regions of plug welds are conservatively assumed to be crack along outer shell.

Table 7.2-1 shows membrane and bending stresses of housings for load cycles. The stresses surrounded by red lines are used to the calculation of critical crack length. Applying 4.3.2(3) the critical crack lengths are calculated, shown in Table7.2-2, where membrane plus bending stress is considered as membrane stress because of crack model of circumferentially cracked cylinder. The limits of 75 percents of housing thickness are larger than those corresponding to collapse loads. Then the critical crack lengths are obtained to be the limits of fracture assessment. Crack propagation has been calculated using stress intensity factor of 4.3.5(5) and crack propagation rate of 4.3.5(7). Fig.7.2-2 shows the crack propagation of housings. Allowable crack lengths of housings are summarized in Table 7.2-2. The allowable crack lengths of No.7 housings are estimated to be 38.6mm considering inspection error of 4.4mm [7-1]. The length is a little bit shorter than that of an inboard typical housing of 39.5mm.

Table 7.2-3 shows membrane and bending stresses of ribs for load cycles. The stresses surrounded by red lines are used to the calculation of critical crack length. Applying 4.3.1(1) and (2) the critical crack lengths are calculated, shown in Table7.2-4. Crack propagation has been calculated using stress intensity factor of 4.3.5(4) and crack propagation rate of 4.3.5(7). Fig.7.2-3 shows the crack propagation of ribs. Allowable crack lengths of ribs are summarized in Table 7.2-4. The allowable crack lengths of ribs are estimated to be 12.2mm considering inspection error of 4.4mm. The length is larger than that of an inboard typical side rib of 8.8mm.

Table 7.2-1 Stress conditions for crack growth evaluation of Housings (un-welded part of plug weld)

Unit [MPa]

Housing		Cycle			
		3180	101	1	30000
#7+	M	1.40	1.57	1.55	-0.55
	B	34.72	35.99	43.89	11.08
	M+B	36.12	37.56	45.43	10.53
	Fracture assessment stress		112.68(=3×37.56)		
#8-	M	1.26	1.46	1.32	-0.69
	B	32.28	33.48	40.35	17.27
	M+B	33.54	34.94	41.67	16.58
	Fracture assessment stress		104.81(=3×34.96)		

M : Membrane Stress

B : Bending Stress

: **Applied stress for the crack growth evaluation**

Table 7.2-2 Critical and Allowable crack depths of Housing for plug weld (un-welded part of plug weld)

Unit [mm]

	Housing #h7+	Housing #h8+
(1)Housing radius	105	105
(2)Crack length corresponding 75% of housing radius*	78.8	78.8
(3) Critical crack length corresponding fracture assessment	43.2	45.4
(4)Critical crack length (larger length between (2) and (3))	43.2	45.2
(5)Allowable crack depth	43.0	45.1
(6)Allowable crack depth including sizing error of 4.4mm	38.6	40.7

* 75% of thickness is defined as the limit in Rules on Fitness-for-Service for Nuclear Power Plant (JSMES NA1-2002)

Table 7.2-3 Stress conditions for crack growth evaluation of Rib (un-welded part of plug weld)

Unit [MPa]

Rib		Cycle			
		3180	101	1	30000
R-1-2	M	38.10	40.80	45.10	-12.90
	B	5.50	5.80	7.30	0.00
	M+B(inside)	32.70	35.10	37.80	-12.90
	M+B(outside)	43.60	46.60	52.40	-12.90
	Fracture assessment stress		M=110.16 B=13.34		
R-1-3	M	40.70	43.20	47.90	-15.90
	B	2.10	2.40	2.70	0.00
	M+B(inside)	38.50	40.80	50.70	-15.90
	M+B(outside)	42.80	45.60	45.20	-15.90
	Fracture assessment stress		M=116.64 B=5.52		
R-1-4	M	11.20	12.70	12.60	2.58
	B	13.50	13.70	18.10	0.02
	M+B(inside)	24.70	26.40	30.70	2.60
	M+B(outside)	-2.37	-1.11	-5.41	2.55
	Fracture assessment stress		M=34.29 B=31.51		

M : Membrane Stress

B : Bending Stress

: **Applied stress for the crack growth evaluation**

Table 7.2-4 Critical and Allowable crack lengths of ribs (un-welded part of plug weld)

Unit [mm]

	Rib-1-2	Rib-1-3	Rib-1-4
(1)rib thickness	60	60	60
(2)Crack length corresponding 75% of housing radius*	45	45	45
(3) Critical crack length corresponding fracture assessment	18.6	18.0	22.5
(4)Critical crack length (lesser length between (2) and (3))	18.6	18.0	22.5
(5)Allowable crack depth	16.6	15.9	21.8
(6)Allowable crack depth including sizing error of 4.4mm	12.2	12.2	17.4

* 75% of thickness is defined as the limit in Rules on Fitness-for-Service for Nuclear Power Plant (JSMES NA1-2002)

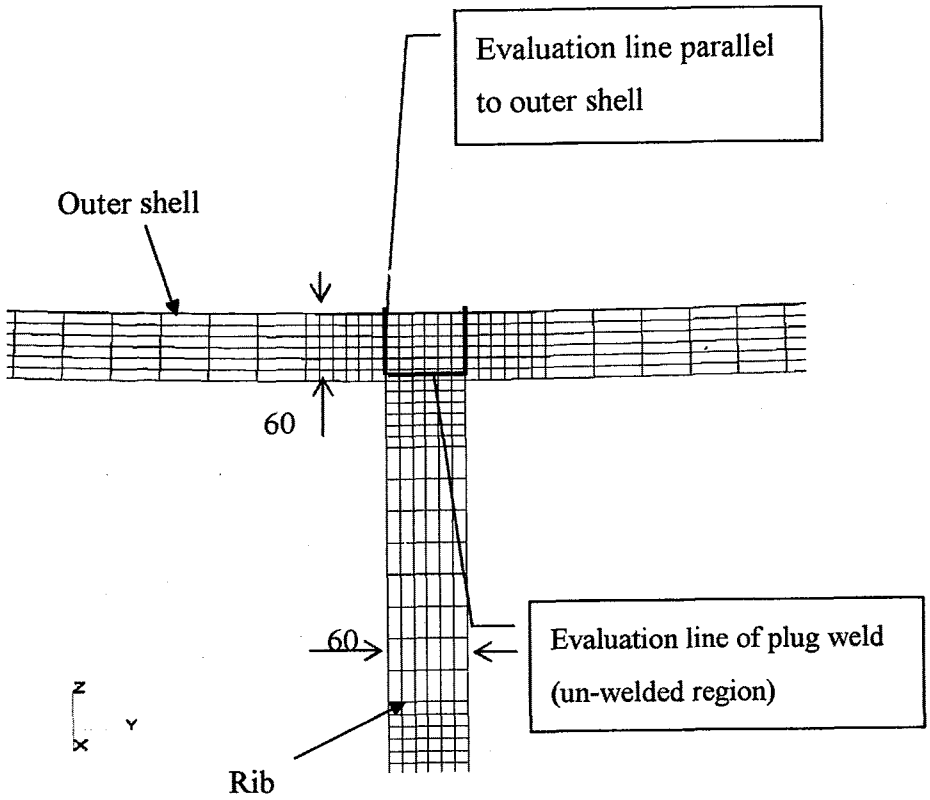

(a)Rib

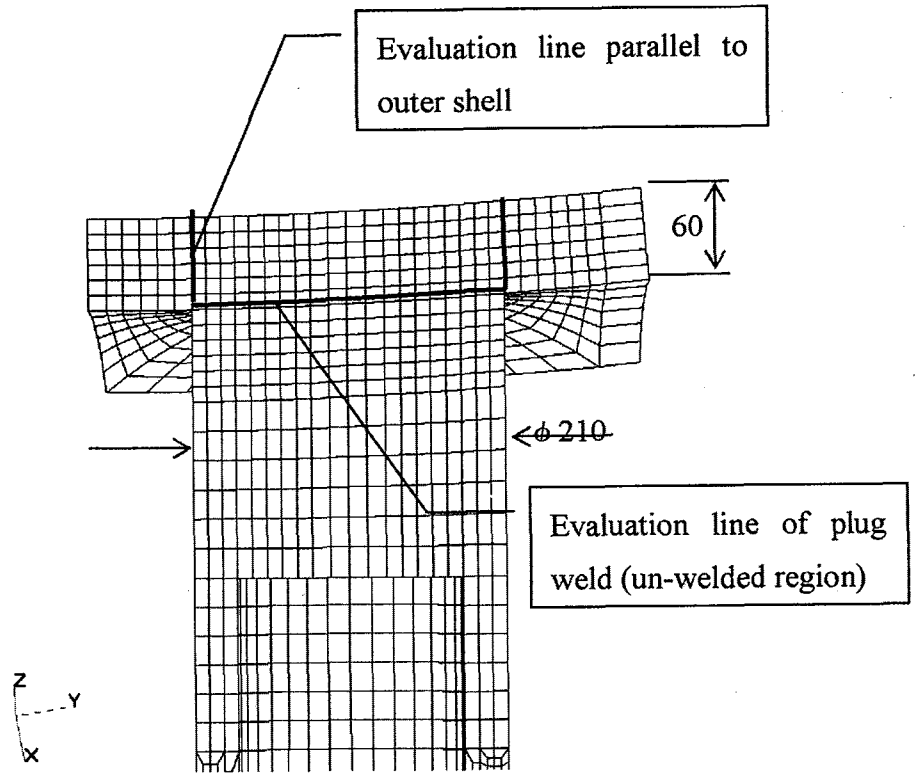

(b) Housing

Fig.7.2-1 Evaluation line for crack analysis

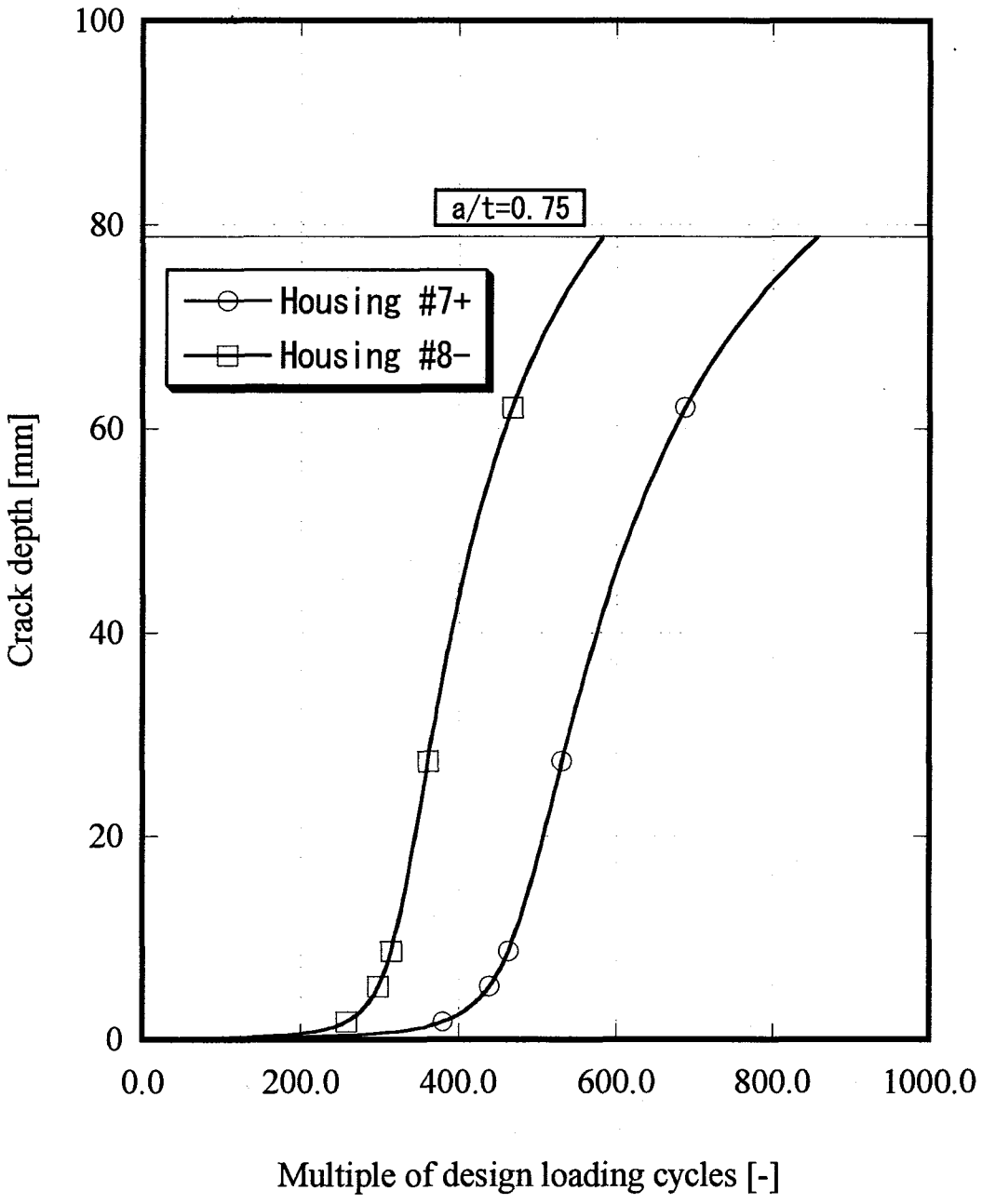

Fig. 7.2-2 Crack growth evaluation result of Housing (Un-welded part of plug weld)

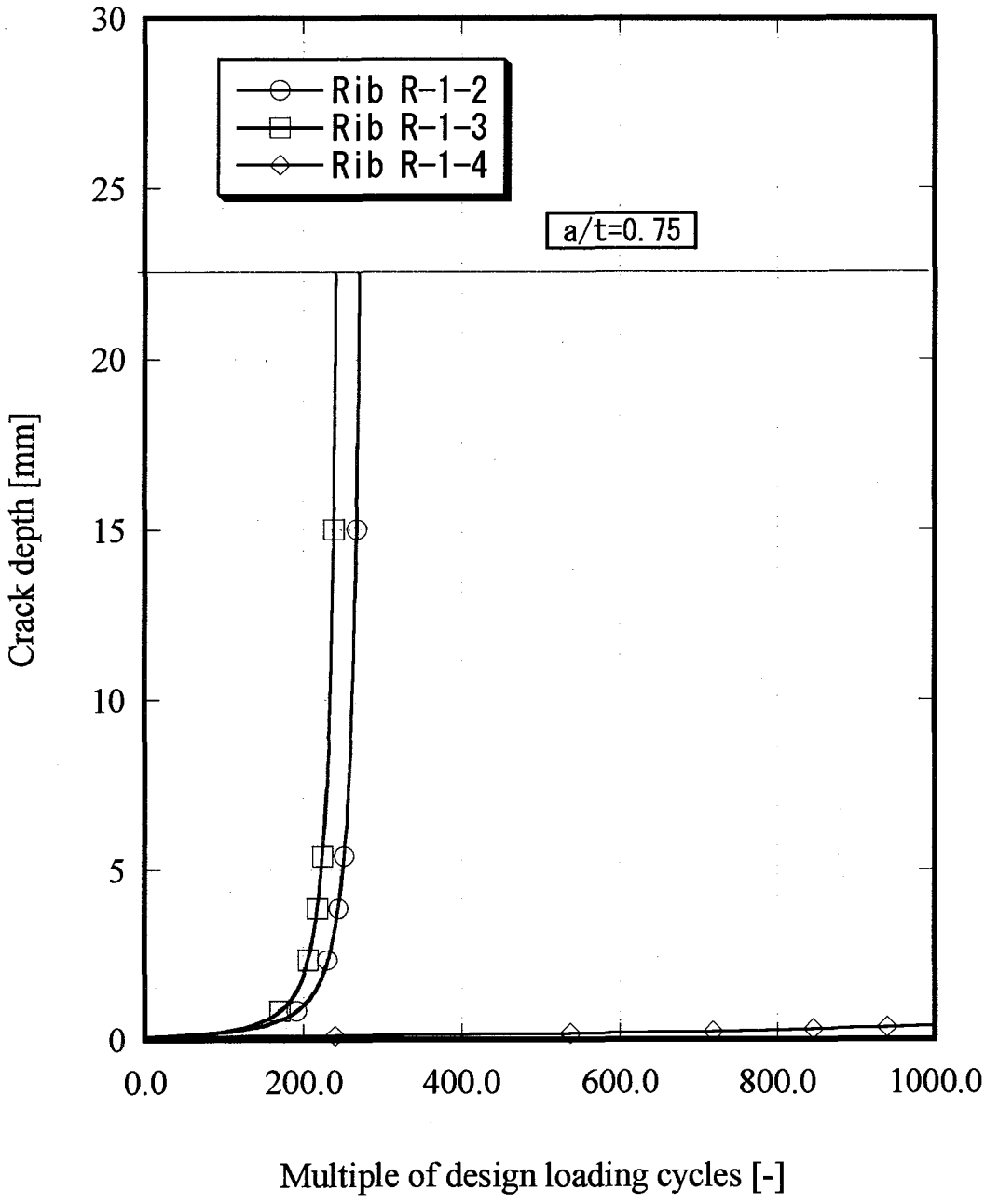

Fig. 7.2-3 Crack growth evaluation result of Rib (Un-welded part of plug weld)

7.3 Allowable crack lengths perpendicular to outer shell surface

Crack lengths perpendicular to outer shell surface, which mean defects of weld metal, might occur not only in plug weld but also in ordinary butt weld. For the application of plug weld, the crack propagations have been additionally calculated for the defects of housings and ribs.

For the crack of housings perpendicular to outer shell surface, surface crack is assumed for the assessment of allowable crack length. Table 7.3-1 shows membrane and bending stresses of the evaluate cross section. The stresses surrounded by red lines are used to the calculation of critical crack length. For fracture assessment, several procedures of multiplying stresses by the safety factor of 3 are assumed; (1)multiplying only membrane stress, (2)multiplying membrane plus bending stresses, (3)assessment of multiplying only membrane stress plus bending stress, (4) assessment of membrane stress without multiplying safety factor, (5) assessment of membrane and bending stresses without multiplying safety factor. The stresses for fracture assessment are summarized in Table 7.3-2. Crack propagation has been calculated using stress intensity factor of 4.3.5(6) and crack propagation rate of 4.3.5(7). Figs.7.3-1(a) and (b) show the crack propagation of housings. Allowable crack lengths of ribs are summarized in Table 7.3-3. The shortest allowable crack length is 4.7mm of No.8 housing in the case of fracture assessment multiplying membrane plus bending stresses by safety factor of 3. The case may be too conservative for the fracture assessment. Except the conservative fracture assessment case, allowable crack is 30.1mm which is enough to weld housings.

For the crack of ribs perpendicular to outer shell surface, assessment procedure is the same as that of housings. Table 7.3-4 shows membrane and bending stresses of the evaluate cross section. The stresses surrounded by red lines are used to the calculation of critical crack length. The stresses for fracture assessment are summarized in Table 7.3-5. Crack propagation has been calculated using stress intensity factor of 4.3.5(6) and crack propagation rate of 4.3.5(7). Figs.7.3-2(a) and (b) show the crack propagation of ribs. Allowable crack lengths of ribs are summarized in Table 7.3-6. The allowable crack is shortest in the case of fracture assessment multiplying membrane plus bending stresses by safety factor of 3. The case may be also too conservative for the fracture assessment. Except the conservative fracture assessment case, allowable crack is more than 24mm which is enough to weld ribs.

Table 7.3-1 Stress conditions for crack growth evaluation of housing (welded part in shell thickness direction)

Unit [MPa]

Housing		Cycle			
		3180	101	1	30000
#7-M-H-1	M	31.30	29.70	39.40	4.08
	B	42.90	40.20	53.00	5.78
	M+B(inside)	74.20	69.90	92.40	9.86
	M+B(outside)	-11.60	-10.50	-13.60	-1.70
#7-M-H-2	M	44.00	46.80	53.60	-5.98
	B	52.80	56.20	64.40	7.52
	M+B(inside)	96.80	103.00	118.00	-13.50
	M+B(outside)	-8.78	-9.08	-10.80	1.48
#8-M-H-1	M	28.80	23.60	30.00	3.15
	B	38.30	31.60	40.20	4.22
	M+B(inside)	67.10	55.20	70.20	7.37
	M+B(outside)	-9.58	-8.08	-10.20	-1.07
#8-M-H-4	M	42.00	45.80	49.40	-16.40
	B	57.00	62.20	67.60	22.20
	M+B(inside)	99.00	108.00	117.00	-38.60
	M+B(outside)	-15.00	-16.10	-17.80	5.85

M : Membrane Stress

B : Bending Stress

: **Applied stress for the crack growth evaluation**

Table 7.3-2 Stress conditions for fracture assessment of housing (Including safety factor)
(Welded part in shell thickness direction)

Unit [MPa]

Housing	Fracture assessment				
	(1)SF×M	(2)SF × (M+B)	(3)SF × M+B	(4)M	(5)M+B
#7-M-H-1	93.9 (=3×31.30)	222.6 (=3×74.20)	136.8 (=3×31.3+42.9)	39.4	92.4
#7-M-H-2	140.4 (=3×46.80)	309.0 (=3×103.0)	196.6 (=3×46.8+56.2)	53.6	118.0
#8-M-H-1	86.4 (=3×28.80)	201.3 (=3×67.10)	124.7 (=3×28.8+38.3)	30.0	70.2
#8-M-H-4	137.4 (=3×45.80)	324.0 (=3×108.0)	199.6 (=3×45.8+62.2)	49.4	117.0

Table 7.3-3 Critical and allowable crack depths of housing
(Welded part in shell thickness direction)

Unit [mm]

	Housing	Fracture assessment				
		(1)SF×M	(2)SF × (M+B)	(3)SF × M+B	(4)M	(5)M+B
Critical crack depth	#7-M-H-1	45.0 *	45.0 *	45.0*	45.0 *	45.0 *
	#7-M-H-2	45.0*	29.3	45.0 *	45.0 *	45.0 *
	#8-M-H-1	45.0*	45.0 *	45.0 *	45.0 *	45.0 *
	#8-M-H-4	45.0 *	11.1	45.0 *	45.0 *	45.0 *
Allowable crack depth	#7-M-H-1	41.6	41.6	41.6	41.6	41.6
	#7-M-H-2	37.5	25.1	37.5	37.5	37.5
	#8-M-H-1	42.5	42.5	42.5	42.5	42.5
	#8-M-H-4	34.5	9.1	34.5	34.5	34.5
Allowable crack depth (Including sizing error)	#7-M-H-1	37.2	37.2	37.2	37.2	37.2
	#7-M-H-2	33.1	20.7	33.1	33.1	33.1
	#8-M-H-1	38.1	38.1	38.1	38.1	38.1
	#8-M-H-4	30.1	4.7	30.1	30.1	30.1

* 75% of thickness is defined as the limit in Rules on Fitness-for-Service for Nuclear Power Plant (JSMES NA1-2002)

Table 7.3-4 Stress conditions for crack growth evaluation of Rib (Welded part in shell thickness direction)

Unit [MPa]

Rib		Cycle			
		3180	101	1	30000
R-2-1-1	M	13.40	-54.20	-77.40	27.50
	B	41.00	56.80	31.60	39.00
	M+B(inside)	54.50	2.16	-45.40	-11.60
	M+B(outside)	-27.60	-111.00	-109.00	66.50
R-2-5-2	M	25.50	18.00	33.80	28.70
	B	85.50	88.00	100.20	1.60
	M+B(inside)	111.00	106.00	134.00	27.10
	M+B(outside)	-59.40	-69.70	-66.00	30.30

M : Membrane Stress

B : Bending Stress

□ : **Applied stress for the crack growth evaluation**

Table 7.3-5 Stress conditions for fracture assessment of rib including safety factor (Welded part in shell thickness direction)

Unit [MPa]

Rib	Fracture assessment				
	(1)SF×M	(2)SF × (M+B)	(3)SF × M+B	(4)M	(5)M+B
R-2-1-1	82.5 (=3×27.50)	199.5(=3×66.50)	121.5(=3×27.5+39.0)	27.5	66.5
R-2-5-2	86.1 (=3×28.70)	333.0(=3×111.0)	162.0(=3×25.5+85.5)	33.8	134.0

Table 7.3-6 Critical and allowable crack depths of rib
(Welded part in shell thickness direction)

Unit [mm]

	Rib	Fracture assessment				
		(1)SF×M	(2)SF × (M+B)	(3)SF × M+B	(4)M	(5)M+B
Critical crack depth	R-2-1-1	45.0 *	45.0 *	45.0*	45.0 *	45.0 *
	R-2-5-2	45.0 *	0.0	45.0*	45.0 *	45.0 *
Allowable crack depth	R-2-1-1	28.4	28.4	28.4	28.4	28.4
	R-2-5-2	33.2	0.0	33.2	33.2	33.2
Allowable crack depth (Including sizing error)	R-2-1-1	24.0	24.0	24.0	24.0	24.0
	R-2-5-2	28.8	0.0	28.8	28.8	28.8

* 75% of thickness is defined as the limit in Rules on Fitness-for-Service for Nuclear Power Plant (JSMES NA1-2002)

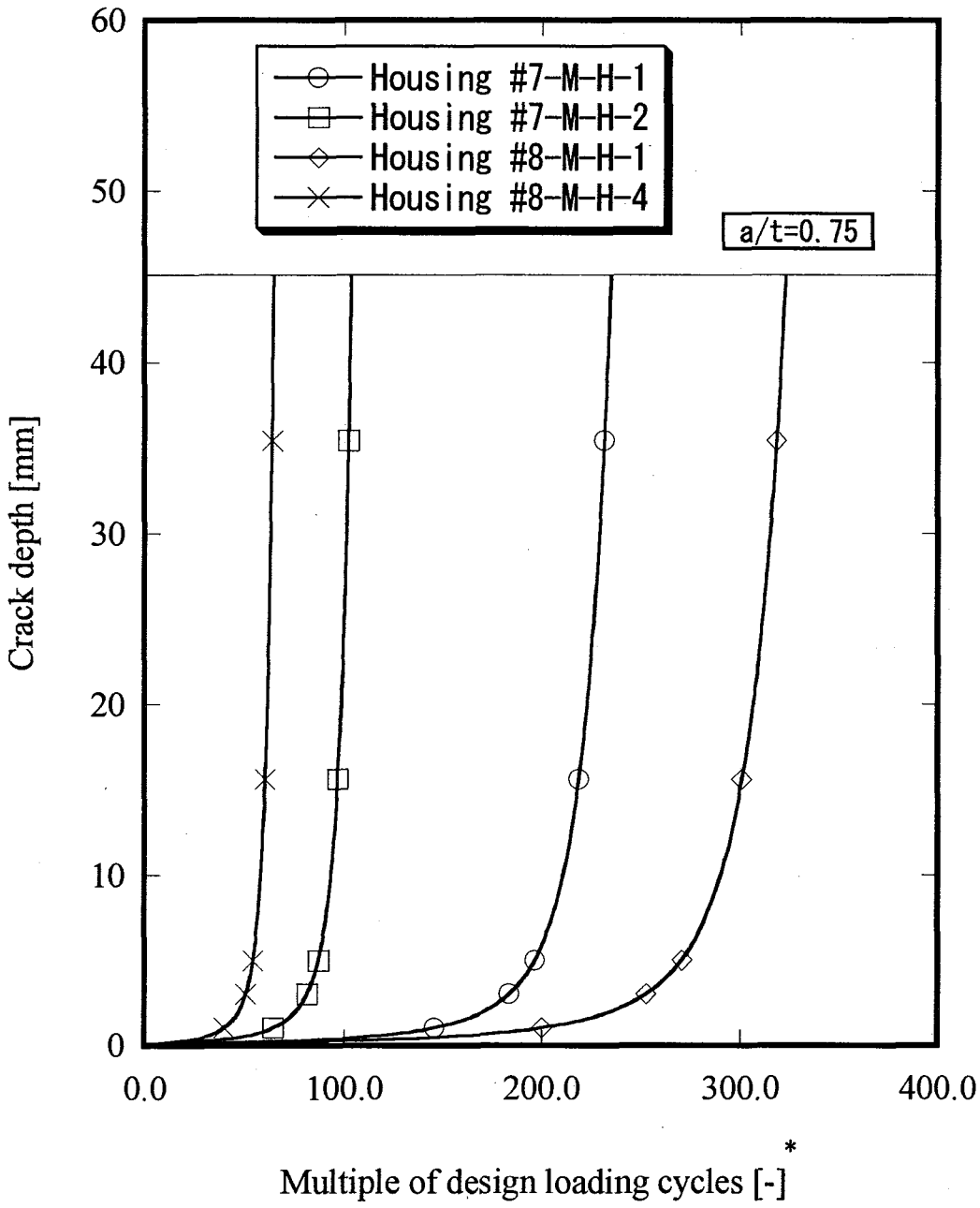

Fig. 7.3-1(a) Crack growth evaluation result of housing (welded part, crack depth from the surface)

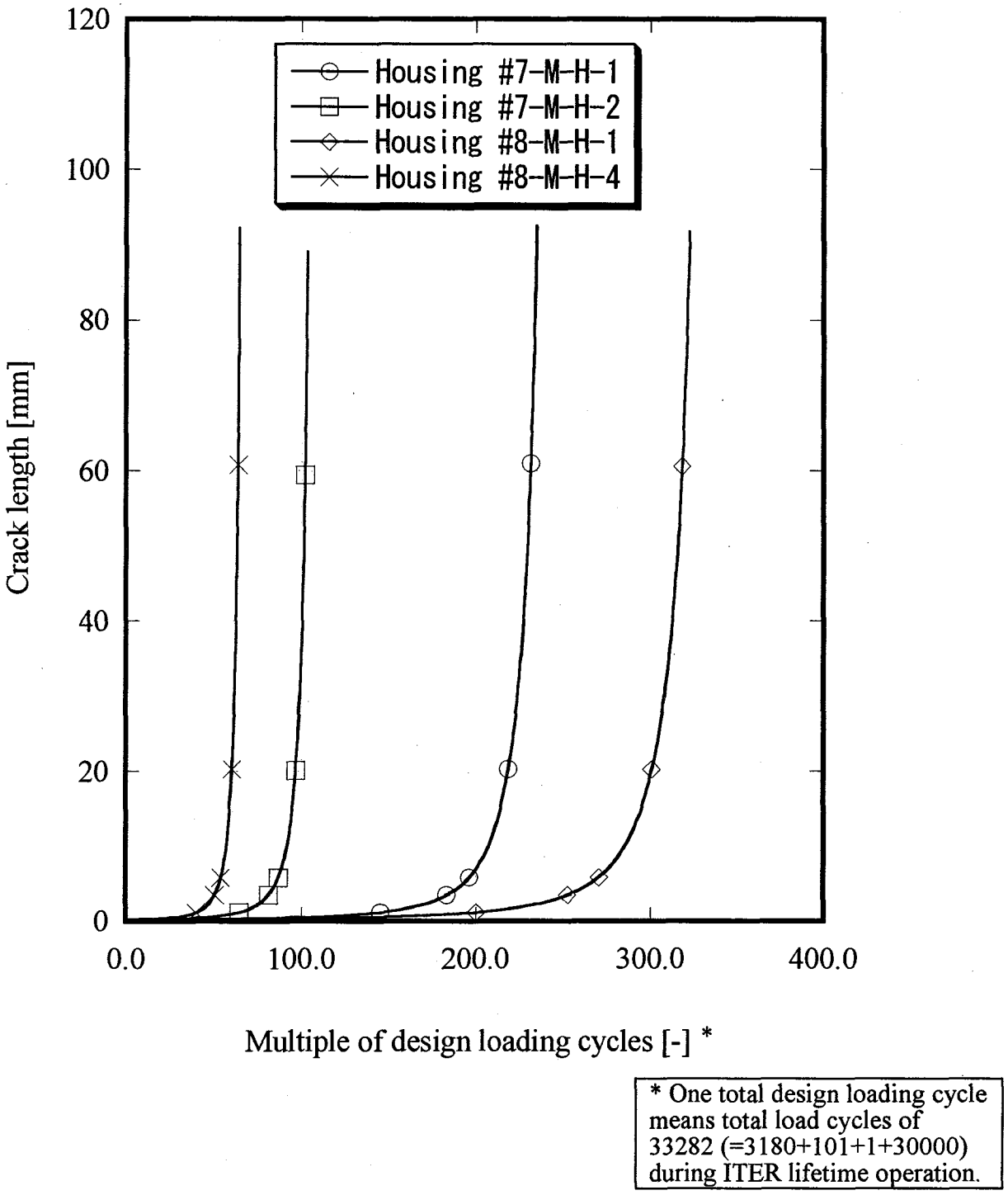

Fig.7.3-1 (b) Crack growth evaluation result of housing (welded part, crack depth from the surface)

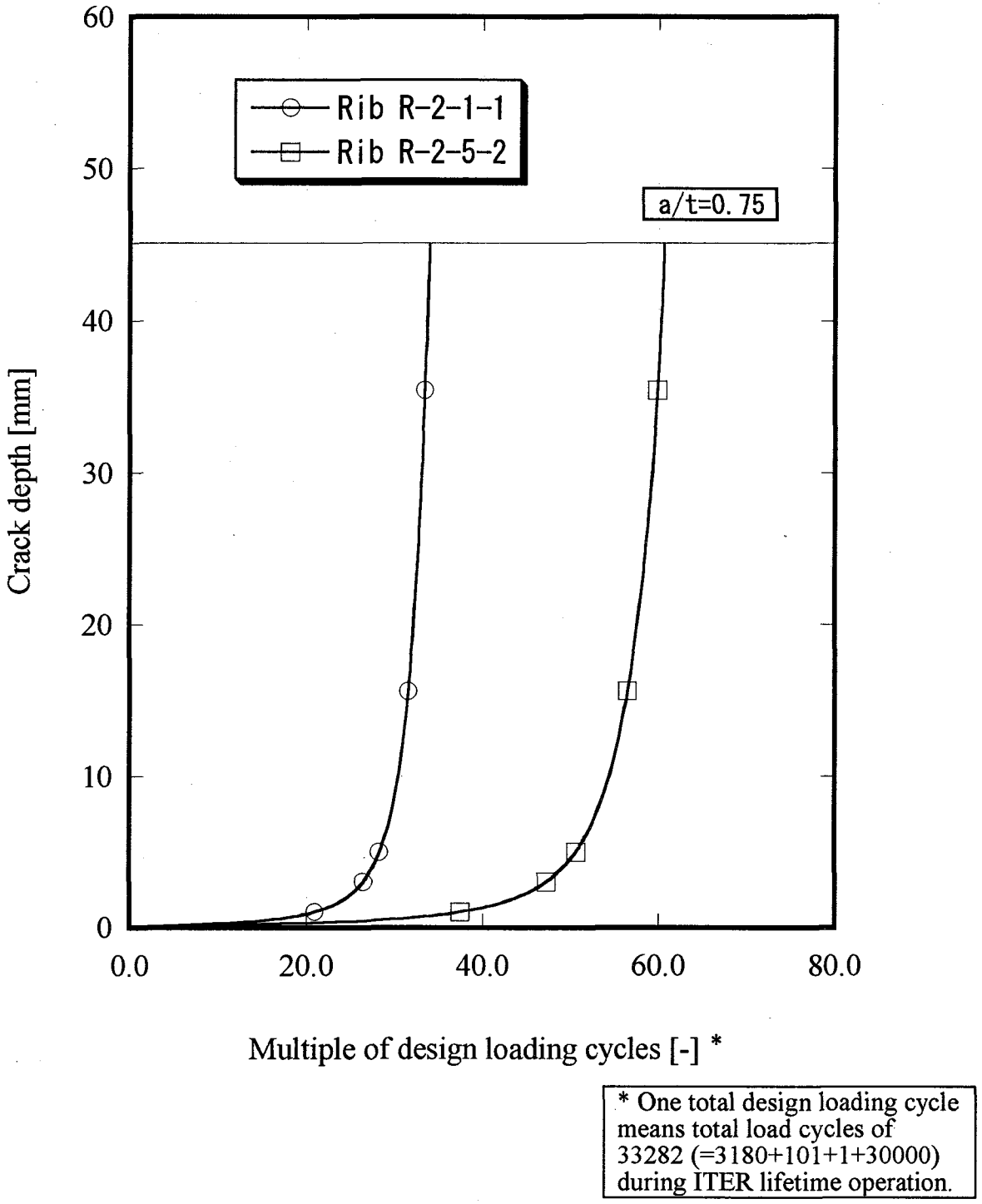

Fig. 7.3-2(a) Crack growth evaluation result of rib (welded part, crack depth from the surface)

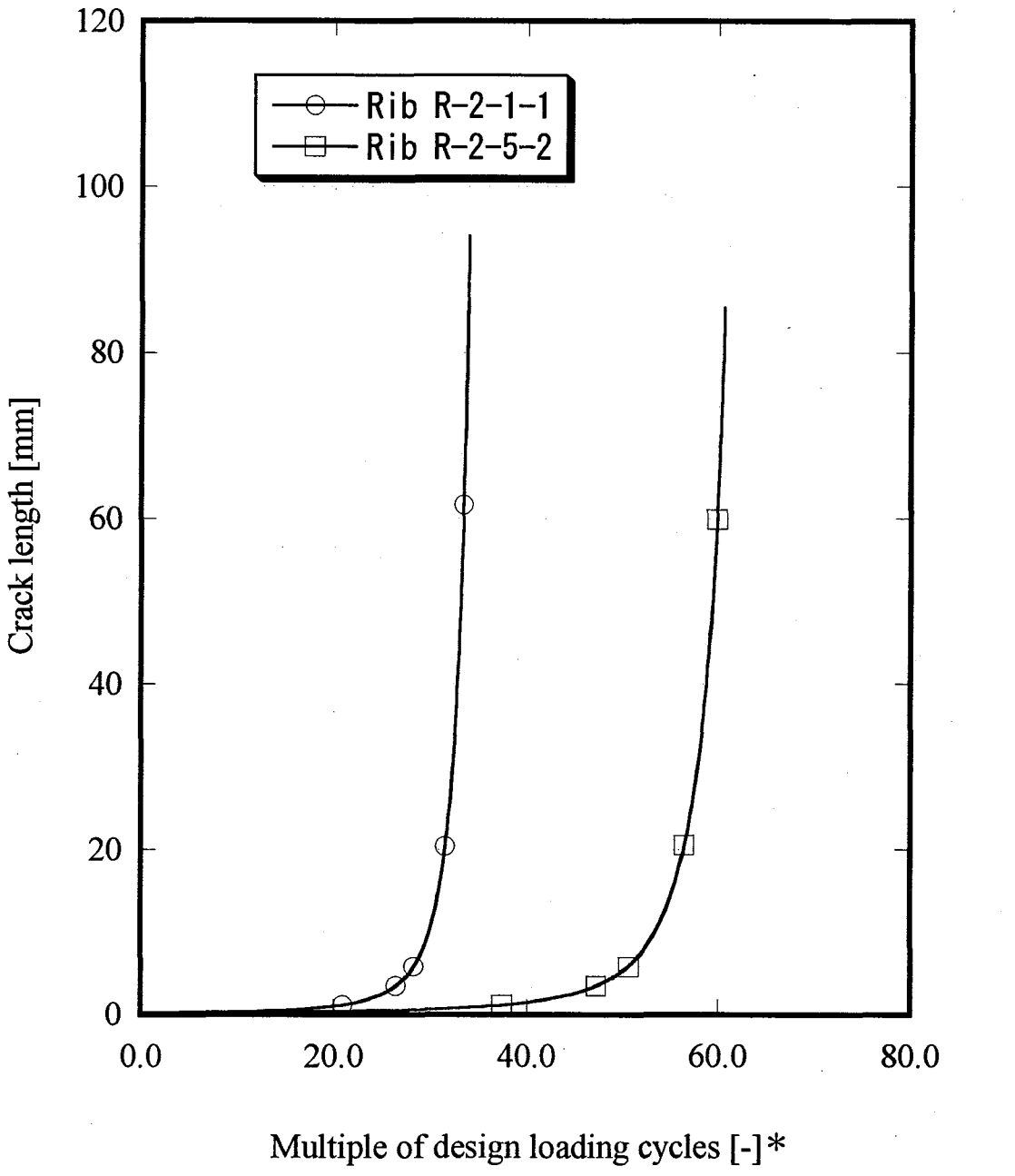

Fig.7.3-2(b) Crack growth evaluation result of rib (welded part, crack depth from the surface)

7.4 Summary

Allowable cracks for the plug welds between outer shell and ribs/housings have been estimated in the inboard upper region. Following results are obtained;

(1) Allowable crack lengths of plug welded ribs are estimated to be 12.2mm considering inspection error of 4.4mm. The length is larger than that of typical inboard area of 8.8mm.

(2) Allowable crack length of plug welded housing is estimated to be 38.6mm, which is a little bit shorter than that of typical inboard area of 39.5mm.

(3) Additionally allowable crack lengths of ribs and housings perpendicular to outer shell surface, which are defects of weld metal, are calculated for the plug weld application. Those are 24mm and 30.1mm except the too conservative fracture assessment case multiplying membrane plus bending stresses by safety factor of 3. For the assessment of allowable crack length, safety factors are important for the fracture assessment.

Reference

[7-1] Application of UT for inspection of pipes etc. in primary loop recirculation system, Nuclear and Industrial Safety Agency in Japan, July, 2004.

8 Conclusions

Applicability of plug weld has been investigated in order to improve fabricability of ITER Vacuum Vessel. A lot of ribs and housings should be welded to inner and outer shells of ITER Vacuum Vessel. Especially, welding ribs/housings to outer shell, access of weld is limited to the outer shell side. Moreover, by welding outer shells, weld deformations of the outer shells seem to be produced due to heat deposition of a lot of weld joints. Precise adjustment of groove gaps is required for welding outer shells.

Plug weld has advantages to adjust weld grooves comparing with butt weld. For the butt weld, groove gaps should be adjusted less than 1mm in case of automatic welding. For the plug weld, outer shell with slits is set on ribs/housings then the outer shell and ribs/housings are welded. However un-welded region is unavoidable at the edge of welding. The un-welded length can be conservatively assumed to be a crack. This report describes the assessment of applicability of the plug weld using crack propagation analyses for typical inboard region and inboard upper region. The allowable crack lengths are calculated for un-welded region of plug weld along outer shell surface and defects perpendicular to outer shell surface. Following results are obtained.

(1) Plug welding for welding between outer shell and ribs/housings could be applicable.

(2) For typical inboard region, allowable crack lengths of plug welded ribs are estimated to be 8.8mm and 12.7mm for side rib and center rib, respectively, considering inspection error of 4.4mm. For inboard upper region that is 12.2mm.

(3) For typical inboard upper region, allowable crack lengths of plug welded housings are estimated to be 39.5mm, considering inspection error of 4.4mm. For inboard upper region that is 38.6mm. This means that housings with smaller diameter less than 210mm might be applicable for welding between outer shell and housings.

(4) Additionally allowable crack lengths of ribs and housings perpendicular to outer shell surface, which are defects of weld metal, are calculated for the plug weld application. Those are 24mm and 30.1mm except the too conservative fracture assessment case multiplying membrane plus bending stresses by safety factor of 3. For the assessment of allowable crack length, safety factors are important for the fracture assessment.

Acknowledgement

The authors would like to express their gratitude to department of ITER Project for their valuable discussions and comments. They would acknowledge Drs. T.Tsunematsu and M.Mori for their support.